



**HAL**  
open science

# Synthesis and Characterization of Vanadium-containing Mesoporous Silica and its Application in the Catalysis of Oxidation Reaction

Yuting Zheng

► **To cite this version:**

Yuting Zheng. Synthesis and Characterization of Vanadium-containing Mesoporous Silica and its Application in the Catalysis of Oxidation Reaction. Material chemistry. Ecole normale supérieure de lyon - ENS LYON; East China normal university (Shanghai), 2014. English. NNT : 2014ENSL0944 . tel-01086424

**HAL Id: tel-01086424**

**<https://theses.hal.science/tel-01086424>**

Submitted on 16 Feb 2015

**HAL** is a multi-disciplinary open access archive for the deposit and dissemination of scientific research documents, whether they are published or not. The documents may come from teaching and research institutions in France or abroad, or from public or private research centers.

L'archive ouverte pluridisciplinaire **HAL**, est destinée au dépôt et à la diffusion de documents scientifiques de niveau recherche, publiés ou non, émanant des établissements d'enseignement et de recherche français ou étrangers, des laboratoires publics ou privés.

# THÈSE

en vue de l'obtention du grade de

**Docteur de l'Université de Lyon, délivré par l'École Normale Supérieure de Lyon**

**En cotutelle avec East China Normal University**

**Discipline : Chimie**

**Laboratoire de Chimie de l'ENS de Lyon / GCCP, East China Normal University**

**École Doctorale de Chimie**

présentée et soutenue publiquement le 2 Novembre 2014

par Madame Yuting ZHENG

---

**Synthèse et caractérisation de matériaux mésoporeux à base d'oxyde de vanadium pour l'oxydation de composés organiques**

---

Directeur de thèse : M. Laurent BONNEVIOT

Co-directeur de thèse : M. Mingyuan HE

Devant la commission d'examen formée de :

Mme. Anne GIROIR-FENDLER, IRCE Lyon, Membre

M. Dongyuan ZHAO, Fudan University, Membre

M. Jean-Marc CLACENS, E2P2-UMI 3464 CNRS, Membre/Rapporteur

M. Laurent BONNEVIOT, ENS de Lyon, Membre/Directeur

M. Mingyuan HE, East China Normal University, Membre/Directeur

M. Peng WU, East China Normal University, Membre

M. Yanglong GUO, East China University of Science and Technology, Membre/Rapporteur

**École Normale Supérieure de Lyon**

**East China Normal University**

**Synthesis and Characterization of Vanadium-containing  
Mesoporous Silica and its Application in the Catalysis of  
Oxidation Reaction**

Academy: Laboratoire de chimie in ENS-Lyon  
Department of Chemistry in ECNU

Major: Physical Chemistry  
Direction: Catalysis and Green Chemistry

Supervisor: Prof. BONNEVIOT Laurent  
Prof. HE Mingyuan

Doctor: ZHENG Yuting

**Shanghai, September 2014**

## Abstract

Vanadium-based materials are widely used as catalysts for oxidation of organic compounds. The catalytic properties of vanadium catalysts for oxidation are related closely to the state and the stability of vanadium species. Therefore, a series of vanadium-containing MCM-41 silica were designed and developed in this study, and their catalytic application for oxidation reactions was evaluated as well.

In the first part of work, the chemical anchoring effect of Al(III) or Ti(IV) heteroatoms on the dispersion of V(V) in MCM-41 type silica was investigated using a quantitative analysis of diffuse reflectance UV-visible spectra. The characteristic properties of prepared materials were determined by various characterization such as X-ray diffraction (XRD), N<sub>2</sub> sorption measurement, Electron paramagnetic resonance (EPR) spectroscopy, UV-visible spectroscopy and Raman spectroscopy. UV-visible spectra of hydrated and dehydrated samples evidenced the coexistence of several V(V) species of different oligomerization and hydration levels. The global blue shift of the band in the presence of Al(III) or Ti(IV) additives was then assigned to a higher proportion of less clustered and isolated V(V) species. The stronger beneficial effect of Ti on the vanadium dispersion is consistent with a higher stability of the X-O-V bridges moving from X = Si to X = Al and Ti.

In the second part, new mesoporous silica materials containing vanadium species were synthesized according to the molecular stencil patterning technique. Molecular stencil patterning is developed specifically for silica templated with ionic surfactants used as masking agent to sequentially immobilize via covalent bonding (grafting) different functions. This molecular surface engineering was proved to improve the vanadium species dispersion according to Thermogravimetric Analysis (TGA),

Nuclear Magnetic Resonance spectroscopy (NMR), Infrared spectroscopy (IR) and UV-visible spectroscopy. The incorporation of titanium species played again the role to immobilize the vanadium species as the results in previous work. The V/Ti ratio should be less than 1 to control the formation of clusters of vanadium species.

Lastly, the vanadium-containing materials were applied to the liquid phase oxidation of cyclohexane into cyclohexanol (A) and cyclohexanone (K). A mixture of these two products is often called K/A oil in the industrial chemical production. K/A oil is widely used as a raw material for adipic acid and caprolactam in the nylon industry. The catalysis results proved that the modification by adding titanium chemical anchors combined with the MSP technique improve the catalytic properties of vanadium-containing heterogeneous catalysts.

In conclusion, the dispersion and stability of vanadium active sites has been improved in new syntheses of vanadium-containing MCM-41 type silica by combining both anchoring heteroatoms and molecular stencil patterning techniques. Such a novel design leads to better catalytic performance in oxidation reaction in correlation with the structural and physical characteristics of the material.

**Key words:** vanadium, mesoporous silica, MCM-41, UV-visible spectroscopy, Molecular stencil patterning technique, leaching, oxidation of cyclohexane.

## Résumé

Les matériaux à base de vanadium sont largement utilisés comme catalyseurs pour l'oxydation de composés organiques. Les propriétés catalytiques des catalyseurs au vanadium pour l'oxydation dépendent de l'état et de la stabilité des espèces de vanadium. Dans cette étude, nous développons des nouveaux catalyseurs hétérogènes au vanadium pour la réaction d'oxydation.

Dans la première partie du travail, les matériaux mésoporeux à base de silice (MCM-41) contenant du Al (III) et du Ti (IV) sont envisagés comme supports. L'effet d'ancrage chimique de ces hétéroatomes sur les ions V (V) et leur dispersion dans la silice MCM- 41 ont été étudiés à l'aide d'une analyse quantitative des spectres UV-visible de réflectance diffuse. En complément, les matériaux ont été caractérisés par diffraction des rayons X (DRX), mesure de sorption d'azote, spectroscopie de résonance magnétique électrique (RPE) et la spectroscopie Raman. Les spectres UV-visible des échantillons hydratés et déshydratés mettent en évidence la coexistence de plusieurs espèces V (V) de différente nucléarité et différent taux d'hydratation. Le décalage vers le bleu de la bande UV des échantillons contenant comme des additifs les ions Al(III) ou Ti(IV) est cohérent avec une meilleure dispersion des ions vanadium présentant entre autres plus d'espèces mononucléaires (isolés). L'effet bénéfique du titane sur la dispersion de vanadium est compatible avec la formation directe de ponts covalents de type Ti-O-V.

Dans la seconde partie, les ions V(IV) ont été déposés sur des matériaux mésoporeux à base de silice en utilisant une nouvelle stratégie dite de pochoir moléculaire ou «Molecular-Stencil Patterning ». La stratégie de pochoir moléculaire s'applique à la silice contenant des tensioactifs ioniques en utilisant ces derniers comme agent de

masquage lors du greffage covalent de diverses fonctions. Cette stratégie de surface moléculaire permet de contrôler à la fois le voisinage moléculaire et la dispersion à longue distance des espèces de vanadium entre elles. La caractérisation a été effectuée en utilisant plusieurs méthodes telles l'analyse thermogravimétrique (ATG), la spectroscopie de résonance magnétique nucléaire (RMN), la spectroscopie infrarouge (IR) et la spectroscopie UV-visible. L'incorporation des ions titane (IV) joue le rôle d'ancre chimique pour les ions V(IV) comme dans le chapitre précédent. Il est montré qu'une proportion de V/Ti inférieure à un et proche de trois génère les meilleures conditions pour éviter la formation de gros agrégats d'oxyde de vanadium.

Enfin, ces nouveaux matériaux au vanadium ont été testés en phase liquide pour catalyser l'oxydation partielle du cyclohexane en une huile désignée par son rapport molaire K/A de cyclohexanone (K) et de cyclohexanol (A). Ce mélange est utilisé comme telle en chimie industrielle de base, en particulier comme précurseurs de l'acide adipique et de caprolactame pour la synthèse du nylon. Les tests ont démontré que l'introduction de titane combiné à la stratégie de pochoir moléculaire a notablement amélioré les propriétés catalytiques de ce type de catalyseurs au vanadium.

En conclusion, la silice MCM-41 au vanadium a été conçue par l'introduction des hétéroatomes d'ancrage et de la stratégie de pochoir moléculaire, afin d'améliorer la dispersion et la stabilité des sites actifs. Les matériaux conçus ont montré de meilleures propriétés et caractéristiques catalytiques dans divers caractérisation et la réaction d'oxydation.

## 摘要

含钒催化剂被广泛用于催化有机化合物氧化反应,其催化性能与所含钒物种状态及其稳定性有着密切联系。因此,本研究设计合成了一系列的含钒 MCM-41 型介孔二氧化硅,对其物理化学性质进行了多种表征并且评估了它们在催化氧化过程中的性能。

本工作的第一部分致力于将钒物种负载于含有 Al(III) 及 Ti(IV) 杂原子的 MCM-41 型介孔二氧化硅中,并对漫反射紫外可见光谱进行定量分析以证明杂原子对于钒物种的固载作用。一系列表征手段被用于分析材料的各种物理化学性质,如粉末 X 射线衍射 (XRD), 氮气吸脱附测试, 电子顺磁共振 (EPR), 紫外可见光谱 (UV-visible) 以及拉曼光谱 (Raman)。对含水与脱水样品的紫外可见光谱详细解析表明了多种聚合态的钒物种存在于不同样品中。含有 Al(III) 及 Ti(IV) 杂原子作为载体的含钒材料的紫外可见光谱较之纯硅含钒样品的光谱出现了明显蓝移现象,说明在前者样品中的钒物种颗粒相对较小并具有较多的单分散钒活性位,并以此推断 Ti-O-V 键与 Al-O-V 键相对于 Si-O-V 键更加稳定。

在第二部分工作中,分子模板法被用于设计修饰含钒介孔二氧化硅材料表面。分子模板法是专用于修饰并功能化某些使用离子型模板剂导向的介孔二氧化硅材料表面。使用分子模板法所得的样品经一系列表征手段如热重分析 (TGA), 核磁共振 (NMR), 红外光谱 (IR) 以及紫外可见光谱 (UV-visible) 后表明,有机官能团的引入可以限制钒物种的生长获得活性位分散良好的样品。在此基础上,钛原子作为固载原子同样被引入并被证明当钒钛比小于 1 时,钛原子可有效控制钒物种的聚合。

最后,前两部分工作所获得的材料被应用于液相催化氧化反应以考察其催化性能。环己烷环氧化生成重要工业原料 K/A 油反应过程在此被选择为探针反应。K/A

油作为己二酸及己内酰胺的前驱体被广泛使用于尼龙工业中,因此选择此反应作为探针反应旨在提高含钒催化剂的工业应用前景。结果表明,使用 Ti 原子掺杂以及分子模板法修饰样品可提高含钒介孔二氧化硅催化剂的催化性能及活性位的稳定性。

综上所述,使用固载原子 Ti 原子掺杂以及使用分子模板法修饰二氧化硅表面都可以有效地提高钒物种在二氧化硅基材中的分散性及稳定性,由此所得的含钒多相催化剂在液相氧化反应中也表现出了较高的催化性能。

关键词:钒氧化物,介孔二氧化硅, MCM-41, 紫外可见光谱, 分子模板法, 环己烷氧化。

# Contents

<b>Abstract</b> .....	<b>I</b>
<b>R ésum é</b> .....	<b>III</b>
<b>摘要</b> .....	<b>V</b>
<b>List of schemes, figures and tables</b> .....	<b>i</b>
<b>Chapter 1. General Introduction</b> .....	<b>1</b>
1.1 History of vanadium catalyst .....	1
1.2 Heterogeneous catalysis .....	3
1.2.1 History of heterogeneous catalysis .....	3
1.2.2 Mesoporous silica: a way from homogeneous to heterogeneous.....	5
1.3 Conclusion .....	7
1.4 Reference .....	8
<b>Chapter 2. Literature Survey</b> .....	<b>9</b>
2.1 Mesoporous silica and the modification of surface .....	9
2.1.1 Mesoporous silica .....	9
2.1.1.1 The M41S family .....	10
2.1.1.2 Formation mechanism.....	12
2.1.1.3 Synthesis of MCM-41 type silica and general physico-chemical properties .....	15
2.1.2 Modification of the surface of mesoporous silicas .....	18
2.1.2.1 The surface of mesoporous silicas .....	18
2.1.2.2 Modification of the surface of mesoporous silicas .....	19
2.2 Vanadium-containing heterogeneous catalysts .....	23
2.2.1 Vanadium species in the heterogeneous catalysts .....	23
2.2.1.1 Molecular structure of surface VO <sub>4</sub> species.....	24
2.2.1.2 Active species of vanadium supported materials .....	25
2.2.2 Spectroscopic characterization of vanadium species in heterogeneous catalysts.....	27
2.2.2.1 Diffuse reflection UV-visible spectroscopy (DR UV-vis) .....	27
2.2.2.2 Electron paramagnetic/spin resonance spectroscopy (EPR/ESR) .....	30
2.2.2.3 Raman spectroscopy .....	31
2.2.2.4 Nuclear magnetic resonance spectroscopy (NMR).....	33
2.2.3 Vanadium-containing heterogeneous catalysts .....	34
2.2.3.1 Oxides supported vanadium catalysts .....	34
2.2.3.2 Vanadium-containing zeolites and microporous molecular sieves.....	37
2.2.3.3 Vanadium-containing mesoporous materials .....	41
2.3 Catalysis applications of vanadium-containing heterogeneous catalysts .....	44
2.3.1 Oxidation reaction of alcohol.....	44
2.3.2 Oxidation reaction of saturated and unsaturated hydrocarbons .....	45
2.3.2.1 Oxidation reaction of alkene and cycloalkene.....	46
2.3.2.2 Oxidation reaction of linear alkane and cycloalkane .....	47

2.3.2 Hydroxylation of aromatic compounds .....	48
2.3.3 Dehydrogenation of alkanes .....	49
2.3.4 Oxidative halogenation .....	52
2.3.4.1 Haloperoxidases .....	52
2.3.4.2 Vanadium catalyzed bromination reaction.....	53
2.3.4.3 Oxidative bromination of phenol red catalyzed by V-containing materials.....	54
2.4 Conclusion .....	56
2.5 Reference .....	57
<b>Chapter 3. Chemicals and Characterization .....</b>	<b>70</b>
3.1 Commercial products.....	70
3.1.1 Solvents and gases .....	70
3.1.2 Reagents.....	70
3.2 Characterization method.....	71
3.3 Reference .....	73
<b>Chapter 4. Effect of Al(III) and Ti(IV) additives on vanadium dispersion in MCM-41 type silicas .....</b>	<b>74</b>
4.1 Introduction .....	74
4.2 Experimental.....	76
4.2.1 Synthesis of 2D hexagonal mesoporous silica: <sup>19-21</sup> .....	76
4.2.2 Preparation of vanadium-containing materials: .....	77
4.3 Results and discussion .....	78
4.3.1 Synthesis of materials and textural characterization.....	78
4.3.1.1 Preparation of the materials .....	78
4.3.1.2 Textural characterization.....	79
4.3.2 Vanadium state during the preparation.....	82
4.3.3 Analysis of vanadium species polymerization based on Tauc's plot. .	84
4.3.4 Quantitative investigation of vanadium state on the different supports by DR UV-visible spectroscopy.....	89
4.3.5 Investigation the Ti-O-V bonds based on Raman spectroscopy. ....	95
4.4 Conclusion .....	99
4.5 Reference .....	100
<b>Chapter 5. Improvement of vanadium dispersion using molecular surface engineering.....</b>	<b>103</b>
5.1 Introduction .....	103
5.2 Experimental.....	105
5.2.1 Synthesis of 2D hexagonal mesoporous silica.....	105
5.2.2 Preparation of vanadium-containing silica .....	106
5.2.2.1 Preparation of LUS-V(x) .....	106
5.2.2.2 Preparation of LUS-Ti(y)-V(x) .....	107
5.2.2.3 Preparation of LUS-E-V(x).....	107
5.2.2.4 Preparation of LUS-E-Ti(y)-V(x) .....	108
5.3 Results and discussion .....	110
5.3.1 Synthesis of materials and textural characterization.....	110

5.3.1.1 Preparation of samples .....	110
5.3.1.2 Textural characterization.....	111
5.3.1.3 Organic groups in the LUS-E-V(x) and LUS-E-Ti(y)-V(x) series. ....	114
5.3.2 The influence of EBDMS groups on dispersion of vanadium species. ....	122
5.3.3 The influence of Titanium species on dispersion of vanadium species. ....	129
5.4 Conclusion.....	137
5.5 Reference.....	139
<b>Chapter 6. Investigation of catalytic application of vanadium containing mesoporous silica .....</b>	<b>140</b>
6.1 Introduction .....	140
6.2 Experimental.....	143
6.2.1 Leaching test .....	143
6.2.2 Oxidation reaction of cyclohexane .....	143
6.3 Results and discussion .....	144
6.3.1 Redox behaviors of vanadium-containing silica.....	144
6.3.2 Leaching test .....	146
6.3.3 Catalytic performance of oxidation of cyclohexane .....	149
6.3.3.1 Catalytic performance of vanadium-containing MCM-41 type silica prepared by impregnation.....	149
6.3.3.2 Recycling and reusing of vanadium-containing MCM-41 type silica prepared by impregnation.....	151
6.3.3.3 Catalytic performance of vanadium-containing MCM-41 type silica prepared by grafting with or without molecular patterning stencil technique .....	154
6.3.3.4 Recycling and reusing of vanadium-containing MCM-41 type silica prepared by grafting with or without molecular patterning stencil technique .....	158
6.4 Conclusion.....	161
6.5 Reference.....	163
<b>Chapter 7. Conclusions and perspectives .....</b>	<b>165</b>
7.1 General conclusions.....	165
7.2 Future perspectives .....	168
<b>Acknowledgements .....</b>	<b>170</b>

## List of schemes, figures and tables

### Chapter 1

**Scheme 1.** Overall reaction scheme of vanadium haloperoxidases. P2

**Figure 1.** Examples of the reaction types mediated by peroxovanadium (V) complexes. P3

**Table 1.** Examples of major industrial processes using heterogeneous catalysis. P4

### Chapter 2

**Scheme 1.** Halogenation of organic substrates. P53

**Figure 1.** The M41S family of mesoporous molecular sieves including MCM-41, MCM-48, and MCM-50. P10

**Figure 2.** Two mechanisms proposed for the formation of mesoporous silica: A) cooperative self-assembly (CSA) mechanism, and B) liquid-crystal templating (LCT) mechanism. P12

**Figure 3.** Liquid crystal templating mechanistic pathways for M41S. P13

**Figure 4.** Powder X-ray diffraction pattern of calcined MCM-41 silica. P16

**Figure 5.** N<sub>2</sub> adsorption-desorption isotherm of MCM-41 silica without surfactant. P17

**Figure 6.** TEM images of MCM-41 silicas with pore sizes of (a) 2.0, (b) 4.0, (c) 6.5, and (d) 10.0 nm. P17

**Figure 7.** Types of silanol groups and siloxane bridges on the surface of amorphous silica. P18

**Figure 8.** Schematic representation of the hierarchical porous materials with ordered nanoporosities and microcavities in the long-chain molecular monolayer coating. P20

**Figure 9.** Synthetic routine from as-made silica LUS 1 to ruthenium supported

complex <b>6</b> via Molecular Stencil Patterning (MSP) technique.	P21
<b>Figure 10.</b> Synthetic routine from the as-made silica <b>1</b> to the multifunctional metallated material <b>7</b> via MSP technique.	P22
<b>Figure 11.</b> Three different forms of VO <sub>x</sub> species on the surface of inorganic supports.	P24
<b>Figure 12.</b> Possible molecular structures of monomeric VO <sub>4</sub> species on silica support.	P25
<b>Figure 13.</b> VO <sup>2+</sup> Crystal Field Splitting Diagram.	P28
<b>Figure 14.</b> Attribution of vanadium oxide species based on results of the deconvolution of experimental spectra (left), and relative abundance of various vanadium oxide species in the dependence of vanadium concentration (right). Oh-coordinated species, orange square; Td-coordinated oligomeric units, green circle; Td-coordinated isolated monomeric units, blue triangle.	P29
<b>Figure 15.</b> EPR spectra at 293 K of (a) V/Ti-MCM-41, (b) V/Zr-MCM-41, (c) V/MCM-41 and (d) V/Al-MCM-41.	P31
<b>Figure 16.</b> Raman spectra of dehydrated V <sub>2</sub> O <sub>5</sub> /SiO <sub>2</sub> catalyst as a function of vanadia loading (exciting wavelength: 532nm).	P32
<b>Figure 17.</b> <sup>51</sup> V MAS NMR spectra of VO <sub>x</sub> /Al <sub>2</sub> O <sub>3</sub> samples prepared from: vanadyl sulfate (4VS), ammonium metavanadate (4VM) and vanadyl acetylacetonate (4VA).	P34
<b>Figure 18.</b> Model for the structure of the supported hydrated, dehydrated and reduced vanadium species on the surface.	P35
<b>Figure 19.</b> Topology of MFI molecular sieve.	P38
<b>Figure 20.</b> Three different types of tetrahedral V species and their possible position in the V-BEA zeolite.	P39
<b>Figure 21.</b> Dissociative chemisorption of methanol on a surface vanadium site of supported vanadium catalysts.	P44

<b>Figure 22.</b> Main products at the earlier stage of hydroxylation of biphenyl catalyzed by V-containing MCM-41.	P48
<b>Figure 23.</b> Primary products and further oxidized products of hydroxylation of naphthalene.	P49
<b>Figure 24.</b> Simulated example of propane oxidative dehydrogenation over VO <sub>x</sub> -based catalyst.	P51
<b>Figure 25.</b> The vanadium site of V-bromoperoxidase. Vanadium cofactor is represented as a gray/red stick and ball model.	P52
<b>Figure 26.</b> Catalytic cycle for V-BrPO showing coordination of H <sub>2</sub> O <sub>2</sub> before oxidation of bromide.	P53
<b>Figure 27.</b> Oxidative bromination of phenol red catalyzed by V-MCM-41.	P55
<b>Table 1.</b> Summary of the catalytic activity and selectivity of the Ti and V nanostructured systems towards the oxidation of 1-hexene, cyclohexene and cyclohexane.	P46
<b>Table 2.</b> Oxidation of <i>n</i> -hexane over TS-2 and VS-2.	P47
 <b>Chapter 3</b>	
<b>Table 1.</b> Solvents utilized in this study.	P70
<b>Table 2.</b> Gases utilized in this study.	P70
<b>Table 3.</b> Reagents utilized in this study.	P70
 <b>Chapter 4</b>	
<b>Scheme 1.</b> Preparation process of impregnated vanadium containing materials.	P78
<b>Figure 1.</b> Low-angle XRD powder pattern of a.LUS, b. Al(5)-LUS, and c. Ti(7)-LUS.	P79
<b>Figure 2.</b> Low angle powder XRD of a. LUS-V(2.5) before calcination, and b. LUS-V(2.5) after calcination.	P80

**Figure 3.** N<sub>2</sub> adsorption-desorption isotherms of LUS (black up-triangle), LUS-V(2.5) (red star), Al(5)-LUS (blue square), Al(5)-LUS-V(2.5) (pink down-triangle), Ti(7)-LUS (green sphere) and Ti(7)-LUS-V(2.5) (diamond). P80

**Figure 4.** EPR spectra of a. LUS-V(2.5) before calcination, b. Al(5)-LUS-V(2.5) before calcination, c. Ti(7)-LUS-V(2.5) before calcination and d. Si-LUS-V(2.5) after calcination. P82

**Figure 5.** DR UV-visible spectra of a. LUS-V(2.5) before calcination, and b. LUS-V(2.5) after calcination. P84

**Figure 6.** Tauc's plot based on UV-visible spectra of LUS-V(x), Al(5)-LUS-V(x) and Ti(7)-LUS-V(x). P86

**Figure 7.** Tauc's plot based on UV-visible spectra of LUS-V(2.5), Al(y)-LUS-V(2.5), Ti(z)-LUS-V(2.5). P88

**Figure 8.** DR UV-visible spectra of a. Ti(2.8)-LUS, b. Ti(7)-LUS, and c. Ti(12.5)-LUS. P89

**Figure 9.** DR UV-visible spectra fitted by Gaussian curve of a. LUS-V(2.5), b. Al(5)-LUS-V(2.5), c. Ti(7)-LUS-V(2.5) and a\*. dehydrated LUS-V(2.5), b\*. dehydrated Al(5)-LUS-V(2.5), c\*. dehydrated Ti(7)-LUS-V(2.5) P90

**Figure 10.** Relative fitted peak area of LUS-V series, Al-LUS-V series and Ti-LUS-V series. P93

**Figure 11.** Raman spectra (exciting wavelength: 514 nm) of a. LUS, b. Ti(7)-LUS c. LUS-V(2.5), and d. Ti(7)-LUS-V(2.5). P95

**Figure 12.** Raman spectra (exciting wavelength: 514 nm) of a. Ti(7)-LUS-V(2.5) (blue solid line), b. Ti(7)-LUS, c. LUS-V(2.5), and d. [LUS-V(2.5)+Ti(7)-LUS]\*0.4 (pink dash line). P96

**Figure 13.** Raman spectra (exciting wavelength: 244 nm) of a. LUS, b. Ti(7)-LUS, c. LUS-V(2.5), and d. Ti(7)-LUS-V(2.5). P97

**Figure 14.** Raman spectra (exciting wavelength: 244 nm) of a. Ti(7)-LUS-V(2.5), b.

Ti(7)-LUS, c. LUS-V(2.5), and d. [LUS-V(2.5)+Ti(7)-LUS]\*0.5 (pink line). P98

**Table 1.** Textural analysis of supports and materials with vanadium. P81

**Table 2.** Edge energies of obtained from Tauc's plot of LUS-V(x), Al(5)-LUS-V(x), and Ti(7)-LUS-V(x). P87

**Table 3.** Edge energies of obtained from Tauc's plot of LUS-V(2.5), Al(y)-LUS-V(2.5), and Ti(y)-LUS-V(2.5). P88

**Table 4.** The detail of fitting Gaussian curve of all the sample. P94

## Chapter 5

**Scheme 1.** Preparation procedure of LUS-V(x), LUS-Ti(y)-V(x), LUS-E-Ti(y)-V(x) and LUS-E-V(x). P109

**Scheme 2.** Possible structures of EBDMS surface species in the samples. P122

**Scheme 3.** Possible model of vanadium species distribution in the LUS-V(x) and LUS-E-V(x). P129

**Scheme 4.** The ideal anchored V species moieties with a single V=O species linked to the silica support by one V-O-Si and 2 V-O-Ti on a dimeric Ti site. P136

**Figure 1.** Low angle power XRD patterns (A) and N<sub>2</sub> adsorption-desorption isotherms (B) of a. LUS-V(5), b. LUS-E-V(5), c. LUS-Ti(5)-V(5), and d. LUS-E-Ti(5)-V(5). P111

**Figure 2.** TG-DTG curves of a. LUS-V(5), b. LUS-Ti(5)-V(5), c. LUS-E-Ti(5)-V(5), and d. LUS-E-V(5). P114

**Figure 3.** ATR-IR spectra of a. LUS-V(5), b. LUS-Ti(5)-V(5), c. LUS-E-V(5), and d. LUS-E-Ti(5)-V(5). P115

**Figure 4.** Difference spectra obtained by normalization and substraction of the spectrum of genuine LUS, to a. LUS-V(5), b. LUS-Ti(5)-V(5), b. LUS-E-V(5) and c. LUS-E-Ti(5)-V(5). P119

**Figure 5.** <sup>29</sup>Si solid NMR spectra of a. LUS, b. LUS-V(1.25), c. LUS-V(5), d. LUS-E,

e. LUS-E-V(1.25), f. LUS-E-V(5), g. LUS-E-Ti(5), h. LUS-E-Ti(5)-V(1.25) and i. LUS-Ti(5)-V(5) P121

**Figure 6.** UV-vis spectra of non-calcined samples: a. LUS-V(1.25), b. LUS-V(2.5), c. LUS-V(5), a\*. LUS-E-V(1.25), b\*. LUS-E-V(2.5), and c\*. LUS-E-V(5). P123

**Figure 7.** EPR spectra of a. LUS-V(1.25), b. LUS-V(2.5), c. LUS-V(5), a\*. LUS-E-V(1.25), b\*. LUS-E-V(2.5), and c\*. LUS-E-V(5). P123

**Figure 8.** UV-vis spectra of a. LUS-V(1.25)-cal, b. LUS-V(2.5)-cal, c. LUS-V(5)-cal, a\*. LUS-E-V(1.25)-cal, b\*. LUS-E-V(2.5)-cal, and c\*. LUS-E-V(5)-cal. P124

**Figure 9.** Tauc's plot ( $[F(R_{\infty})hv]^2$  vs.  $hv$  for both LUS-V(x) and LUS-E-V(x) series. P125

**Figure 10.** Relative fitted peak area LUS-V(x), LUS-E-V(x), LUS-V(x)-cal and LUS-E-V(x)-cal. Orange bar represented the bands at  $20000\text{ cm}^{-1}$  -  $25000\text{ cm}^{-1}$  (polymer) Green bar represented the bands at  $30000\text{ cm}^{-1}$  (oligomer) ; Blue bar represented the bands at  $38000\text{ cm}^{-1}$  (monomer); Violet bar represented the bands at  $46000\text{ cm}^{-1}$  (monomer). P126

**Figure 11.** UV-vis spectra of a. LUS-E-Ti(5)-V(1.25), b. LUS-E-Ti(5)-V(2.5), c. LUS-E-Ti(5)-V(5), a\*. LUS-Ti(5)-V(1.25), b\*. LUS-Ti(5)-V(2.5), and c\*. LUS-Ti(5)-V(5). P130

**Figure 12.** UV-vis spectra of a. LUS-E-Ti(5)-V(1.25)-cal, b. LUS-E-Ti(5)-V(2.5)-cal, c. LUS-E-Ti(5)-V(5)-cal, a\*. LUS-Ti(5)-V(1.25)-cal, b\*. LUS-Ti(5)-V(2.5)-cal, and c\*. LUS-Ti(5)-V(5)-cal. P131

**Figure 13.** Tauc's plot ( $[F(R_{\infty}) hv]^2$  vs.  $hv$  of LUS-E-Ti(5)-V(x) and LUS-Ti(5)-V(x). P132

**Figure 14.** Relative fitted peak area LUS-E-Ti(5)-V(x), LUS-Ti(5)-V(x), LUS-E-Ti(5)-V(x)-cal and LUS-Ti(5)-V(x)-cal. Orange bar represented the bands at  $20000\text{ cm}^{-1}$  -  $25000\text{ cm}^{-1}$  (polymer) Green bar represented the bands at  $30000\text{ cm}^{-1}$  (oligomer) ; Blue bar represented the bands at  $38000\text{ cm}^{-1}$  (monomer); Violet bar

represented the bands at $46000\text{ cm}^{-1}$ (monomer).	P134
<b>Figure 15.</b> UV-visible spectra of a. LUS-Ti(5) and b. LUS-E-Ti(5).	P136
<b>Table 1.</b> Elemental analysis of samples.	P110
<b>Table 2.</b> Textural properties of samples analyzed by $\text{N}_2$ sorption.	P113
<b>Table 3.</b> Percentage of $Q_n$ , $M_n$ obtained from $^{29}\text{Si}$ NMR	P120
<b>Table 4.</b> Data of deconvolution for LUS-V(x), LUS-E-V(x), LUS-V(x)-cal and LUS-E-V(x)-cal.	P127
<b>Table 5.</b> Data of deconvolution for LUS-E-Ti(y)-V(x), LUS-Ti(y)-V(x), LUS-E-Ti(y)-V(x)-cal and LUS-Ti(y)-V(x)-cal.	P135

## Chapter 6

<b>Figure 1.</b> $\text{H}_2$ -TPR patterns of a. LUS, b. LUS-V(1.25)-I, c. LUS-V(2.5)-I, and d. LUS-V(5)-I.	P145
<b>Figure 2.</b> $\text{H}_2$ -TPR patterns of a. LUS-V(2.5)-I, b. Al(5)-LUS-V(2.5)-I, and c. Ti(7)-LUS-V(2.5)-I.	P145
<b>Figure 3.</b> Loss of vanadium species of Si-LUS-V-I series, Al(5)-LUS-V-I series and Ti(7)-LUS-V-I series.	P146
<b>Figure 4.</b> Tauc's plot based on UV-visible spectra of LUS-V(x)-I, Al(5)-LUS-V(x)-I and Ti(7)-LUS-V(x)-I after leaching test.	P148
<b>Figure 5.</b> Cyclohexane conversion of LUS-V(5)-I and Ti(7)-LUS-V(5)-I during four times reusing.	P153
<b>Figure 6.</b> Cyclohexane conversion of LUS-V(1.25)-I and Ti(7)-LUS-V(1.25)-I during five times reusing.	P154
<b>Table 1.</b> Elemental analysis of LUS-V, Al-LUS-V and Ti-LUS-V series before and after leaching test.	P147
<b>Table 2.</b> Edge energies of obtained from Tauc's plot of LUS-V(x), Al(5)-LUS-V(x),	

and Ti(7)-LUS-V(x).	P149
<b>Table 3.</b> Catalytic performance of LUS-V-I series and Ti(7)-LUS-V-I series.	P150
<b>Table 4.</b> Catalytic performance of LUS-V(5), Ti(7)-LUS-V(5), LUS-V(1.25) and Ti(7)-LUS-V(1.25) in reusing process.	P152
<b>Table 5.</b> Catalytic performance of vanadium-containing MCM-41 type silica prepared by MSP technique.	P157
<b>Table 6.</b> Catalytic performance of LUS-Ti(5)-V(1.25)-G, LUS-Ti(5)-V(1.25)-G-cal, LUS-E-Ti(5)-V(1.25)-G-cal and LUS-E-V(1.25)-G-cal in reusing process.	P159
<b>Figure 7.</b> Cyclohexane conversion of LUS-Ti(5)-V(1.25)-G and LUS-Ti(5)-V(1.25)-G-cal during four times reusing.	P160
<b>Figure 8.</b> Cyclohexane conversion of LUS-Ti(5)-V(1.25)-G-cal, LUS-E-Ti(5)-V(1.25)-G-cal and LUS-E-V(1.25)-G-cal during four times reusing.	P160

## Chapter 1. General Introduction

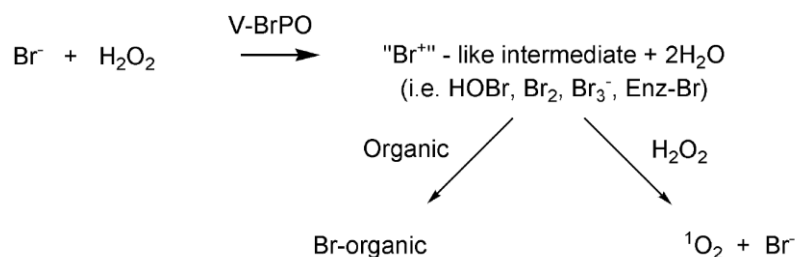
### 1.1 History of vanadium catalyst

*Learning from Mother Nature* is an eternal topic to worldwide human beings even with different culture background. In ancient China, Taoists advocated to respect the philosophy of nature, which was first proposed by Laozi, the author of *Daodejing* in 6th century BC.<sup>2</sup> The idea from *Daodejing* influenced not only the literary researchers but also the scientific researchers. Many scientists mentioned that *Daodejing* inspired them during their scientific life, such as Hideki Yukawa<sup>3</sup>, the Japanese theoretical physicist and the first Japanese Nobel laureate. In the development of modern science, the bio mimicry plays magic in all the fields, especially in the engineering because the design of nature is always more efficient and less wasteful.

It was believed that marine organisms in the ocean inspired the discovery of vanadium catalyst. Due to the high halogen content in the ocean, it is not surprising that halogenation plays an important role in the metabolism of marine seaweeds. Considering the chemical defense roles of the halogenated compounds to keep predators away from a particular organism, these products from the oxidation of halides were thought to have biological activity such as antifungal, antibacterial, antineoplastic, antiviral and antiinflammatory. These biological active products were suggested to be biosynthesized via haloperoxidase enzymes in the 1980s. The vanadium-dependent haloperoxidases was the most prevalent one in the discovery of haloperoxidase.<sup>1,4</sup> This was considered as an origin of vanadium catalysis.

The mechanism of the halogenation by vanadium haloperoxidases includes two steps (Scheme 1). In the first step, vanadium haloperoxidases catalyze the oxidation of halides by H<sub>2</sub>O<sub>2</sub> producing a two electron oxidized halogen intermediate. Secondly,

the oxidized intermediate can halogenate an appropriate organic substrate or react with another equivalent of  $\text{H}_2\text{O}_2$ .<sup>1</sup>



Scheme 1. Overall reaction scheme of vanadium haloperoxidases.<sup>1</sup>

Inspired by the vanadium haloperoxidase enzymes, a variety of vanadium complexes were mimicked and studied as catalysts to get better understanding of the mechanism of vanadium haloperoxidase enzymes and to suggest the importance of vanadium active site. The acquaintance of mechanism and behavior of vanadium active site in the aid of hydrogen peroxide, the reactivity of peroxovanadium(V) complexes is receiving renewed attention. Peroxovanadium complexes perform a variety of net two-electron oxidation reaction, which are presented in detail below (Figure 1). Alkenes and allylic alcohols can be epoxidized and hydroxylated. Sulfides can be oxidized to sulfoxides and sulfones. Benzene and other arenes and alkanes can be hydroxylated. Primary and secondary alcohols are oxidized to aldehydes and ketones.<sup>5,6</sup>

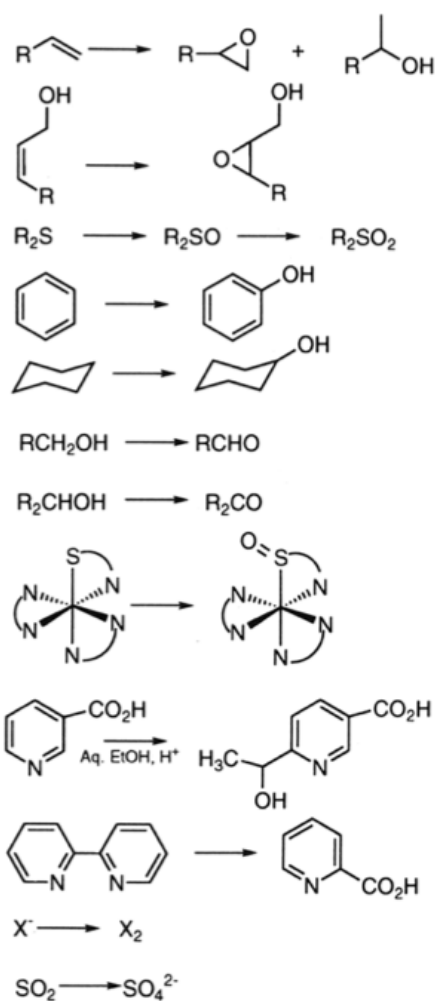


Figure 1. Examples of the reaction types mediated by peroxovanadium (V) complexes.

## 1.2 Heterogeneous catalysis

### 1.2.1 History of heterogeneous catalysis

In general, catalysis is divided to three categories: homogeneous catalysis, heterogeneous catalysis, and biocatalysis. In homogeneous catalysis, the catalyst is in the same phase as the reactants and products. As its name implied, heterogeneous catalysis is related to all the cases where the catalyst and the reactants are in the different phase. In most situations, heterogeneous catalysis was considered as a gas/solid or liquid/solid process. The gas/solid and the liquid/solid combination is so common that some books or journals refer to it as “classic” heterogeneous catalysis or even simply as “catalysis”.<sup>7</sup>

The “classic” saying of heterogeneous catalysis is originated from the widely application of heterogeneous catalysis in petrochemical and bulk-chemicals industry. In fact, heterogeneous catalysis not only impelled the development of chemistry, but also influenced the history of human beings because its potential power in energy and resource field. In 1908, the German chemist Fritz Haber synthesized successfully ammonia by nitrogen and hydrogen at high pressures over an osmium catalyst, which opened the door for gas/solid heterogeneous catalysis. As a coin has two sides, industrial nitrogen fixation provided mankind with much-needed fertilizer, brought the 1918 Nobel Prize to Haber, it also strengthened Germany’s position in World War I because of its supply for making explosives. It was believed that, in World War II, the Allied forces applied heterogeneous catalyst to develop new cracking and alkylation process so as to obtain higher-octane aviation fuel, which gave the Spitfires superior performance over the Messerschmitts in the famous Battle of Britain. Similarly, catalytic dehydrogenation of methylcyclohexane supplied both sides with the necessary toluene for making TNT. Today, heterogeneous catalysis dominates the petrochemicals and the bulk chemicals industry. Table 1 gives some examples of the key processes, catalysts, and products involved. Following the trend of chemistry development, heterogeneous catalysts move into the field of green chemistry, fine-chemicals industry and so on.<sup>8</sup>

Table 1. Examples of major industrial processes using heterogeneous catalysis.<sup>8</sup>

Process	Catalyst	Reactants	Products	End usage
Haber–Bosch NH <sub>3</sub> synthesis	magnetite (Fe)	H <sub>2</sub> , N <sub>2</sub>	NH <sub>3</sub>	fertilizer, gunpowder, explosives
Methanol synthesis	Cu/ZnO/Al <sub>2</sub> O <sub>3</sub>	CO, CO <sub>2</sub> , H <sub>2</sub>	CH <sub>3</sub> OH	bulk chemicals, fuel
Fischer–Tropsch	Co, Fe	coal, natural gas	C <sub>5</sub> –C <sub>11</sub> hydrocarbons	automotive fuel
Cracking	clays	long alkanes, C <sub>12</sub> +	C <sub>7</sub> –C <sub>9</sub> alkanes	fuel, detergents
Alkylation	zeolites, clays, silicates	C <sub>3</sub> –C <sub>5</sub> alkanes	C <sub>7</sub> –C <sub>9</sub> isoalkanes	high-octane fuel
Dehydrogenation/reforming	Pt/Al <sub>2</sub> O <sub>3</sub>	alkanes	alkenes	polymers, bulk chemicals
Hydrodesulfurization	Co/Mo sulfides	diesel fuel	sulfur-free diesel	automotive fuel
Hydrocracking	Pt on zeolites or aluminosilicates	aromatics mixture	saturated hydrocarbons	automotive/aviation fuel
Isomerization	H-ZSM-5 zeolites	xylenes, toluene	<i>p</i> -xylene	polymers, bulk chemicals
Polymerization	Ti, Ziegler–Natta	ethene	poly(ethylene)	polymers, bulk chemicals
Oxidation	vanadium oxide	xylenes	phthalic acids	polymers

### 1.2.2 Mesoporous silica: a way from homogeneous to heterogeneous

Silica is an excellent support in many cases of heterogeneous catalysts due to its high stability and ease of separation. According to IUPAC definition, the materials contain pores with pore diameters  $> 50$  nm are named as macroporous materials, the ones  $< 2$  nm are called as microporous materials, and the one between them ( $2$  nm  $<$  pore diameter  $< 50$  nm) are named as mesoporous materials. The invention of mesoporous silica, which started in 1990s although the first patent for producing mesoporous silica was released around 1970, provided attractive advantages such as high specific surface area and large opened pores. The most famous mesoporous silica series is M41S family, which was developed by Mobil Corporation laboratories and named as **Mobil Crystalline Materials**. The family was composed of three crystalline phase type:

- 1) MCM-41, which possesses hexagonal mesophase belonging to  $p6mm$  space group,
- 2) MCM-48, whose structure shows cubic mesophase, can be visualized as a two interlinked networks of spherical cages separated by continuous silicate frameworks.
- 3) MCM-50, in uncalcined form, shows lamellar structure, but after surfactant removal and post treatment, results into pillared layer material.<sup>9</sup>

In these three mesophase crystalline material, MCM-41 is widely used because its high stability and ease to be prepared. The specific surface area of MCM-41 can exceed  $1000$  m<sup>2</sup>/g. The open mesopores with long-range ordered channels provide the accessibility to reagents, which means that it would be easy not only to modify and functionalize the surface of silica, but also to allow the substrate reach active sites anchoring on the surface during the catalysis reaction. Considering that a lot of catalysis reactions proceed in the liquid phase, a catalyst based on silica takes obvious advantages during separation, recycling and reusing after reaction. In another word, these catalysts can transform homogeneous catalysis process to heterogeneous process, which is widely used in the industrial production due to its low-cost.

The heterogeneous reaction catalyzed by catalysts based on mesoporous silica included acid catalysis, redox catalysis and so on. Acid sites in the silica can be achieved by introduction of trivalent cations such as aluminum, boron atoms and also by incorporating of an acidic ingredient such as a heteropolyacid. The aluminum-containing mesoporous silica materials were tested in a number of petroleum refining processes such as cracking and hydrocracking applications. On the other hand, titanium, vanadium and other transition metal atoms were incorporated and considered as active sites in the oxidation reaction.<sup>10</sup> Inspired by the discovery of titanium-modified zeolites, which use H<sub>2</sub>O<sub>2</sub> as oxidant and were believed as a green and efficient process, titanium-containing mesoporous silica was synthesized to make up the shortage of zeolites in the application of bulky substrates. A large amount of oxidation reactions have been reported to be catalyzed by titanium-containing mesoporous silica such as epoxidation of cycloalkenes and hydroxylation of aromatic compounds. Vanadium-containing mesoporous silica is also useful catalyst in the oxidation reactions due to their different selectivity from titanium-containing silica. However, the efforts on the development of vanadium-containing materials are much less than those on the titanium ones maybe because of the leaching problem which exists widely in the vanadium-containing silica.

### **1.3 Conclusion**

As a conclusion, incorporation of vanadium into silica could solve separation and recycling problems in the multiphase catalysis reactions, and also a vanadium-containing mesoporous silica catalyst may own the same properties as the homogeneous vanadium catalysts. Although this sort of catalysts exists some shortcoming, it still shows potential in various catalysis processes.

In this thesis, we aimed at designing vanadium-containing mesoporous silica with better diffusion of vanadium active sites and solving the leaching problem. The physical and chemical properties of materials were characterized by different kinds of physical techniques such as X-ray diffraction, nitrogen sorption, thermo gravimetric analysis, diffused reflection UV-visible spectroscopy, Raman spectroscopy, infrared spectroscopy, nuclear magnetic resonance, and electron paramagnetic resonance. The reactivity of synthesized materials was tested by probe reaction to evaluate the catalytic performance.

## 1.4 Reference

- (1) Butler, A; Carter-Franklin. J. N. *Natural Product Reports* **2004**, 21, 180.
- (2) 老子 道德经; Vol. 第二十五章.
- (3) [http://en.wikipedia.org/wiki/Hideki\\_Yukawa#Awards\\_and\\_honours](http://en.wikipedia.org/wiki/Hideki_Yukawa#Awards_and_honours).
- (4) Butler, A.; Walker, J. V. *Chemical Reviews* **1993**, 93, 1937.
- (5) Butler, A.; Clague, M. J.; Meister, G. E. *Chemical Reviews* **1994**, 94, 625.
- (6) Ligtenbarg, A. *Coordination Chemistry Reviews* **2003**, 237, 89.
- (7) Rothenberg, G. In *Catalysis*; Wiley-VCH Verlag GmbH & Co. KGaA: 2008,  
p 1.
- (8) Rothenberg, G. In *Catalysis*; Wiley-VCH Verlag GmbH & Co. KGaA: 2008,  
p 127.
- (9) Naik, B.; Ghosh, N. N. *Recent Patents on Nanotechnology* **2009**, 3, 213.
- (10) Sayari, A. *Chemistry of Materials* **1996**, 8, 1840.

## Chapter 2. Literature Survey

### 2.1 Mesoporous silica and the modification of its surface

Mesoporous silica is a form of silica that contains pores in the range of meso-scale range (2-50nm). The most famous type of mesoporous silica are MCM-41 and SBA-15. They present a large specific surface area, a narrow pore size distribution, and the surface can be easily functionalized. A large diversity of functions can be incorporated opening potential applications in many fields such as catalysis, adsorption, sensing and biochemistry.

#### 2.1.1 Mesoporous silica

Zeolites are microporous solids that have been largely used in the field of catalysis.<sup>2,26</sup> However, due to the small pore size (usually smaller than 1 nm) they often present diffusion problems concerning applications with bulky compounds. The development of mesoporous materials was considered as a strategy to copy with this problem. Before the spring up of mesoporous materials, a lot of efforts was devoted to enlarge the pore size of molecular sieves: pore sizes can approach 0.8-1.3nm in the  $\text{AlPO}_4\text{-8}$ <sup>27</sup>, VIP-5<sup>28</sup> and cloverite.<sup>29</sup>

In 1992, Mobil Corporation reported a new family of mesoporous molecular sieves designated as M41S.<sup>13,30</sup> This discovery was considered as a milestone in the history of mesoporous materials. Furthermore, other types of mesoporous silicas were synthesized with different structure such as SBA series<sup>31,32</sup> (*Santa Barbara Amorphous*, invented by University of California, Santa Barbara), FSM-16 (*Folded Sheets Mesoporous materials*), HMS (*Hexagonal Mesoporous Silica*), MSU series (*Michigan State University Material*), KIT-1 (*Korea Advanced Institute of Science and Technology*).

### 2.1.1.1 The M41S family

M41S family is the earliest, most famous series family in the field of mesoporous silicas. There are three members in this family:

- 1) MCM-41 with hexagonal channels and belonging to  $p6mm$  space group.
- 2) MCM-48, which is also a hot research subject in the mesoporous materials field. It owns cubic meso-structure and belongs to  $Ia3d$  space group.
- 3) MCM-50 with lamellar structure and belonging to  $p2$  space group.<sup>13,30</sup>

Their structures and X-ray diffraction patterns were shown in Figure 1.

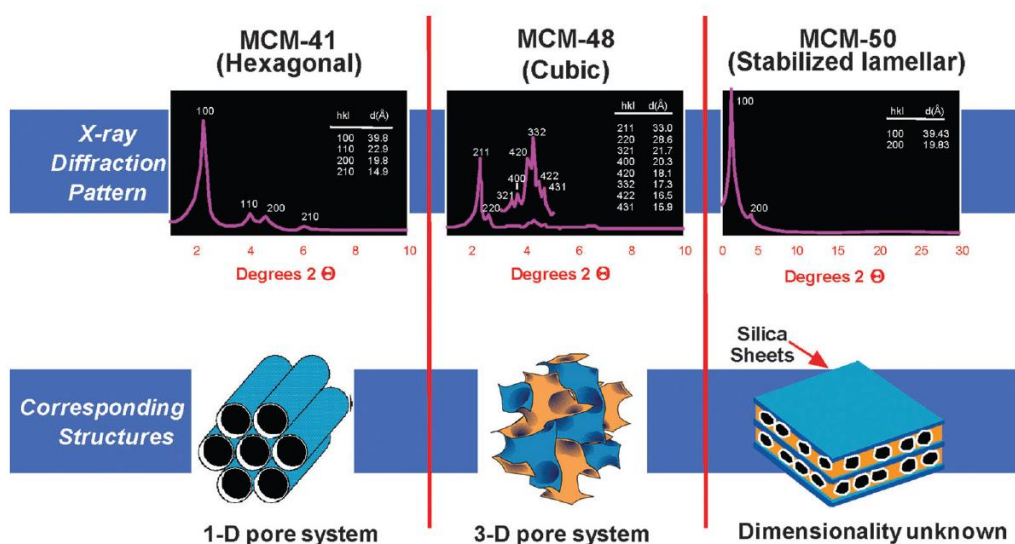


Figure 1. The M41S family of mesoporous molecular sieves including MCM-41, MCM-48, and MCM-50.<sup>5</sup>

In the classical synthesis of these three materials, the silicate source, which is generally tetraethyl orthosilicate (TEOS), is firstly hydrolyzed and condensed in the presence of cationic surfactants (cetyltrimethylammonium halides) as structure-directing agents (SDA) under basic conditions. During the synthesis, the surfactant/silicon (SUR/Si) ratio plays an important role to determine the structure of the final materials. When the ratio is less than 1, the predominant product appears to be the hexagonal phase, MCM-41. As the SUR/Si ratio increases, the mesophase turns

to a cubic one, which is named as MCM-48. MCM-50 with lamellar structure can be achieved upon further increasing of the SUR/Si ratio. MCM-41 and MCM-48 have been the two phases the most studied.

A lot of efforts has been dedicated to the study of MCM-41 type silica in all the aspects: synthesis method<sup>33-40</sup>, structural characterization<sup>41-46</sup> and applications<sup>47-55</sup>. The pore diameter can be varied from ~1.8 up to 10 nm either by changing surfactant chain length or by adding and auxiliary swelling organic agent into the starting gel. This was proved by X-ray diffraction and benzene sorption.<sup>13</sup> Besides X-ray diffraction, other techniques were utilized to characterize the MCM-41 type silica such as gas sorption (N<sub>2</sub>, Ar), microscopy (Scanning Electron Microscopy (SEM) and Transmission Electron Microscopy(TEM)). Due to the opened long-ranged channels and large specific surface area of this type of silica, it has been used as a support for introducing active sites to design heterogeneous catalysts.<sup>56-62</sup>

The second popular member in the M41S family, MCM-48, is another hotspot in the research of mesoporous silicas. MCM-48 contains two independent three-dimensional pore systems, which are interweaved and situated in a mirror-plane position one to each other.<sup>63</sup> This special pore system provides a more favorable mass transfer kinetics in catalysis and separation applications than MCM-41, which presents a one-dimensional hexagonal directional pore system.<sup>64</sup> However, the generation of the cubic phase during the synthesis is more critical. The ratio of cationic surfactant to silicon needs to be controlled and is reported to be between 0.55-0.15 in the initial recipe. A lot of research work has been devoted to the synthesis of this type silica with cubic mesophase and it is still a research topic now.<sup>64-67</sup>

### 2.1.1.2 Formation mechanism

The mechanism of formation and assembly of mesoporous silicas has been largely investigated. Understanding the details of the mechanism helps to control and even to predict the properties of mesoporous materials. Two mechanisms are now accepted as the main pathways of the formation of mesoporous materials. The first one, the liquid-crystal template (LCT) process, was first proposed by the Mobil's scientists who first published systematically the synthesis of M41S materials. This mechanism is essentially always "true", because the pathways proposed basically include almost all possibilities. The second formation mechanism widely accepted is the cooperative self-assembly processes.<sup>7</sup> Figure 2 shows these two main mechanisms.

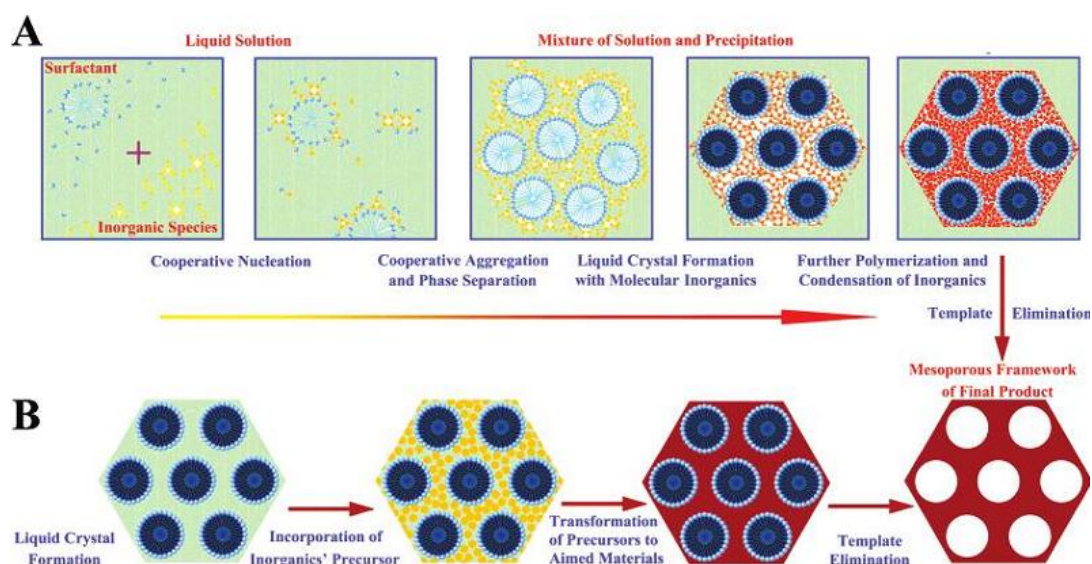


Figure 2. Two mechanisms proposed for the formation of mesoporous silica: A) cooperative self-assembly (CSA) mechanism, and B) liquid-crystal templating (LCT) mechanism.<sup>7</sup>

The liquid-crystal templating mechanism was suggested by the microscopy and diffraction results presented for MCM-41, which are similar to those obtained earlier for surfactant/water liquid crystal or micellar phases.<sup>13</sup> In this process, the surfactant molecules first formed micelles, which aggregated into rods upon increase of the

surfactant concentration. These micellar rods arranged into hexagonal array and become further organized into liquid crystals phases, which play the role as template for the formation of MCM-41 (Figure 3 lower part). The anionic inorganic species (silicate species under basic condition) balance the cationic hydrophilic surface of the micelles (Figure 2B). Inorganic silicate with hexagonal structure may be formed in this reaction mixture. In this mechanism, the silicate condensation is not considered as a dominant factor during the formation. The micellar liquid crystals are thought to play the most important role here. However, silicate species may affect the organization of the surfactant template, which generates the mesostructure of the final material. MCM-48 and MCM-50 phases are obtained by just tuning the surfactant concentration in the synthetic solution (Figure 3 upper part), which was believed as a proof of LCT mechanism.<sup>5</sup>

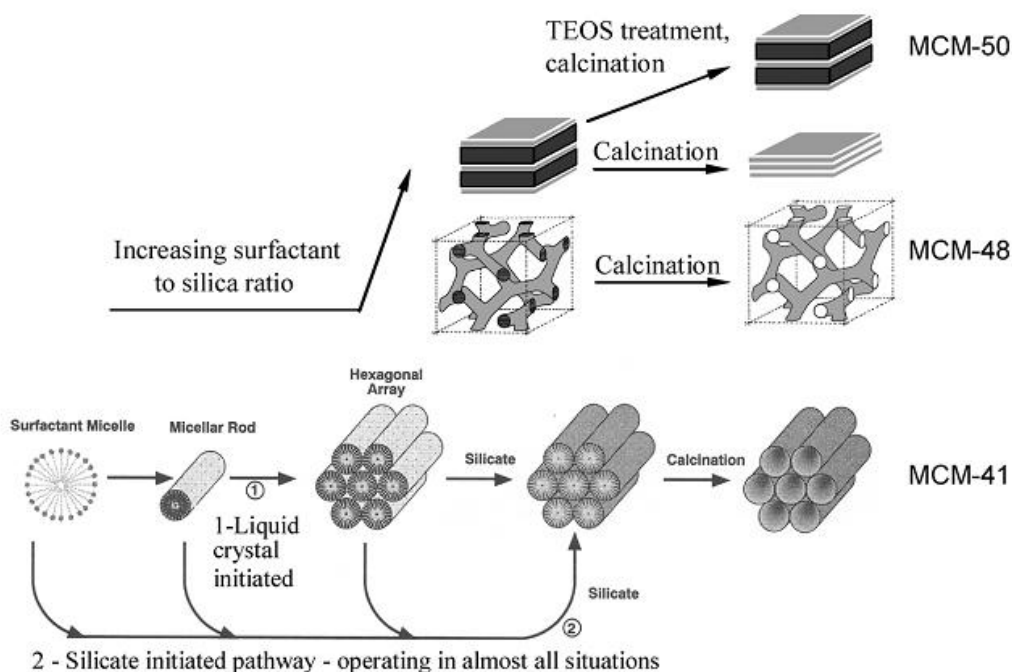


Figure 3. Liquid crystal templating mechanistic pathways for M41S.<sup>5</sup>

When the M41S family was discovered, the synthesis and the proposed LCT mechanism caught all the eyes of experts in the field of porous materials. Latter, the

LCT mechanism was a controversial topic to be investigated. There are some research results that support this mechanistic process.<sup>68,69</sup> Attard *et al.* succeeded in the synthesis of mesoporous silica by using nonionic surfactants and they proposed a LCT mechanism for the formation of such materials.<sup>70</sup> However, Zana *et al.* proposed that the LCT mechanism only fits to the systems containing high concentration of surfactant such as the case of Attard, in which the concentration of nonionic surfactants was up to 50% and the liquid crystal phase was therefore present.<sup>71</sup> They proved that the interaction between surfactants micelles and silicate species is very weak in the precursor solution. They proposed a new strategy of formation mechanism, where the key step is the formation of silica pro-polymers.<sup>72,73</sup>

Another popular mechanism of formation of mesoporous silica is the cooperative self-assembly (CSA) process. This process is based on the interactions between surfactants and silicates to form inorganic-organic materials.(Figure 2A) The organic-inorganic self-assembly is generally driven by weak noncovalent bonds such as hydrogen bonds, van der Waals forces.

There are several remarkable investigations about the formation mechanism of SBA-15 which is related to the cooperative self-assembly process. The group of Goldfarb investigated this process via in-situ EPR (electron paramagnetic resonance) spectroscopy, ESEEM (electron spin-echo envelope modulation) experiments<sup>74</sup> and direct imaging cryo-TEM (transmission electron microscopy)<sup>75</sup>. The micrographs showed directly the imaging of the formation of SBA-15. It was proved that it exists a continuous transformation from initial spheroidal micelles into threadlike micelles. The interesting point is that the size of these micelles is quite similar to those ones found in the final products while there did not exist any hexagonal arrangement.<sup>75</sup> This is a direct proof to show a totally different formation mechanism from the former

LCT mechanism. Flodstrom proposed four stages in the formation of SBA-15 by using time-resolved *in-situ*  $^1\text{H}$  NMR and TEM: 1) silicate adsorption on spheroidal micelles possibly with some aggregates growth, 2) the association of these spheroidal micelles into flocs, 3) precipitation of these flocs and 4) micelle-micelle coalescence to generate cylinders that form the final SBA-15.<sup>76</sup>

Both mechanisms are accepted by the researchers working in the area of mesoporous silica. The difference is focused on the formation of hexagonal structure.

### **2.1.1.3 Synthesis of MCM-41 type of silica and general physico-chemical properties**

MCM-41 type of mesoporous silica is generally synthesized by hydrothermal methods. CTABr (Cetyl Trimethyl Ammonium Bromide) is added into the reaction mixture as a surfactant that is considered as a template to form the hexagonal structure according to the LCT mechanism. In a typical synthesis of MCM-41 silica, the surfactant is dissolved in the water to prepare a homogeneous surfactant solution. And then a silicate solution (e.g. sodium silicate) is added into the former surfactant solution. The resulting gel is stirred for 0.5-2h at room temperature, then heated at a temperature around or higher than 100 °C for hours or days. The crystalline solid is separated by filtration after the hydrothermal process and dried at lower temperature (80 °C). The surfactant can be removed either by calcination or by extraction. L. Bonneviot *et al.*<sup>77</sup> synthesized MCM-41 type of silica named as LUS (Laval University Silica) with CTATos (Cetyl Trimethyl Ammonium Tosylate) as surfactant. This protocol uses a lower amount of surfactant than the classical ones and affords a well-structured silica.

Various general characterization methods are applied to obtain basic information of

the structure of the synthesized materials. XRD (X-ray diffraction) is used to determine the mesostructure, a hexagonal lattice in the case of MCM-41 (Figure 4). The pore size and specific surface area are measured by  $N_2$  sorption. The adsorption-desorption isotherm of MCM-41 type of silica shows a typical type (IV) isotherm according to IUPAC classification (Figure 5). At the beginning of the adsorption, the  $N_2$  adsorbed amount increases gradually with an increase in relative pressure by multilayer adsorption. A sudden uptake of the adsorbed amount is observed over a narrow range of relative pressure between 0.3 and 0.4 caused by capillary condensation of nitrogen in mesopores. The desorption branch coincides with the adsorption one<sup>33</sup>. The specific surface area is around  $1000 \text{ m}^2/\text{g}$  and the pore size is around 3-4 nm or even larger if a surfactant with a longer chain is used. TEM (transmission electron microscope) is utilized to show the hexagonal structure of the material. Figure 6 shows the hexagonal arrangement pores of MCM-41 silicas with different diameters, which were investigated by the Mobil's scientists in the original study.

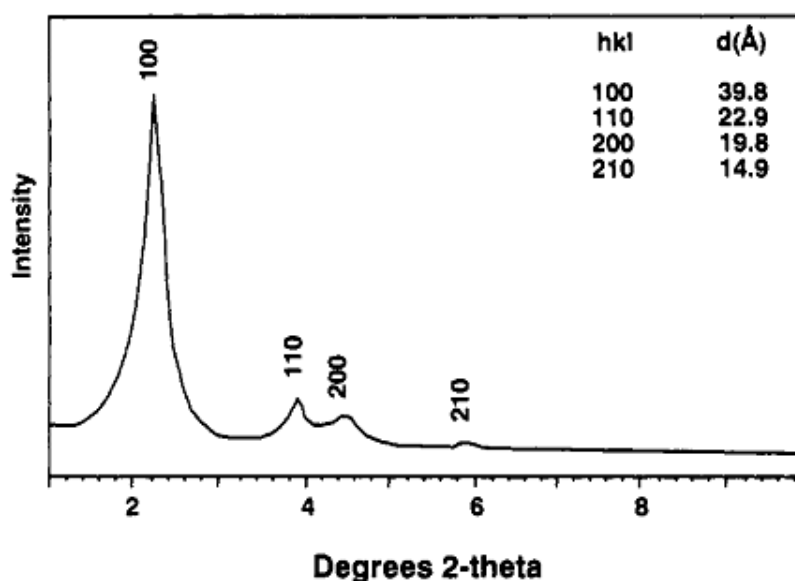


Figure 4. Powder X-ray diffraction pattern of calcined MCM-41 silica.<sup>13</sup>

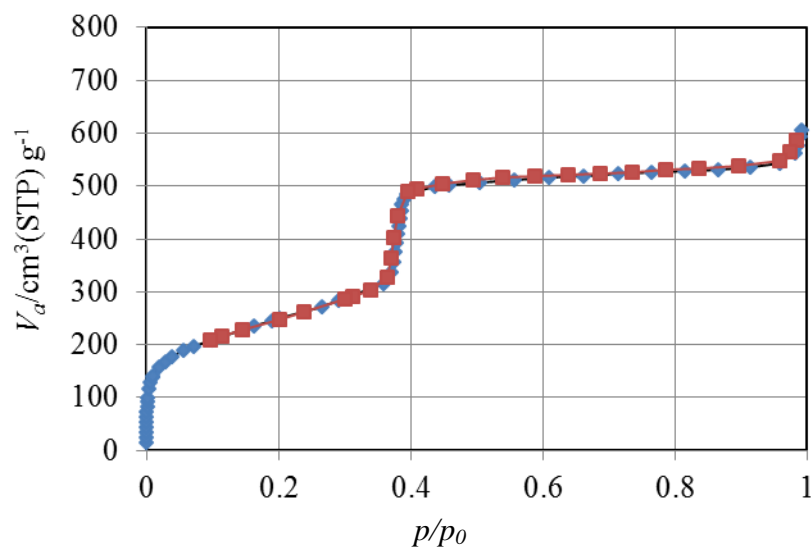


Figure 5.  $\text{N}_2$  adsorption-desorption isotherm of MCM-41 silica without surfactant.

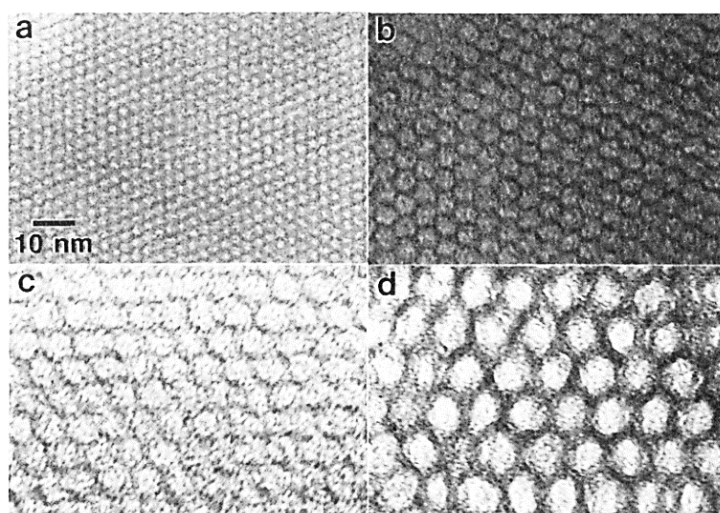


Figure 6. TEM images of MCM-41 silicas with pore sizes of (a) 2.0, (b) 4.0, (c) 6.5, and (d) 10.0 nm.<sup>13</sup>

Other characteristic methods such as TGA (Thermogravimetry analysis), FT-IR (Fourier transform infrared) spectroscopy, NMR (Nuclear Magnetic Resonance) spectroscopy are also used to study the properties of MCM-41 when necessary.

## 2.1.2 Modification of the surface of mesoporous silicas

### 2.1.2.1 The surface of mesoporous silicas

The walls of M41S mesoporous silicas are composed of amorphous silica. Numerous spectral and chemical data have proved the presence of various silanols species on the surface of amorphous silicas (Figure 7): 1) isolated silanols, which are linked to other silicon atoms by three Si-O-Si legs, 2) geminal silanols, also called silanediols, which possess two Si-OH bonds and one Si-O-Si, and 3) surface siloxanes Si-O-Si. Besides, the Si-OH from both isolated silanols and geminal silanols, vicinal silanols can also be formed by hydrogen bonding.<sup>18</sup>

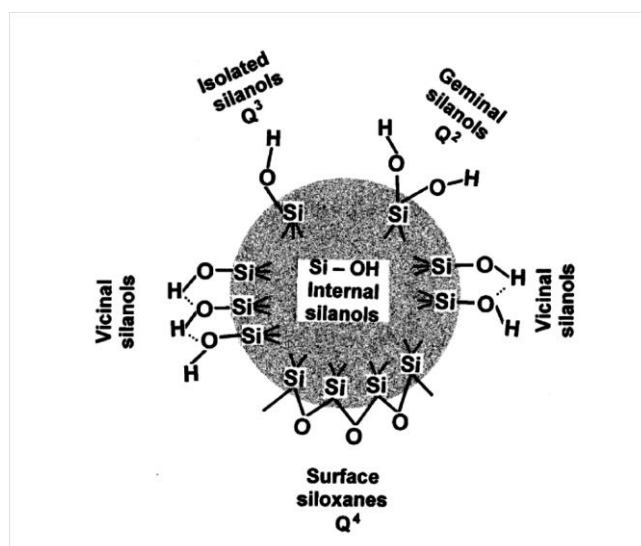


Figure 7. Types of silanol groups and siloxane bridges on the surface of amorphous silica.<sup>18</sup>

The abundance of Si-OH groups make the surface of amorphous silicas to highly hydrophilic. These silanol groups can easily adsorb molecules that can interact with Si-OH by covalent or non-covalent interactions. This provides the possibility to modify and functionalize the surface of amorphous silicas depending on the final use of the solid. It is also the reason why the amorphous silicas are potential supports in many fields of applications.

### 2.1.2.2 Modification of the surface of mesoporous silicas

The surface of mesoporous silicas can be modified through different interaction (covalent, electrostatic, hydrogen bonding, Van der Waals ...) between the functional groups and Solano groups on the surface of the solid. The functionalized mesoporous silicas are promising materials with potential applications in many fields such as drug delivery, catalysis, sensing and adsorption. In order to modify the hydrophilic nature of the surface, a hydrophobic organosilane can be grafted to the silica surface. In addition, functional groups with metallic sites can be introduced to generate heterogeneous catalysts widely used in chemical and biochemical fields. Other potential application are separation, ion-exchange, chromatography, removal of heavy metals, stabilization of some dyes and polymer composites, and so on.<sup>78</sup> Following the demands of applications, various new approaches have been reported, including direct silanation, surface rehydration and silanation, co-condensation, and molecular imprinting.<sup>19</sup>

Based on the results of the study of F. Goettmann and C. Sanchez about the confinement effects in mesoporous materials<sup>79</sup>, the mesoporous silica with amorphous wall can be compared to zeolites, that possess size and shape selectivity. In addition, the high surface area and large pore size of mesoporous silicas provides enough space to graft more than one species of functional groups to lead to more sophisticated materials.<sup>19,80-83</sup> J. Liu and his colleagues use a new approach of molecular imprinting technique, which was proposed by A. Katz and M. E. Davis in 2000<sup>84</sup>, to synthesize a hierarchical porous material with MCM-41 type channels and a soft, “microporous” molecular monolayer.<sup>19</sup> As shown in Figure 8 inorganic microporous materials (red triangular shape in Figure 8) are introduced as the microcavities with long-chain molecular monolayers around. The size and shape of the cavities can be systematically varied by properly choosing the long-chain template molecules.

Furthermore, changing the long-chain template molecules in the monolayer coating can also regulate the accessibility of the microcavities. This material shows preliminary results in the Knoevenagel condensation between malononitrile and benzaldehyde or 3-pentanone.<sup>19</sup>

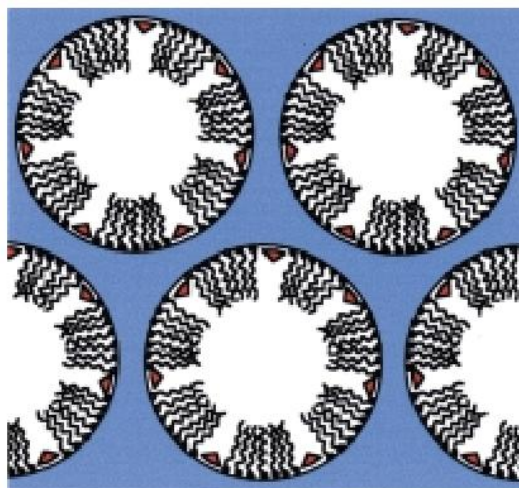


Figure 8. Schematic representation of the hierarchical porous materials with ordered nanoporosities and microcavities in the long-chain molecular monolayer coating.<sup>19</sup>

On the other hand, these functionalized materials can mimic living life such as enzymes.<sup>85</sup> In the biocatalysis of enzymes, the confinement effect is also an important parameter to afford selectivity in the catalytic reaction. G. Wulff and his group are considered as the first ones to attempt to use a molecular spacer to separate two vicinal amine sites on amorphous silica.<sup>86</sup> Later on, there were a lot of efforts devoted to this kind approach.<sup>81,82,87</sup> A new approach combining multi-functionalities, hydrophobicity and confinement necessitates specific techniques like the novel molecular stencil patterning (MSP) developed by our group.<sup>14,24,83,85,88,89</sup> In this technique, the vicinity between two different species is controlled in templated nanostructured mesoporous silica of MCM-41 type. In the sequence of this technique, the surfactant cations in the channels, considered as a molecular mask, are firstly partially removed to provide vacancy for the first functional groups. The

self-repulsion between the positively charged surfactants provides a regular pattern homogeneously distributed all through the channel. The first functional groups, generally an organosilane, are introduced to occupy the vacant Si-OH on the surface of silica. Then, the remaining surfactant is removed by using an ethanolic solution of HCl. Finally, the second functional group is introduced. In the final material, the

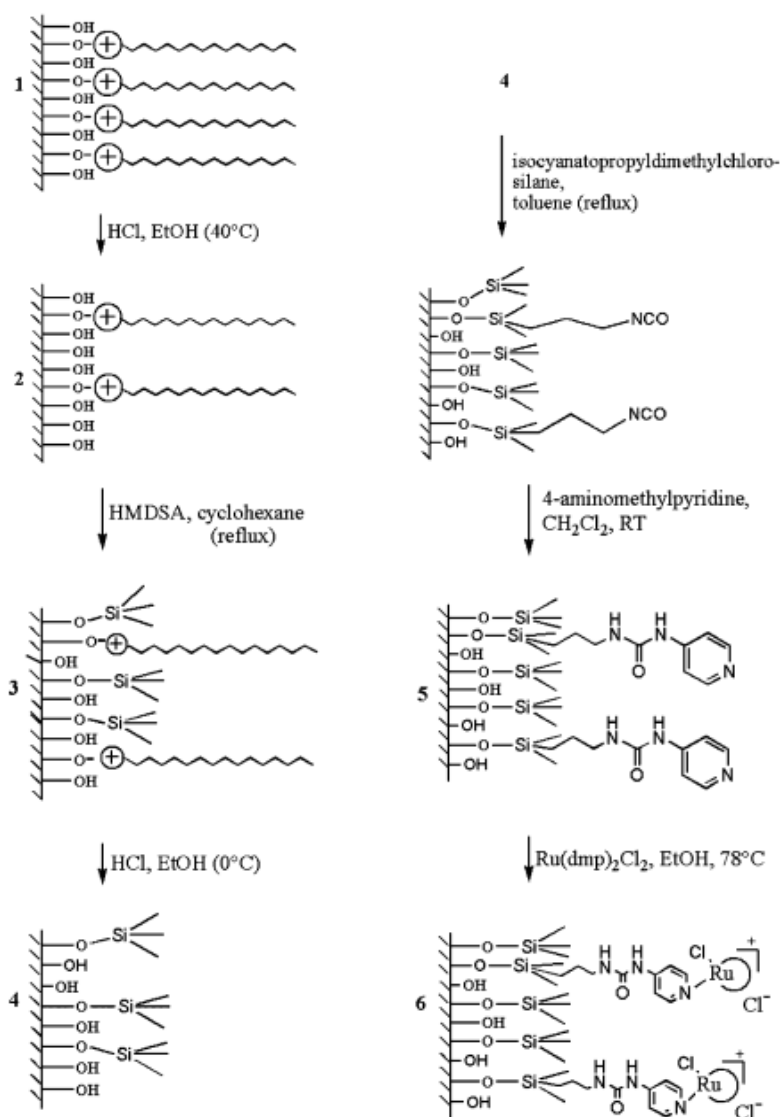


Figure 9. Synthetic routine from as-made silica LUS **1** to ruthenium supported complex **6** via Molecular Stencil Patterning (MSP) technique.<sup>14</sup>

second functional group grafted on the surface is diluted by the first one. For example, S. Abry *et al.* incorporated an aminoligand using MSP technique, which is isolated by

trimethylsilyl functions, and which can be further complexed to Cu(II) ions.<sup>85</sup> Figure 9 shows the step-by-step synthesis of ruthenium supported catalyst for sulfide oxidation. In this study, the ruthenium-containing silica with isolated active sites in the confined space of the mesopores of the silica matrix was achieved. The probe reaction, oxidation reaction of methylphenylsulfide into sulfoxide, proved that the materials owned special selective activity.<sup>14</sup> A series of metallic active sites such as copper<sup>24,85,90</sup>, nickel<sup>88</sup>, iron<sup>89</sup> were incorporated into the hexagonal channels of MCM-41 type silica based on the MSP technique. This technique was improved by K. Zhang during his research of copper supported silica catalysts.<sup>24</sup> In this improvement,

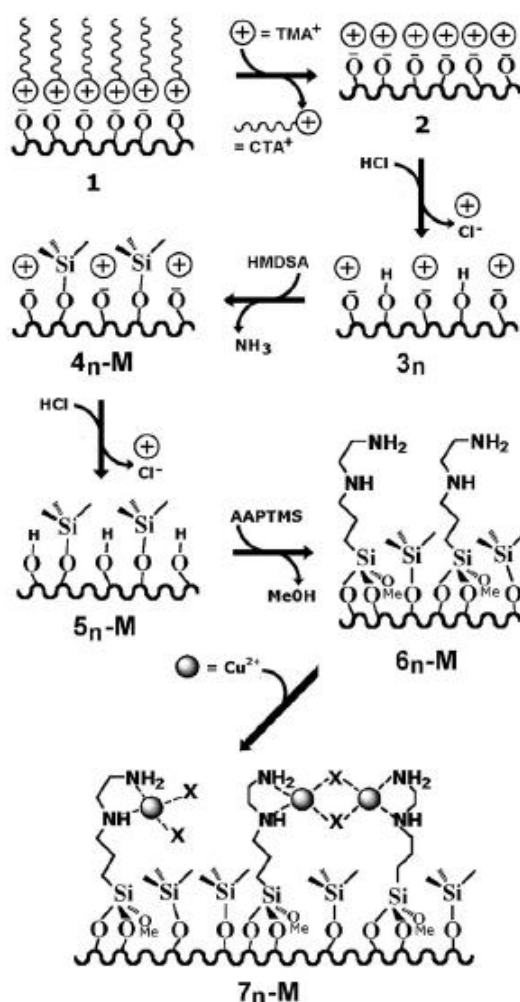


Figure 10. Synthetic routine from the as-made silica **1** to the multifunctional metallated material **7** via MSP technique.<sup>24</sup>

the long-chain surfactant CTA<sup>+</sup> cations were replaced by a smaller cations, tetramethylammonium ions (TMA<sup>+</sup>) as a masking agent (shown in Figure 10). This technique was widely used in later researches in our group.

As a conclusion, the researches about mesoporous silica and its modification are hot topics in the materials chemistry in recent years. It deserved more efforts not only to improve the synthesis but also to enlarge the applications.

## **2.2 Vanadium-containing heterogeneous catalysts**

One of the most widely developed applications of mesoporous silicas is the design of a catalyst with metal atoms loaded. The transition metal supported material always plays an important role in catalytic oxidation such as Ti-containing silicate, which shows remarkable performance in the selective oxidation with H<sub>2</sub>O<sub>2</sub> as a green oxidant.<sup>26,91</sup> On the other hand, vanadium chemistry also attracts lots of attention since the discovery of bromo peroxidase vanadium(V) in marine algae.<sup>3</sup> Vanadium(V) peroxy complexes are known as catalysts for various oxidation reaction such as epoxidation and hydroxylation of alkenes<sup>92</sup>, and oxidation of aromatics<sup>6,9</sup>, alkanes<sup>93,94</sup> and alcohols<sup>95</sup>. Titanium based porous materials such as TS-1<sup>96</sup> are known to be efficient heterogeneous catalysts for oxidation reactions while vanadium equivalent systems are still under development and more effort needs to be done to develop efficient catalysts.

### **2.2.1 Vanadium species in the heterogeneous catalysts**

One of the most interesting subjects in the research of vanadium-containing materials is to understand which vanadium species are involved in the catalytic cycle. There is a lot of contributions in the literature to understand the nature of the vanadium species present in vanadium-containing materials. Herein, we will only discuss about the

surface  $\text{VO}_4$  species deposited on the oxides such as  $\text{SiO}_2$ ,  $\text{Al}_2\text{O}_3$  and  $\text{TiO}_2$  since the situation in zeolites or in other molecular sieves is more complicated and will be described later on.

### 2.2.1.1 Molecular structure of surface $\text{VO}_4$ species

There were three different forms of vanadium species as a function of the degree of isolation on the surface. The first one was isolated monomeric  $\text{VO}_4$  species with a terminal  $\text{V}=\text{O}$  and three legs  $\text{V}-\text{O}$ -support connecting it with the support (Figure 11A). With increasing aggregation degree of vanadium species, one or two dimensional oligomeric species connected by  $\text{V}-\text{O}-\text{V}$  bridges (Figure 11B) are generated, as well as three dimensional bulky vanadium oxide clusters (Figure 11C).

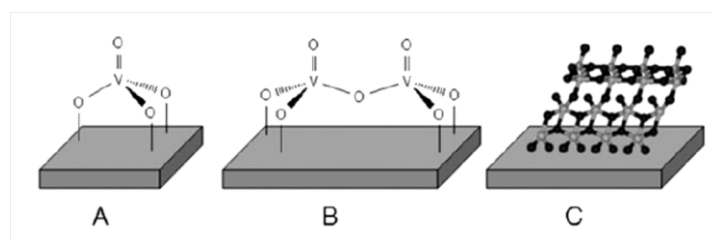


Figure 11. Three different forms of  $\text{VO}_x$  species on the surface of inorganic supports.<sup>22</sup>

In vanadium supported silica, the vanadium species aggregate upon increase of the vanadium loading. The best-dispersed vanadium materials can be obtained at low vanadium loading, considering in that case that mainly isolated monomeric species are present in the solid. The isolated monomeric species are believed to be the most active species during the catalytic process due to the higher accessibility of the vanadium site compared to other polymeric species.<sup>22</sup>

The structure of monomeric vanadium species is unanimous accepted to be a distorted tetrahedron with a mono-oxo  $\text{V}=\text{O}$  bond on top. However, there is no consensus on

the precise structure. Four different structures were suggested for the way how the monomeric vanadium species are anchored on the support.<sup>97</sup> These four structures are shown in Figure 12: 1). A pyramidal structure with V=O bond on top and three legs of V-O-support with  $C_{3v}$  symmetry (Figure 12A). This model is considered as the most popular one and it has been proved by several spectroscopic measurements.<sup>98-101</sup> 2). A hydrogenated variant structure in which one of V-O-support bond is replaced by V-OH (Figure 12B). 3). An umbrella model consisting of a V=O bond, a V-O-support bond and a peroxide O-O moiety linked to the central vanadium atom (Figure 12C). 4). A variation on the umbrella model with the peroxide replaced by two OH groups (Figure 12D). The B, C, D structures were also proposed and studied on the basis of various characteristic measurements<sup>102,103</sup> and even theoretical calculations<sup>104,105</sup>.

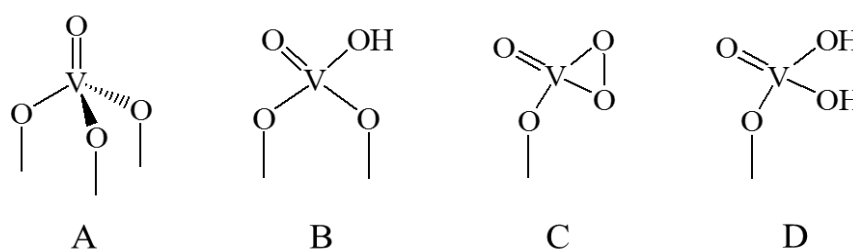


Figure 12. Possible molecular structures of monomeric  $VO_4$  species on silica support.<sup>22</sup>

### 2.2.1.2 Active species of vanadium supported materials

The next question is to identify the bonds that offer a real catalytic contribution for oxidation reactions. Three different bonds exist in the  $VO_4$  active sites: terminal V=O bonds, bridging V-O-V bonds and bridging V-O-support bonds.

#### V=O bond

The terminal V=O bonds were proposed as the catalytic active site in oxidation reaction in 1954.<sup>106</sup> However, further catalysis studies with vanadium containing materials demonstrated that the V=O bonds do not contain the catalytically active

oxygen which affected the reactivity during hydrocarbon oxidation reactions. The possible reason is that the M=O bonds are more stable than other single bonds to be broken during the reaction.<sup>22,107</sup> On the other hand, the catalytic role of terminal V=O cannot be completely neglected. As a result, the role of V=O in the catalytic process is still not totally clear.

### **V-O-V bonds**

The bridging V-O-V bonds are widely present in oligomeric and polymeric vanadium species. In the gas phase oxidation reaction of methanol catalyzed by V<sub>2</sub>O<sub>5</sub> supported materials, several research groups found that the TOF (turnover frequency) decreased with increasing of the amount of V-O-V bonds resulting from increasing of surface vanadium coverage. This indicates that the oxygen in the V-O-V bonds did not participate in the catalytic reaction. As a result, the V-O-V are generally considered not to be involved in the catalytic process.<sup>22,108</sup>

### **V-O-support bonds**

The role of the V-O-support bonds in the process of catalysis comes from some indirect evidences. In the selective oxidation of methanol to formaldehyde catalyzed by supported vanadium oxide, it was found that changing the specific support oxide composition influenced the TOF. Therefore, it was proved that the oxygen in the V-O-support bonds played an important role in the catalytic oxidation reaction. As a consequence, the careful choice of the support to load vanadium species turned to be very important in the preparation of vanadium-containing heterogeneous materials. In the review of I. Muylaert and P. Van Der Voort about vanadium species in heterogeneous catalysis, they concluded that the catalytic TOF values increased as the support is varied: SiO<sub>2</sub> < Al<sub>2</sub>O<sub>3</sub> < Nb<sub>2</sub>O<sub>3</sub> < Ta<sub>2</sub>O<sub>5</sub> < TiO<sub>2</sub> < ZrO<sub>2</sub> < CeO<sub>2</sub>. This order is the opposity to the electronegativity of the support cations, which indicates that higher

TOF values correspond to lower electronegativity of the support cations. This correlation can be explained as follows: a lower electronegativity of the support cations results in a higher electron density on the V-O bond in the bridging V-O-Support bonds, which enhances the specific rate of the redox cycle of the catalytic active site.<sup>22</sup> These results may be helpful to the design of vanadium containing materials.

### **2.2.2 Spectroscopic characterization of vanadium species in heterogeneous catalysts**

There are numerous reports describing the vanadium species in various heterogeneous catalysts. The spectroscopic characterization is the main tool to understand the state of vanadium in the solid. The basic measurement techniques include diffuse reflectance UV-visible spectroscopy, electron paramagnetic resonance (also called electron spin resonance) spectroscopy, nuclear magnetic resonance spectroscopy and Raman spectroscopy. Each characteristic method is described as following.

#### **2.2.2.1 Diffuse reflectance UV-visible spectroscopy (DR UV-vis)**

DR UV-visible spectroscopy is an absorption electronic spectroscopy widely used in solution to characterize transition metal ions because it is a relatively cheap and simple technique. In solid state, diffuse reflectance is used. Two kinds of transitions can be measured in the UV-visible spectrum of vanadium species: d-d transitions and charge transfer transitions. The energy of d-d transitions depends on vanadium oxidation state, and the one of charge transfer transitions is influenced by the local coordination environment and the polymerization. Thus, DR UV-visible technique can provide the information about different oxidation states and local coordination state of vanadium species in the solid materials.

In general,  $V^{4+}$  and  $V^{5+}$  are the two possible ions present in the final solids based on the vanadium sources used during the synthesis of the materials. There are no free electrons in the  $d$  orbit in  $V^{5+}$  species ( $d^0$ ). Therefore,  $V^{4+}$  shows weak d-d absorption

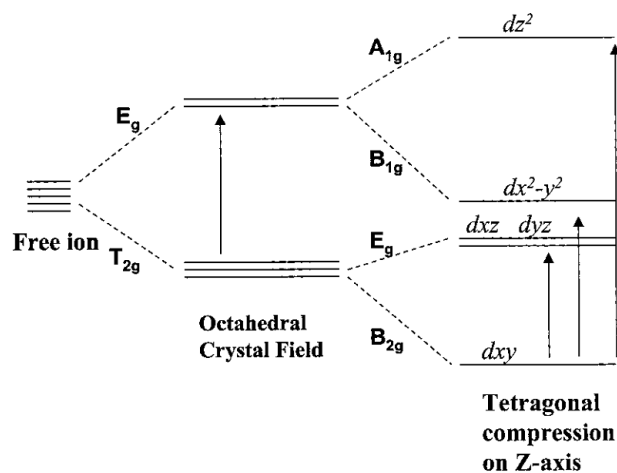


Figure 13.  $VO^{2+}$  Crystal Field Splitting Diagram.<sup>15</sup>

bands in the region of low energy around 1.55-2.07 eV (corresponding to 600-800 nm).<sup>22</sup> For example, in the spectroscopic study of a zeolite containing vanadium (V/USY), two weak absorption bands of  $VO^{2+}$  are observed at 770nm and 625 nm, respectively. Combining these results with EPR studies and crystal field theory, these two bands can be attributed to  $B_{2g} \rightarrow E_g$  and  $B_{2g} \rightarrow B_{1g}$ , respectively. (Figure 13) The  $B_{2g} \rightarrow A_{1g}$  transition located at around 330-250 nm is overlapped by the background signal of the zeolite support.<sup>15</sup>

The UV-vis spectrum of  $V^{5+}$  is often more complicated compared to  $V^{4+}$  species. Indeed, adsorption bands corresponding to charge transfer (CT) transitions involving  $V^{5+}$  species appear at the higher energy region of 3-6 eV (412-206 nm) and the intensity of these bands are 30 times stronger than d-d transitions.<sup>109</sup> However, the peak shown in the spectrum is always broad and the individual absorption bands are overlapped one with each other because of the different coordination environment of vanadium (V) species. A Czech group has developed a new methodology to measure and evaluate the DR UV-vis spectra of vanadium oxide species supported on the

mesoporous silica.<sup>10</sup> The details of the broad peak containing the information of different vanadium (V) species was interpreted by deconvoluting the spectrum by a set of several Gaussian or Lorentzian shaped absorption bands (Figure 14 left). The bands located at around 2.5 eV (~500 nm) and 3 eV (~413 nm) are ascribed to the octahedrally ( $O_h$ ) coordinated species that form vanadium oligomers. These species have significant intensity in those samples with a higher concentration of vanadium (Figure 14 right). The band located at 4.1-3.75 eV (~300 nm-330 nm) is attributed to the tetrahedral ( $T_d$ ) oligomers. The 5.1-4.6 eV (~243-270 nm) band is attributed to both  $T_d$  oligomers and monomers. The intensity of these two bands increases as the concentration of the vanadium increases while their positions changes from higher to

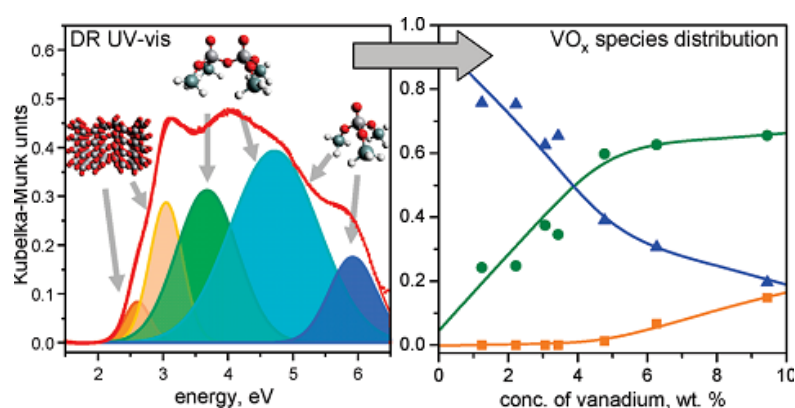


Figure 14. Attribution of vanadium oxide species based on results of the deconvolution of experimental spectra (left), and relative abundance of various vanadium oxide species in the dependence of vanadium concentration (right).

$O_h$ -coordinated species, orange square;  $T_d$ -coordinated oligomeric units, green circle;

$T_d$ -coordinated isolated monomeric units, blue triangle.<sup>10</sup>

lower energy. The last band at 6 eV (~207 nm) was ascribed to the isolated  $T_d$  monomeric vanadium species which did not change its position significantly.<sup>10</sup> In addition, a new methodology is developed to improve the utilization of DR UV-vis spectra in this work. The authors indicates that the previous studies using DR UV-vis spectroscopy often neglected that the intensity of measured spectra was frequently not

proportional to the concentration of samples which is the limitation of Kubelka-Munk (KM) function. The author demonstrated that a linear relation between the intensity of UV-vis bands and the concentration of vanadium only existed for KM values lower than approximately 0.5. As a result, the measured sample should be diluted by pure silica or with a nonabsorbent solid such as MgO to avoid the intensity of the bands turning to too high.<sup>10</sup>

### 2.2.2.2 Electron paramagnetic/spin resonance spectroscopy (EPR/ESR)

Electron paramagnetic resonance (electron spin resonance) spectroscopy is a technique to study materials with unpaired electrons. Therefore, only vanadium (IV) species, which are  $d^1$ , will give a signal in EPR. Indeed, the  $\text{VO}^{2+}$  moiety presents a characteristic eight-line hyperfine patterns due to the interaction between the unpaired electron and nuclear spin  $I = 7/2$  of  $^{51}\text{V}$  (natural abundance 99.8%).<sup>59</sup>

In the study of Z. Luan and L. Kevan<sup>12</sup>, vanadium species were loaded onto pure silica MCM-41 support and MCM-41 containing different heteroatoms (Al, Ti or Zr). The EPR spectra of V/MCM-41 and V/Al/MCM-41 show eight hyperfine lines centered at  $g=1.981$  with a hyperfine coupling constant  $A=114$  G (Figure 15). This isotropic signal corresponds to free vanadyl ions, indicating that there was no interaction of between the siliceous surface of the support and the vanadium species. However, the spectrum of V/Ti-MCM-41 shows a strong anisotropy characterized by  $g_{//} = 1.937$ ,  $A_{//} = 192$  G and  $g_{\perp} = 1.984$ ,  $A_{\perp} = 69$  G. The same signal is observed in the V/Zr-MCM-41. These results suggest that the vanadium species are immobilized on the surface of Ti-MCM-41 and Zr-MCM-41. Nevertheless, some mobile isotropic  $\text{VO}^{2+}$  ions were also observed in the spectrum of V/Zr-MCM-41. This means that the interaction between vanadium and Zr-MCM-41 is weaker than that in Ti-MCM-41. The detailed analysis of EPR spectra can also afford a lot of information

about the vanadium species in the material such as dispersion and coordination environment.<sup>12,59,110</sup>

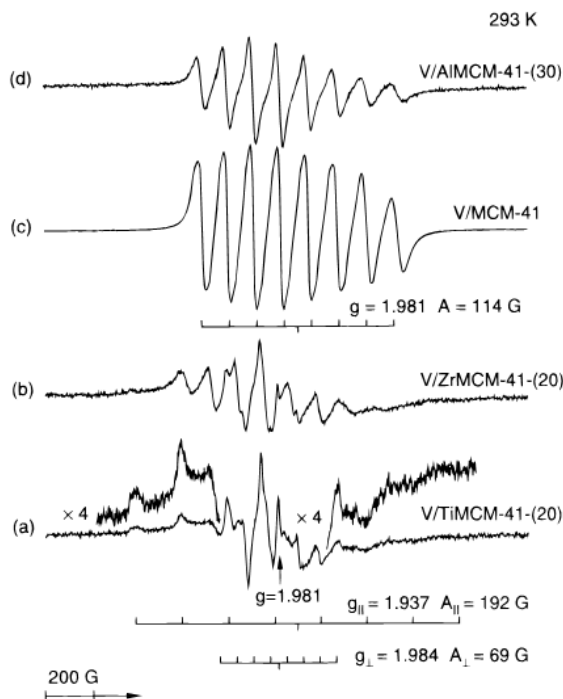


Figure 15. EPR spectra at 293 K of (a) V/Ti-MCM-41, (b) V/Zr-MCM-41, (c) V/MCM-41 and (d) V/Al-MCM-41.<sup>12</sup>

### 2.2.2.3 Raman spectroscopy

Raman spectroscopy is a spectroscopic technique widely used to investigate vibrational, rotational, and other low-frequency modes in various materials. In the study of vanadium-containing materials, Raman spectroscopy can complete the information about different state of vanadium species from the UV-visible spectroscopy.

I. E. Wachs has largely studied the Raman spectra of vanadium supported oxides materials, and he describes the attribution of the different signals in several works. The Raman spectra of dehydrated  $V_2O_5/SiO_2$  materials with different vanadia contents

were studied and compared with pure  $\text{SiO}_2$  (Figure 16).<sup>11</sup> In the spectrum of pure  $\text{SiO}_2$ , the Raman band at  $976\text{ cm}^{-1}$  is ascribed to the Si-OH vibration, and the bands at 802, 607, and  $487\text{ cm}^{-1}$  to three to five Si-containing siloxane rings, respectively. The band at  $976\text{ cm}^{-1}$  decreases upon addition of vanadium to  $\text{SiO}_2$ , due to the consumption of surface silanol groups. Meanwhile, some new bands appear. The new bands at  $\sim 1070\text{ cm}^{-1}$  and  $\sim 920\text{ cm}^{-1}$  originate from the Si-O bonds from the breaking of Si-O-Si bonds during the introduction of vanadium. The band at  $\sim 920\text{ cm}^{-1}$  is also believed to come from the vibration of V-O-Si vibration. The sharp peak at  $\sim 1035\text{ cm}^{-1}$  is assigned to the V=O bond of surface  $\text{VO}_4$  species linked with  $\text{SiO}_2$  surface. Otherwise, the bands at 337 and  $465\text{ cm}^{-1}$  are attributed to symmetric and asymmetric bending modes of the

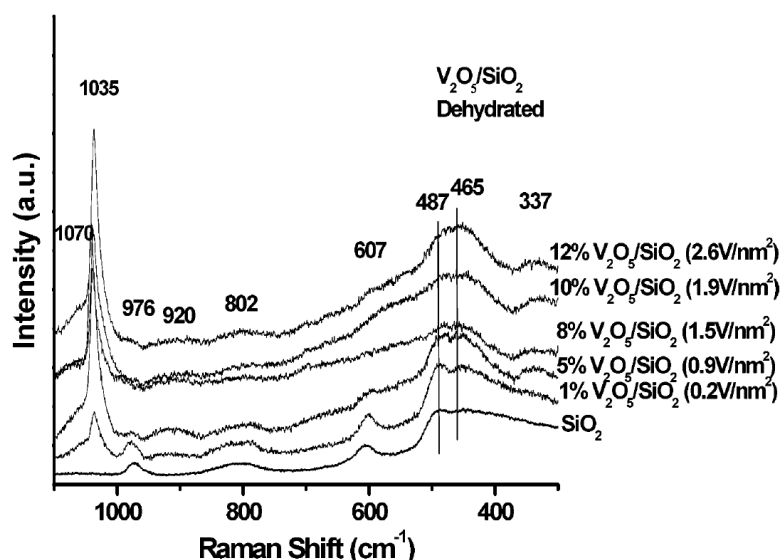


Figure 16. Raman spectra of dehydrated  $\text{V}_2\text{O}_5/\text{SiO}_2$  catalyst as a function of vanadia loading (exciting wavelength: 532nm).<sup>11</sup>

surface  $\text{VO}_4$  moieties. Increasing the vanadium content results in the appearance of a  $994\text{ cm}^{-1}$  band, which is attributed to crystalline  $\text{V}_2\text{O}_5$  nanoparticles. This discrimination in the Raman spectra is clearer than that in the UV-visible spectra in which there are broad bands resulting from the five different bridging V-O-V bonds.

The group of Israel E. Wachs also revealed the characteristic Raman bands of

vanadium species on the other oxide supports such as  $\text{Al}_2\text{O}_3$ <sup>11,111,112</sup>,  $\text{ZrO}_2$ <sup>11</sup>,  $\text{Nb}_2\text{O}_5$ <sup>113</sup> and mixed oxide supports<sup>114,115</sup> or catalysts<sup>116</sup>. Most supports showed Raman activity in the spectra while some like  $\text{Al}_2\text{O}_3$  did not. Nevertheless, there is no doubt that the choice of the support may affect the state of vanadium species on the surface and the influence can be proved by Raman spectroscopy.

#### 2.2.2.4 Nuclear magnetic resonance spectroscopy (NMR)

Besides these three spectroscopic techniques mentioned above, NMR spectroscopy also provide interesting and useful information about the state of vanadium species in the research of vanadium-containing materials despite that the spectra are complicated and the signal is not sensitive enough.<sup>16,57,110,117,118</sup>

In the study of alumina-supported vanadium materials, NMR spectroscopy was used to characterize the vanadium species in different samples obtained from various vanadium precursors such as vanadyl sulfate, ammonium metavanadate and vanadyl acetylacetonate (Figure 17). The signals at -420 and -500 ppm were attributed to the decavanadate polyanions ( $\text{V}_{10}\text{O}_{28}^{6-}$ ). Both signals at -570 and -620 ppm were assigned to the  $\text{VO}_4$  species. The chemical shift at -570 ppm comes from the V-O-Al weak bonds to the surface via either one or two bonds, while the peak at -620 ppm corresponds to the strong V-O-Al bonds belonging to  $\text{VO}_4$  tetrahedral species linking the surface with either two or three bonds. The appearance of a chemical shift at -610 ppm indicates the presence of the crystalline  $\text{V}_2\text{O}_5$  phase. In this case, the results of NMR spectroscopy suggest that the choice of vanadium precursors may affect the dispersion of vanadium species in the final materials. And the quantitative results provide information to compare the distribution of various vanadium species in the prepared materials.<sup>16</sup>

Other techniques such as Fourier Transform infrared spectroscopy (FT-IR)<sup>109,112,119,120</sup>, X-ray absorption spectroscopy (XAFS)<sup>1,115</sup> are also applied to investigate the states of vanadium species on the surface and the relation between vanadium species and the support. Combining all these different spectroscopic techniques, the information of vanadium species in the obtained material can be easily characterized.

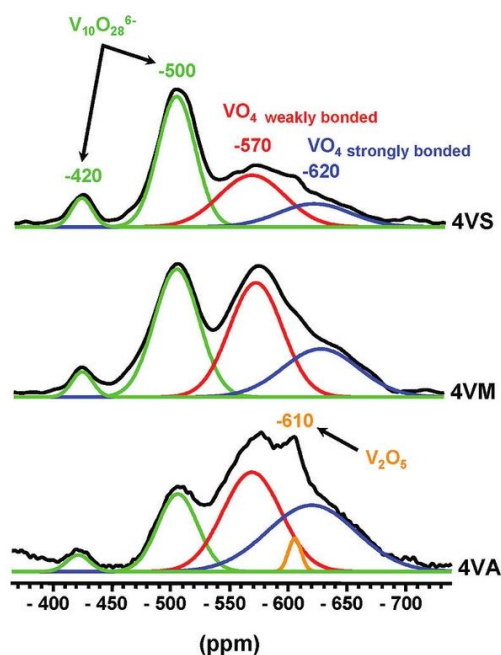


Figure 17.  $^{51}\text{V}$  MAS NMR spectra of  $\text{VO}_x/\text{Al}_2\text{O}_3$  samples prepared from: vanadyl sulfate (4VS), ammonium metavanadate (4VM) and vanadyl acetylacetonate (4VA).<sup>16</sup>

## 2.2.3 Vanadium-containing heterogeneous catalysts

### 2.2.3.1 Oxides supported vanadium catalysts

There are numerous studies about vanadium supported materials, in which vanadium species are generally loaded on different metal oxides. In most cases, vanadium species are introduced in the solid by wetness impregnation method during the preparation of the materials. The final products are characterized by UV-visible, Raman, FT-IR, EPR, NMR, TPR (temperature programmed reduction) and other techniques in order to reveal the nature and properties of vanadium species on the surface.

A lot of effort has been devoted to the investigation of alumina-supported vanadium both in the experimental and theoretical aspects. Furthermore,  $V_2O_5/Al_2O_3$  is a preferred models to understand the structure and catalytic properties of vanadium species on the surface.<sup>1,105,107</sup> In the work of J. N. J. van Lingen, the umbrella structural model of monomeric  $VO_4$  is proposed as a viable and internally consistent model at low metal loading. The experimental results combined with DFT calculation results confirms the umbrella model which can be described as a chemisorbed  $V=O(O_2)$  species. It is proposed that the umbrella model takes less energy to form than the pyramid model. This model gives more possibilities for the catalytic reaction routes and makes the reaction mechanism scheme simpler.<sup>105</sup>

M. Ruitenbeek found that the structure of a well-dispersed vanadium oxide phase is sensitive to parameters such as the reaction temperature and the reactants via X-ray absorption spectroscopy. Another interesting discovery was the migration of vanadium during the reduction process, which was detected by *in-situ* XANES (X-ray absorption near-edge structure). As shown in Figure 18, the fresh vanadium species on the surface turned to tetrahedral species during the dehydration process. The EXAFS data analysis revealed that the reduced vanadium (III) ions migrated into the surface layers of  $Al_2O_3$ . This process is considered reversible and the  $(Al-O)_3-V=O$  species can be restored after re-oxidation.<sup>1</sup>

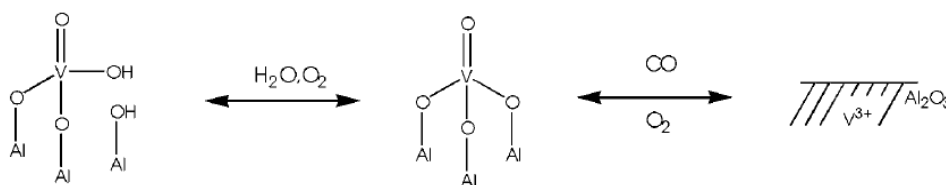


Figure 18. Model for the structure of the supported hydrated, dehydrated and reduced vanadium species on the surface.<sup>1,2</sup>

A new method was developed to introduce vanadium to USY zeolite system via coating a thin film of  $\text{Al}_2\text{O}_3$  on the external surface of zeolite because the preferential adsorption of  $\text{V}^{4+}$  onto the  $\text{Al}_2\text{O}_3$ . This material was believed to possess a potential application for vanadium passivation of fluid catalytic cracking (FCC) catalyst for petroleum refining.<sup>15</sup>

The choice of the support is very important for the catalytic properties of the final material. Back in the 1980s, F. Roozeboom *et al.* studied the incorporation of vanadium on several oxides supports:  $\gamma\text{-Al}_2\text{O}_3$ ,  $\text{CeO}_2$ ,  $\text{Cr}_2\text{O}_3$ ,  $\text{SiO}_2$ ,  $\text{TiO}_2$  and  $\text{ZrO}_2$ .<sup>121</sup> The vanadium species were introduced by ion-exchange and wet-impregnation methods, and the solids were characterized by X-ray fluorescence, Raman spectroscopy and temperature-programmed reduction for both qualitative and quantitative structural analysis. It was found that the crystalline  $\text{V}_2\text{O}_5$  was formed easily on the  $\text{SiO}_2$  by both preparation techniques while others solids contained no crystalline  $\text{V}_2\text{O}_5$ .

In the study of the oxidation reaction of ethanol to acetaldehyde by supported vanadium catalysts, the reactivity ranking of supports was  $\text{TiO}_2 > \text{ZrO}_2 > \text{CeO}_2 > \text{Al}_2\text{O}_3 > \text{SiO}_2$ .<sup>122</sup> In fact, this ranking can be generalized to other reactions such as propane oxidation even in different reaction condition. An exception is the oxidation of methanol, in which the ranking becomes  $\text{CeO}_2 > \text{ZrO}_2 > \text{TiO}_2 > \text{Al}_2\text{O}_3 > \text{SiO}_2$ .<sup>122</sup>

Each support exhibits unique properties, which can influence the catalytic performance of vanadium-containing materials. For example, if alumina is used as support, some vanadium (IV) sites are hard to be oxidized to vanadium (V) even under an oxidizing atmosphere, which was proved by EPR measurements.<sup>123</sup> The ceria support, on the other hand, allows an easy formation of the  $\text{CeVO}_4$  at elevated

temperatures.<sup>122,124</sup>

### **2.2.3.2 Vanadium-containing zeolites and microporous molecular sieves**

Supported vanadium oxides have attracted a lot of attention because of the potential application in catalysis. The limitation of low specific surface area of oxides was overcome by the introduction of vanadium ions into the zeolite structures such as MFI<sup>125-130</sup>, BEA<sup>20,131-135</sup>, MEL<sup>136</sup>, and MTW<sup>137</sup>. And the advantage in shape selectivity and high thermal stability has made zeolites with transition metal ions as a popular heterogeneous catalyst from the end of last century until now. There is no doubt that it possesses a great potential in industrial application.

MFI type zeolite is a famous type of zeolite because its Al-substituted (ZSM-5) and Ti-substituted (TS-1) products, which are already produced in the industrial process and used as heterogeneous catalysts for many years.<sup>96</sup> Other atoms substituted MFI zeolites were also developed for various other application in catalysis. MFI type zeolite contains two systems of 10 rings pore channels: a system of straight channels in the *b* direction and a system of sine-shape channels with an angle around 150° which is perpendicular to the *b* direction (Figure 19). The size of the straight channels is 0.53×0.56 nm while the one of sine-shape channels is 0.51×0.55 nm. These two systems of channels facilitates the shape-selectivity in the catalytic reaction process.

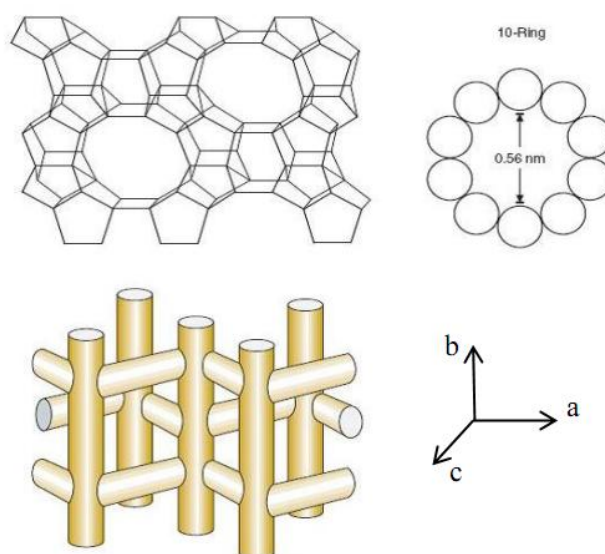


Figure 19. Topology of MFI molecular sieve.

There are two methods to synthesize the V-substituted MFI (VS-1). The first one is direct hydrothermal synthesis which is generally considered as a simple way.<sup>126,128</sup> The second method is post-synthesis treatment.<sup>138,139</sup> The VS-1 synthesized from acidic or alkaline media has different features. In the as-synthesized V-MFI prepared in acidic medium, the  $V^{4+}$  species are present in an octahedral ( $O_h$ ) environment while the vanadium species existed as  $V^{5+}$  in distorted  $T_d$  structure in the alkaline medium. The spectroscopic characterization of the final products proves that the acidic medium is unfavorable for the incorporation of vanadium into the framework.<sup>127</sup> The properties of the final VS-1 during the preparation process also depends on the nature of the vanadium source and of the other additives such as fluoride salt.<sup>129</sup> G. Centi *et al.* have identified four sorts of vanadium species from  $^{51}\text{V}$ -NMR, EPR, DR UV-visible spectroscopies and other characterization techniques: 1) a polymeric vanadium species containing reduced species, 2) a nearly octahedral vanadyl species in the zeolitic channels, 3) a tetrahedral  $V^{5+}$  species which is attributed to atomically dispersed vanadium species anchored to the zeolitic framework, and 4) a nearly tetrahedral  $V^{4+}$  species observed after reduction.<sup>126</sup> The knowledge of vanadium

species in the zeolite provides a lot of assistance in the future research on it.

S. Dzwigaj and his group accomplished abundant work on the synthesis and characterization of vanadium-containing BEA zeolite.<sup>20,132-135,140</sup> Photoluminescence spectroscopy was applied to analyze different types of tetrahedral V species present in V-BEA zeolite. Three different types of vibrational fine structures were found in the spectra which are attributed to three different sorts of tetrahedral V species ( $\alpha$ ,  $\beta$ ,  $\gamma$ ) (Figure 20). The vibration energy increases in the order  $\alpha > \gamma > \beta$ , which indicated the V=O bond length of the tetrahedral V species decreases in this order. The different V=O bonds observed corresponds to a change from a symmetry close to  $T_d$  ( $\alpha$ ) to the one close to vanadium oxo-tertioamlyoxide ( $C_{3v}$  symmetry) ( $\beta$ ). They have also proved that these three sorts of tetrahedral V species can occupy two different sites in

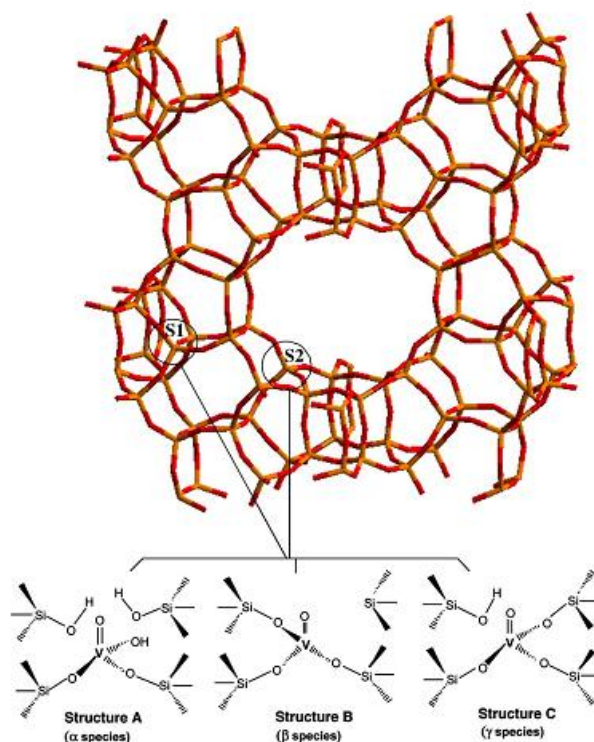


Figure 20. Three different types of tetrahedral V species and their possible position in the V-BEA zeolite.<sup>20</sup>

the framework, accessible and inaccessible to H<sub>2</sub>O molecules such as (S1 and S2 sites depicted in Figure 20).<sup>20</sup>

S. Dzwigaj also found that the synthesis route was an important aspect to influence the nature and local environment of the vanadium species. A two-steps post-synthesis method was developed to control the environment of vanadium species in V-BEA zeolites. In the first step, the vacant T-atom sites with associated hydrogen bonded silanol groups was formed by dealumination from an Al-BEA to Si-BEA. In the second step, V ions were incorporated in the vacant T-atom sites by an aqueous solution with vanadium source such as VOSO<sub>4</sub><sup>140</sup> or NH<sub>4</sub>VO<sub>3</sub><sup>135</sup> as vanadium source. The results show that the dealumination process affects the nature of vanadium species. The V(V) species exist as both pseudo-tetrahedral and pseudo-octahedral form in the sample whose Al-BEA precursors was calcined before the dealumination procedure. In contrast, V-BEA, which is first dealuminated, contains only pseudo-tetrahedral V(V) species.<sup>135</sup>

Besides zeolites, vanadium species can also be introduced into other microporous molecular sieves. ETS-10 is a microporous titanosilicate developed in 1989 by Kuznicki. It is composed of octahedrally coordinated TiO<sub>6/2</sub> units and tetrahedrally coordinated SiO<sub>4/2</sub> units. M. J. Nash and his group reported a study about vanadium-substituted ETS-10. V-containing ETS-10 molecular sieves with various contents of vanadium were prepared. The -V-O-V- chain bonds and -V-O-Ti- bonds were proved by Raman spectroscopy. The photocatalytic performance of samples was evaluated by polymerization of ethylene.<sup>141</sup> On the other hand, microporous vanadosilicate molecular sieves such as VSH-1<sup>142</sup> and other V-containing microporous molecular sieves such as VFI series<sup>143</sup> are also described. All these V-containing materials are proved to have potential applications in catalysis even in

the industrial processes.

### 2.2.3.3 Vanadium-containing mesoporous materials

Although the development of vanadium containing zeolites increased the surface area of the materials and provided the shape selectivity for some catalytic reactions, the pore size that is smaller than 2 nm lead to a diffusion problem in the case of catalysis of bulky substrates. This problem was supposed to be overcome by the development of mesoporous materials, which possess larger pore size between 2 nm to 50nm.

Mesoporous silica was a popular mesoporous support due to its ease synthesis, large specific surface area and high stability. Vanadium species have been introduced into different type of mesoporous silicas such as MCM-41<sup>94,110,117,144-146</sup>, MCM-48<sup>147,148</sup>, SBA-15<sup>57,119,120,149</sup> and HMS<sup>10,150,151</sup>.

The synthesis strategies to afford V-containing mesoporous silica include direct hydrothermal synthesis<sup>93,110,117,144-146,152</sup>, impregnation<sup>10,153,154</sup>, grafting<sup>93,155</sup>, immobilization<sup>6,56,59</sup> and chemical gas deposition<sup>154</sup>. Depending on the synthesis method the final materials can present different features and properties. G. Grubert *et al.*<sup>154</sup> studied V-MCM-41 synthesized by 1) direct hydrothermal synthesis (V-MCM-41-syn), 2) chemical gas deposition of  $\text{VOCl}_3$  as vanadium source on MCM-41 (V-MCM-41-cvd) and 3) impregnation of MCM-41 with vanadyl acetylacetonate (V-MCM-41-imp). Their properties were compared in the aspect of crystallinity, the dispersion of vanadium species and reducibility. The fraction of amorphous species increased in the ranking: V-MCM-41-imp < V-MCM-41-cvd < V-MCM-41-syn. The content of polymeric vanadium species increased in the order: V-MCM-41-syn < V-MCM-41-imp < V-MCM-41-cvd. The reducibility increased in the order: V-MCM-41-syn < V-MCM-41-cvd < V-MCM-41-imp.<sup>154</sup> S. Shylesh *et al.*

also compared the crystallinity of the V-MCM-41 synthesized by direct hydrothermal process, grafting and immobilization. In their case, the direct synthesized sample possessed the best crystallinity. However, in the investigation of catalysis performance of these three sorts of samples, the grafted and the immobilized samples showed higher reactivity than the direct synthesized one due to a better dispersion of vanadium species on the surface. In addition, the immobilized sample avoided the leaching problem during the liquid phase reaction.<sup>6</sup>

The source of vanadium and mesoporous silica are also important parameters that can affect the properties of vanadium-containing mesoporous silica during the preparation.<sup>94,156</sup> P. Selvam *et al.* synthesized V-MCM-41 starting from different vanadium sources in hydrothermal condition. It was found that tetravalent vanadium sources (vanadyl sulfate and vanadyl acetylacetonate) were easier to incorporate to the silicate framework of MCM-41 than pentavalent vanadium ones (sodium vanadate and ammonium vanadate). As a consequence, the products synthesized with tetravalent vanadium source possessed higher reactivity and more excellent selectivity in the oxidation of cyclohexane.<sup>94</sup> On the other hand, it was also found, by comparing V-MCM-41, V-MCM-48 and V-SBA-15, that the properties and the state of vanadium species in the material also depends on the porous characteristics of the silica.<sup>157</sup>

The influence of pH value was investigated in the preparation of V-SBA-15 by a direct synthesis method. The incorporated isolated vanadium species with tetrahedral and square pyramidal coordination increase upon increase of the pH value, while the crystallinity decreases accordingly.<sup>119</sup> Taking into account that temperature has an influence in the hydrothermal synthesis, M. Chatterjee succeeded in the preparation of V-MCM-41 at room temperature. The final solids was found to be catalytically active

in the oxidation of toluene and in the hydroxylation of benzene with  $\text{H}_2\text{O}_2$  as a green oxidant.<sup>152</sup>

Hierarchical microporous-mesoporous materials can resolve the diffusion problem existing in the microporous materials. For example, vanadium silicate-1 (VS-1) nanoparticles can be deposited onto the wall of SBA-15 mesoporous silica to form a hierarchical silica materials.<sup>158</sup> The authors observed that the hydrophilicity of the VS-1 nanoparticles deposited in the channels were different from those full-grown VS-1 particles. Furthermore, the nitrogen of TPAOH (tetrapropylammonium hydroxide, template of VS-1) was found to be in equatorial interaction with  $\text{VO}^{2+}$  species.<sup>158</sup>

Considering the support effect is very important in the vanadium-containing materials, heteroatoms were introduced to the mesoporous silica support<sup>12,159,160</sup>. In the study of Z. Luan and L. Kevan, vanadium species were loaded onto Si-MCM-41, Al-MCM-41, Ti-MCM-41 and Zr-MCM-41 by incipient-wetness impregnation with an aqueous vanadyl sulfate solution. The ESR and UV-visible spectra revealed that the  $\text{VO}^{2+}$  ions were mobile in the V/Si-MCM-41 and V/Al-MCM-41 while they were immobilized in the V/Ti-MCM-41 and V/Zr-MCM-41 samples. And the Ti and Zr atoms on the surface of the supports promoted the oxidation of  $\text{VO}^{2+}$  to  $\text{V}^{5+}$ , which suggests a strong interaction between the vanadium species and Ti or Zr on the surface.<sup>12</sup> Despite the difficulty to synthesis a stable mesoporous titania with high surface area, there are still continuous efforts devoted to vanadium deposition on mesoporous titania.<sup>161-163</sup>

## 2.3 Catalysis applications of vanadium-containing heterogeneous catalysts

Vanadium is an important element widely present in enzymes as bromoperoxidase and nitrogenase in the nature, which reveals its redox properties. In addition, vanadium compounds has been applied as catalysts in various reactions in modern organic synthesis.<sup>164</sup> Finally, vanadium-containing heterogeneous catalysts are involved in many kinds of catalytic process such as oxidation reactions, oxidative halogenations and even photocatalysis.

The oxidation reactions catalyzed by vanadium-containing heterogeneous catalyst include the oxidation of alcohols, alkanes and alkenes, hydroxylation of aromatic compounds, etc.

### 2.3.1 Oxidation of alcohols

Although inorganic materials containing other transition metal atom such as Ti-containing silicas were used for this kind of reaction, the vanadium-containing materials show different chemoselectivities. In the case of oxidation of allyl and methallyl alcohol by Ti-MFI and V-MFI with H<sub>2</sub>O<sub>2</sub> as oxidant, the Ti active centers catalyze preferentially the epoxidation of the double bond, while the V ones catalyze

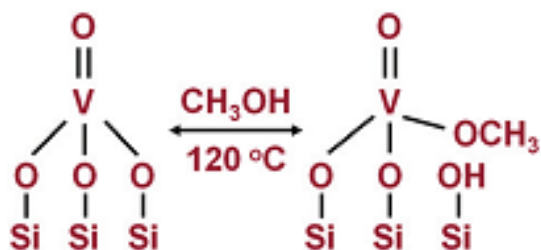


Figure 21. Dissociative chemisorption of methanol on a surface vanadium site of supported vanadium catalysts.<sup>4</sup>

the oxidation of the alcohol moiety.<sup>26,165,166</sup>

A lot of contribution has been deserved to the oxidation of methanol to formaldehyde in gas phase by the group of I. E. Wachs<sup>4</sup>. The decomposition of CH<sub>3</sub>OH on the V<sub>2</sub>O<sub>5</sub>/SiO<sub>2</sub> surface was investigated by *in situ* Raman, IR and UV-vis spectroscopies. It was shown that the chemisorption of CH<sub>3</sub>OH on the surface happened at 120 °C with dissociation into surface methoxy (CH<sub>3</sub>O) and H moieties at the bridging V-O-support bond to form a surface silanol and V-OCH<sub>3</sub> intermediates (Figure 21). The reactivity and kinetics of transformation from CH<sub>3</sub>OH to HCHO was studied via CH<sub>3</sub>OH-temperature-programmed surface reaction (TPSR) spectroscopy. The decomposition of the surface V-OCH<sub>3</sub> intermediate happened above 100 °C to yield HCHO and H<sub>2</sub>O. The surface kinetics showed that the formation of formaldehyde was independent of the presence of O<sub>2</sub> gas. The authors suggest that the oxygen, which is involved in the rate-determining step of the surface methoxy oxidation, is supplied by the surface vanadium sites, and not by gaseous molecular O<sub>2</sub>. This results are in agreement with the lattice oxygen model in the well-known Mars-van Krevelen mechanism.<sup>4</sup>

Concerning the selectivity of methanol oxidation, acidic sites favor the formation of dimethyl ethers, basic sites mainly yield carbon oxides (CO and CO<sub>2</sub>) and redox sites give rise to formaldehyde, methyl formate and dimethoxymethane. The state of vanadium species may have an influence on the nature of the final products. Indeed, an increase of the crystalline vanadium oxide phase in the samples, decreases the formaldehyde yield and carbon oxides are formed.<sup>148</sup>

### **2.3.2 Oxidation of saturated and unsaturated hydrocarbons**

Ti-containing silica is well-known for its remarkable catalytic performance in the

epoxidation of alkenes with  $\text{H}_2\text{O}_2$  as oxidant, and this catalytic process is considered as green process in green chemistry. V-containing silica also shows activity in the oxidation reaction of alkenes and alkanes but with different selectivity compared to Ti-containing ones.

### 2.3.2.1 Oxidation of alkenes and cycloalkenes

In the oxidation of 1-hexene catalyzed by  $\text{TiO}_2/\text{SiO}_2$  and  $\text{V}_2\text{O}_5/\text{SiO}_2$ <sup>23</sup>, the vanadium catalyst leads to less epoxidation products compared to the titanium oxide catalyst, where 100% epoxide is formed. In the case of the epoxidation of cyclohexene, the product obtained in the process catalyzed by  $\text{TiO}_2/\text{SiO}_2$  is still 100% selective in epoxide. By contrast, the oxidized products of  $\text{V}_2\text{O}_5/\text{SiO}_2$  were alcohol and ketone (Table 1).

Table 1. Summary of the catalytic activity and selectivity of the Ti and V nanostructured systems towards the oxidation of 1-hexene, cyclohexene and cyclohexane.<sup>23</sup>

Catalyst (% metal)	Substrate	TOF (mol of product/mol of metal h)	Selectivity (%)			Efficiency TBHP (%)	Conversion (%) <sup>b</sup>
			Epoxide	Alcohol	Ketone		
$\text{SiO}_2$	1-Hexene	3 <sup>c</sup>				–	–
$\text{TiO}_2/\text{SiO}_2$ (1.8)	1-Hexene	54	100	–	–	825	77.5
	Cyclohexene	51.5	100	–	–	507	68.4
	Cyclohexane	22.2	–	57.4	42.5	471	19.2
$\text{V}_2\text{O}_5/\text{SiO}_2$ (0.62)	1-Hexene	198	76.5	10.2 <sup>d</sup>	2.0 <sup>e</sup>	4808	89.8
	Cyclohexene	146	–	38.5	61.5	3539	53.4
	Cyclohexane	94	–	45.5	54.5	2337	37.4

Reaction conditions: 100 mg catalyst, 2 mL substrate, 1 mL TBHP, 80 °C, 6 h reaction time.

The differences observed in the selectivity between Ti-containing catalysts and V-containing catalysts can be explained by the Lewis acidity of the metallic centers. The strong acid site cause the ring opening of the epoxide, which has been proved by the comparative study of the epoxidation catalytic activity of  $\text{TiO}_2/\text{SiO}_2$ ,  $\text{V}_2\text{O}_5/\text{SiO}_2$  and  $\text{Nb}_2\text{O}_5/\text{SiO}_2$ .<sup>23</sup>

### 2.3.2.2 Oxidation of linear alkanes and cycloalkanes

Some oxidation reactions starting from alkane or cycloalkane are very useful and applied in the chemical industry such as the production of cyclohexanone-cyclohexanol mixture (or “KA oil”) via oxidation of cyclohexane. The oxidized products, KA oil, are precursors for the production of adipic acid and caprolactam, which are the key intermediates in the manufacture in nylon.

Vanadium catalysts also show the unique selectivity in the oxidation reaction of alkanes and cycloalkanes. As shown in Table 1, the vanadium-containing material produces more ketone than titanium-containing material in the oxidation reaction of cyclohexane. Cyclohexyl acetate may also be produced as further oxidized product, but in low quantity because the increase of acidity due to the presence of vanadium in the aluminophosphate.<sup>167</sup> The oxidation of larger bulky cycloalkane with more carbon can be catalyzed by vanadium-containing mesoporous materials.<sup>94</sup>

The oxidation reaction of linear alkanes is quite interesting and attractive. In the oxidation of *n*-hexane catalyzed by TS-2 and VS-2 (titanium and vanadium containing MEL type zeolites respectively), the two catalysts showed different selectivity. The products formed using TS-2 are mainly 2-hexanol, 3-hexanol, 2-hexanone and 3-hexanone and no 1-hexanol, hexanal are detected (Table 2). The aldehyde and ketone were formed upon further oxidation of the corresponding alcohols. The presence of the 1-hexanol and hexanal when VS-2 was used as catalysts, Table 2. Oxidation of *n*-hexane over TS-2 and VS-2.<sup>21</sup>

Catalyst <sup>b</sup>	Conv. (mol%)	H <sub>2</sub> O <sub>2</sub> sel. (mol%) <sup>c</sup>	Product distribution (mol%) <sup>d</sup>							Product sel. (mol%) <sup>f</sup>
			1-ol	2-ol	3-ol	1-al	2-one	3-one	others <sup>e</sup>	
TS-2	15.9	58.6	–	19.1	17.1	–	23.7	23.0	16.6	83.4
VS-2	14.6	57.1	3.7	9.2	8.2	7.2	26.3	25.0	21.4	79.5

Reaction conditions: 100 mg catalyst, 5 g *n*-hexane, *n*-hexane / H<sub>2</sub>O<sub>2</sub> (mol) = 3, 20 g solvent (acetonitrile) 100 °C, 8 h reaction time. Reaction carried out with stirring in steel stain autoclave under autogeneous pressure.

suggests that vanadium can activate the primary carbon atom while titanium one cannot.<sup>21,26</sup>

The different selectivity of vanadium catalysts compared to titanium catalysts shows that vanadium possesses a deeper oxidation capability compared to titanium. This may indicate the potential catalytic ability of vanadium-containing catalyst that could be applied in the industrial production as for the Ti-based catalysts.

### 2.3.2 Hydroxylation of aromatic compounds

Hydroxylation of arenes is another interesting and useful reaction for catalysis where transition metal containing materials can be active. Vanadium-containing materials have been applied in the hydroxylation of benzene, phenol and their derivatives as a probe reaction to evaluate the catalytic performance.<sup>6,9,56,59,130,137,151,152,157,168</sup> Hydroxylation of benzene with aqueous H<sub>2</sub>O<sub>2</sub> catalyzed by vanadium-containing materials leads to phenol as the main product with an amount of *p*-benzoquinone in some case.<sup>130,152,168</sup> The oxidized product of hydroxylation of phenol are mainly in the *o* / *p* -positions.<sup>26,137</sup>

The mesopores in the vanadium-containing mesoporous materials allow the diffusion of bulky molecules in the channels, which provides the possibility to catalyze the hydroxylation of larger substrates such as naphthalene and biphenyl.<sup>6,9</sup> In the hydroxylation of biphenyl catalyzed by vanadium-containing MCM-41, the oxidized

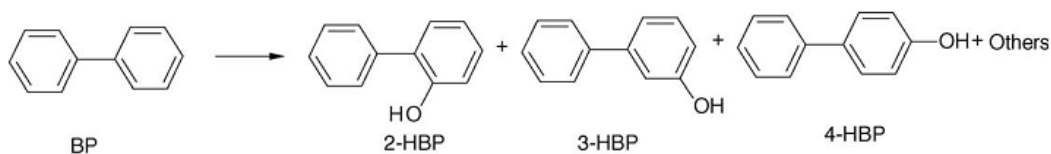


Figure 22. Main products at the earlier stage of hydroxylation of biphenyl catalyzed by V-containing MCM-41.<sup>9</sup>

products were formed following the order: 2-hydroxy biphenyl (2-HBP) > 3-hydroxy biphenyl (3-HBP) > 4-hydroxy biphenyl (4-HBP) (Figure 22) at the beginning of reaction. The formation of quinone derivatives turned to be 80% of the others in the products after 24h.<sup>9</sup>

In the hydroxylation of naphthalene, hydrophilic-hydrophobic interactions are very important for the selectivity of hydroxylated products during the process of hydroxylation. The substrate is nonpolar while the primary products are polar. As a result, a hydrophobic catalyst favors adsorption of the reactant molecules to enhance the conversion. On the other hand, a hydrophilic catalyst leads to deeper oxidation of naphthols earlier formed.<sup>6</sup> (Figure 23)

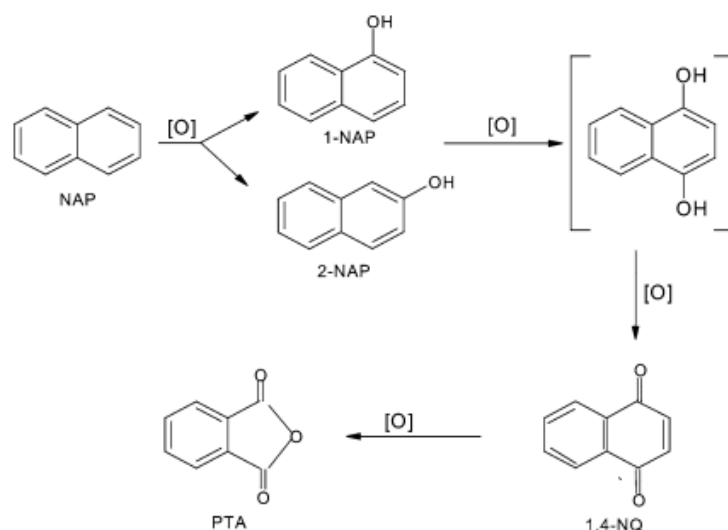


Figure 23. Primary products and further oxidized products of hydroxylation of naphthalene.<sup>6</sup>

### 2.3.3 Dehydrogenation of alkanes

The oxidative dehydrogenation (ODH) reactions are also an attractive classical process in catalysis of vanadium-containing materials. The ODH process of butane is a clear example in the industrial chemistry. The dehydrogenation of paraffins to the corresponding olefins and H<sub>2</sub> needs high temperature, usually above 600 °C, which

always leads to coke in the reactor and regeneration of catalyst is frequently required. In oxydehydrogenation reactions, the produced hydrogen is oxidized to release the heat of reaction, and significant conversion are also observed at lower temperature.<sup>169</sup> Vanadium-containing catalysts have been applied in ODH reaction of ethane,<sup>61,170</sup> propane,<sup>17,57,93,171-179</sup> butane<sup>180-182</sup> and cyclohexane<sup>183</sup> in various studies.

K. Chen *et al.* proposed a possible mechanism of ODH process using vanadium oxide loaded on different oxide supports.<sup>17</sup> They found that the turnover rate of the dissociation of C<sub>3</sub>H<sub>8</sub> and the formation of C<sub>3</sub>H<sub>6</sub> increase, in agreement with decrease of absorption-edge energy in the UV-visible spectrum. Therefore, the lower the dispersion of vanadium species the higher conversion. The authors propose a mechanism involving two adjacent vanadium atoms (Figure 24). Firstly, the methylene C-H bond in propane interacts with a lattice oxygen that is weakly absorbed on the oxide surface. The key step is the adsorption of propane by reacting with a vicinal lattice oxygen atom to form an isopropoxide species and an OH group. The complete mechanism with the elementary steps is shown in Figure 24. Two lattice oxygen atoms are necessary in the C-H activation step. Molecular simulations proved that one-electron reduction of two V<sup>5+</sup> centers to V<sup>4+</sup> using one electron from two adjacent lattice oxygen was possible. As a result, more adjacent vanadium sites are required for the ODH process.<sup>17</sup>

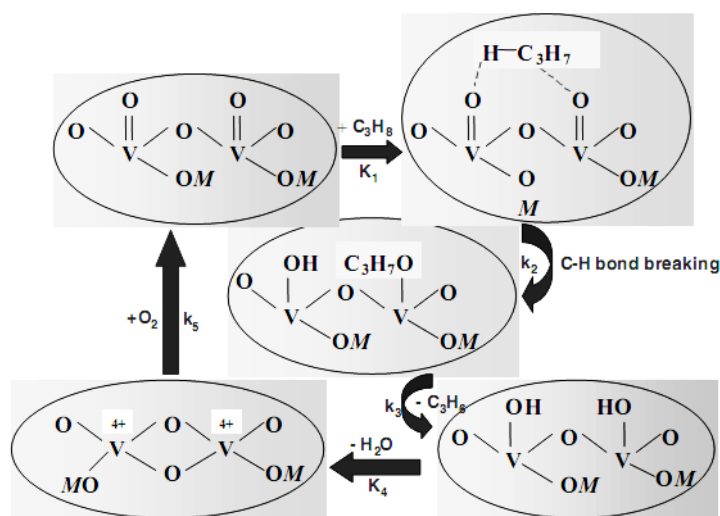


Figure 24. Simulated example of propane oxidative dehydrogenation over  $\text{VO}_x$ -based catalyst.<sup>17</sup>

However, in the research of P. Knotek *et al.* about vanadium supported on hexagonal mesoporous silica, it was proposed that monomeric species are active and selective in the formation of propene, while oxide-like clusters show less activity and selectivity. The oligomeric species are active but do not show selectivity towards the ODH reaction.<sup>176</sup> There is still no consensus in the mechanism of ODH process.

On the other hand, the study of the oxidant is also interesting for ODH process. In the work about oxidative dehydrogenation of propane over V/MCM-41 catalysts by E. V. Kondratenko *et al.*, it was shown that higher propene selectivity is achieved with  $\text{N}_2\text{O}$  compared to  $\text{O}_2$  at similar degrees of  $\text{C}_3\text{H}_8$  conversion although the conversion of  $\text{N}_2\text{O}$  is lower.<sup>173</sup> This phenomenon can be explained by the weaker oxidizing ability of  $\text{N}_2\text{O}$  compared to  $\text{O}_2$ . The weaker oxidizing redox potential of  $\text{N}_2\text{O}$  inhibits the direct oxidation of propane and the oxidation of propene to  $\text{CO}_x$ . Another research group obtained similar results in this topic studying the catalytic performance of  $\text{V}_2\text{O}_5$ ,  $\text{VO}_2$  and  $\text{V}_2\text{O}_3$ .<sup>177</sup>

### 2.3.4 Oxidative halogenation

The oxidative halogenation catalyzed by vanadium-containing materials has been inspired by marine haloperoxidases containing vanadium sites which are widely present in the seaweeds (Figure 25).<sup>3,25,184,185</sup> The halogenated products are believed to be involved in chemical defense roles in organisms, which cause their pharmacological interest such as antifungal, antibacterial, antiviral, antineoplastic, and anti-inflammatory.<sup>3,25</sup>

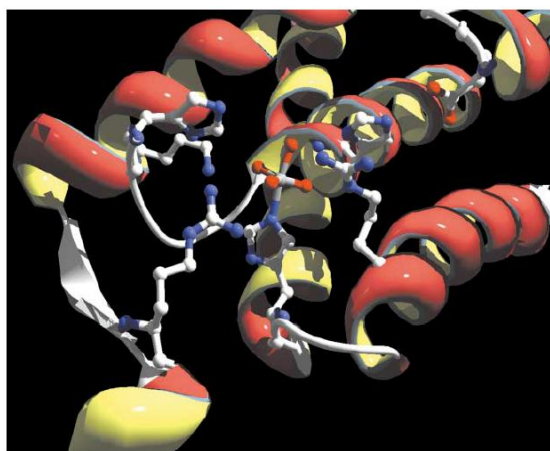
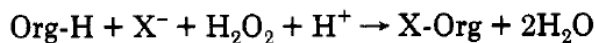


Figure 25. The vanadium site of V-bromoperoxidase. Vanadium cofactor is represented as a gray/red stick and ball model.<sup>25</sup>

#### 2.3.4.1 Haloperoxidases

Haloperoxidases are enzymes that catalyze the oxidation of a halide in the presence of  $H_2O_2$  (Scheme 1). A lot of work has been dedicated to isolate haloperoxidases from all classes of marine algae and marine organisms. Vanadium bromoperoxidase (V-BrPO), a non-Heme BrPO, has been identified from those natural products along with another one, FeHeme bromoperoxidase (FeHeme-BrPO). Vanadium haloperoxidases (V-HPOs) form a family of metalloenzymes that catalyze the oxidation of halides and are classified according to the most electronegative halogen oxidized. The vanadium chloroperoxidases can oxidize chloride, bromide and iodide, whereas the vanadium

bromoperoxidases can oxidize bromide and iodide.<sup>25</sup>



Scheme 1. Halogenation of organic substrates.<sup>3</sup>

In the process of oxyhalogenation, the oxidized halogen intermediate can halogenated an appropriated organic substrate as mentioned in Chapter 1. It was evidenced that the  $\text{H}_2\text{O}_2$  first coordinates to the vanadate site firstly, followed by bromide oxidation, as shown in the cycle depicted in Figure 26.<sup>3,25,186</sup>

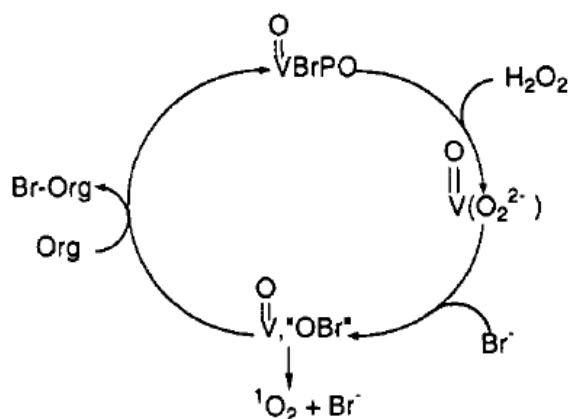


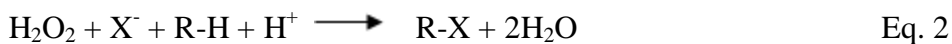
Figure 26. Catalytic cycle for V-BrPO showing coordination of  $\text{H}_2\text{O}_2$  before oxidation of bromide.<sup>3</sup>

The research of halogenation in bio-catalysis evoked the attention to the catalytic ability of vanadium site in halogenation and induced the researches in heterogeneous catalysis.

#### 2.3.4.2 Vanadium catalyzed bromination reaction

A classical bromination reaction is performed using bromine, which is a pollutant and health hazard. Furthermore, half of the bromine ends up as hydrogen bromide waste, which is considered as a non-economic process (Eq. 1). To improve this procedure, a bio-mimetic oxyhalogenation approach has been developed, in which the reoxidation

of HBr with H<sub>2</sub>O<sub>2</sub> under acidic conditions is introduced to replace Br<sub>2</sub> (Eq. 2). This process is believed to be safer and greener.



Vanadium-containing materials and vanadium compounds have been applied to catalyze this reaction.<sup>8,187-191</sup> T. Moriuchi has studied a catalytic system consisted of NH<sub>4</sub>VO<sub>3</sub>, H<sub>2</sub>O<sub>2</sub>, HBr and KBr. This system catalyzes the oxidative bromination of arenes, alkenes, and alkynes in aqueous media efficiently.<sup>188</sup> Replacing vanadium salts by vanadium oxides or supported vanadium materials generated the heterogeneous version of this catalyst. G. Rothenberg *et al.* found that the process of bromination reaction catalyzed by V<sub>2</sub>O<sub>5</sub> could be an option for recycling waste acid streams. It was proved that this method is an efficient way for the bromination of aromatic substrates. In addition, different sorts of mineral acids (HCl, HBr, H<sub>2</sub>SO<sub>4</sub>, HNO<sub>3</sub> and H<sub>3</sub>PO<sub>4</sub>) can be used in this process, which was thought as a potential method for recycling industrial acid wastes.<sup>191</sup> Recently, several new reports have been published about supported vanadium oxides catalyzing bromination of aromatic compounds.<sup>8,190</sup>

#### 2.3.4.3 Oxidative bromination of phenol red catalyzed by V-containing materials

Oxidative bromination of phenol red (phenolsulfonaphthalein) to bromophenol blue (bromo-phenolsulfonaphthalein) can be used as a probe reaction because the substrate and the product are active in the visible region of spectrum and this reaction can be run at room temperature (Figure 27).

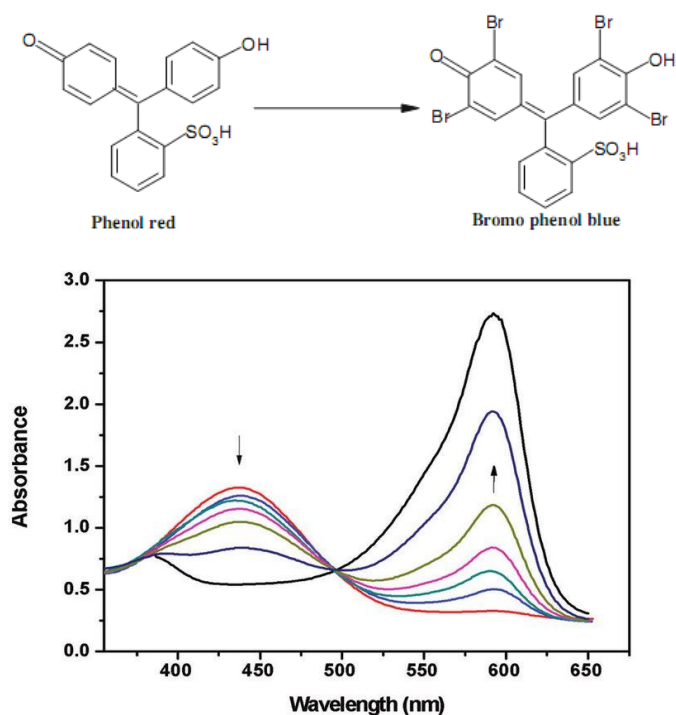


Figure 27. Oxidative bromination of phenol red catalyzed by V-MCM-41.<sup>8</sup>

S. Bhunia studied the oxybromination of phenol red catalyzed by V-MCM-41.<sup>8</sup> In the UV-visible spectrum of the reactant (Figure 27), the peak at 432 nm is attributed to the absorption of phenol red while the one at 592 nm corresponds to the bromophenol blue. The peak of phenol red decreased with the time proceeded whereas the bromophenol blue increased. It was found that after 1h, there was no further changes in the absorption spectrum, which indicated the completion of the reaction.<sup>8</sup> Thus, this reaction provides a facile and simple method to evaluate the catalytic performance of V-containing materials towards oxidative bromination.<sup>8,190</sup>

## 2.4 Conclusion

In this chapter, a panoramic view of the literature related to this dissertation has been accomplished, including the introduction of mesoporous silica, the vanadium-containing materials and catalytic application of vanadium-containing systems.

In the part of mesoporous silica, a brief introduction of M41S family silicas has been presented including the formation mechanism and typical physico-chemical properties. A further description of the techniques available to modify the surface of silica provides more knowledge to develop such related functional materials.

In the second part of this chapter, the nature and characteristic properties of vanadium species in the vanadium-containing materials have been analyzed. Furthermore, different kinds of vanadium-containing materials with different supports, structures and synthesis methods have been described in detail in order to offer a wide state of the art of vanadium heterogeneous catalysts.

In the last part, several typical catalytic processes involving by vanadium-containing materials have been selected from the literature. In fact, there are still other reactions such as oxidation of sulfides widely used to evaluate the catalytic performance of vanadium-containing catalysts. All these catalytic applications show the potential application of vanadium catalysts.

All these information and knowledge will be useful in the development of this dissertation. In addition, other helpful information that was not mentioned here will be detailed in the discussion in following chapters when necessary.

## 2.5 References

- (1) Ruitenbeek, M.; van Dillen, A. J.; de Groot, F. M. F.; Wachs, I. E.; Geus, J. W.; Koningsberger, D. C. *Topics in Catalysis* **2000**, *10*, 241.
- (2) Corma, A. *Chemical Reviews* **1995**, *95*, 559.
- (3) Butler, A.; Walker, J. V. *Chemical Reviews* **1993**, *93*, 1937.
- (4) Wachs, I. E. *Dalton Transactions* **2013**, *42*, 11762.
- (5) Kresge, C. T.; Roth, W. J. *Chemical Society Reviews* **2013**, *42*, 3663.
- (6) Shylesh, S.; Singh, A. *Journal of Catalysis* **2004**, *228*, 333.
- (7) Wan, Y.; Zhao, D. *Chemical Reviews* **2007**, *107*, 2821.
- (8) Bhunia, S.; Saha, D.; Koner, S. *Langmuir* **2011**, *27*, 15322.
- (9) George, J.; Shylesh, S.; Singh, A. P. *Applied Catalysis A: General* **2005**, *290*, 148.
- (10) Bulánek, R.; Čapek, L.; Setnička, M.; Čičmanec, P. *The Journal of Physical Chemistry C* **2011**, *115*, 12430.
- (11) Tian, H.; Ross, E. I.; Wachs, I. E. *The Journal of Physical Chemistry B* **2006**, *110*, 9593.
- (12) Luan, Z.; Kevan, L. *The Journal of Physical Chemistry B* **1997**, *101*, 2020.
- (13) Beck, J. S.; Vartuli, J. C.; Roth, W. J.; Leonowicz, M. E.; Kresge, C. T.; Schmitt, K. D.; Chu, C. T. W.; Olson, D. H.; Sheppard, E. W. *Journal of the American Chemical Society* **1992**, *114*, 10834.
- (14) Calmettes, S.; Albela, B.; Hamelin, O.; Menage, S.; Miomandre, F.; Bonneviot, L. *New Journal of Chemistry* **2008**, *32*, 727.
- (15) Catana, G.; Rao, R. R.; Weckhuysen, B. M.; Van Der Voort, P.; Vansant, E.; Schoonheydt, R. A. *The Journal of Physical Chemistry B* **1998**, *102*, 8005.
- (16) Lewandowska, A. E.; Bañares, M. A.; Khabibulin, D. F.; Lapina, O. B. *The Journal of Physical Chemistry C* **2009**, *113*, 20648.
- (17) Chen, K.; Bell, A. T.; Iglesia, E. *Journal of Catalysis* **2002**, *209*, 35.

- (18) Zhuravlev, L. T. *Colloids and Surfaces A: Physicochemical and Engineering Aspects* **2000**, *173*, 1.
- (19) Shin, Y.; Liu, J.; Wang, L.-Q.; Nie, Z.; Samuels, W. D.; Fryxell, G. E.; Exarhos, G. J. *Angewandte Chemie International Edition* **2000**, *39*, 2702.
- (20) Dzwigaj, S. *Current Opinion in Solid State and Materials Science* **2003**, *7*, 461.
- (21) Ramaswamy, A. V.; Sivasanker, S. *Catalysis Letters* **1993**, *22*, 239.
- (22) Muylaert, I.; Van Der Voort, P. *Physical chemistry chemical physics : PCCP* **2009**, *11*, 2826.
- (23) Martínez-Méndez, S.; Henríquez, Y.; Domínguez, O.; D'Ornelas, L.; Krentzien, H. *Journal of Molecular Catalysis A: Chemical* **2006**, *252*, 226.
- (24) Zhang, K.; Albelá, B.; He, M. Y.; Wang, Y.; Bonneviot, L. *Physical chemistry chemical physics : PCCP* **2009**, *11*, 2912.
- (25) Butler, A.; Carter-Franklin, J. N. *Nat Prod Rep* **2004**, *21*, 180.
- (26) Arends, I. W. C. E.; Sheldon, R. A.; Wallau, M.; Schuchardt, U. *Angewandte Chemie International Edition in English* **1997**, *36*, 1144.
- (27) Dessau, R. M.; Schlenker, J. L.; Higgins, J. B. *Zeolites* **1990**, *10*, 522.
- (28) Davis, M. E.; Saldarriaga, C.; Montes, C.; Garces, J.; Crowdert, C. *Nature* **1988**, *331*, 698.
- (29) Estermann, M.; McCusker, L. B.; Baerlocher, C.; Merrouche, A.; Kessler, H. *Nature* **1991**, *352*, 320.
- (30) Kresge, C. T.; Leonowicz, M. E.; Roth, W. J.; Vartuli, J. C.; Beck, J. S. *Nature* **1992**, *359*, 710.
- (31) Zhao, D.; Feng, J.; Huo, Q.; Melosh, N.; Fredrickson, G. H.; Chmelka, B. F.; Stucky, G. D. *Science* **1998**, *279*, 548.
- (32) Zhao, D.; Huo, Q.; Feng, J.; Chmelka, B. F.; Stucky, G. D. *Journal of the American Chemical Society* **1998**, *120*, 6024.

- (33)Grün, M.; Unger, K. K.; Matsumoto, A.; Tsutsumi, K. *Microporous and Mesoporous Materials* **1999**, *27*, 207.
- (34)Zhang, K.; Chen, H.-L.; Albela, B.; Jiang, J.-G.; Wang, Y.-M.; He, M.-Y.; Bonneviot, L. *European Journal of Inorganic Chemistry* **2011**, *2011*, 59.
- (35)Pang, J.; Na, H.; Lu, Y. *Microporous and Mesoporous Materials* **2005**, *86*, 89.
- (36)Sayari, A.; Yang, Y.; Kruk, M.; Jaroniec, M. *The Journal of Physical Chemistry B* **1999**, *103*, 3651.
- (37)Selvam, P.; Bhatia, S. K.; Sonwane, C. G. *Industrial & Engineering Chemistry Research* **2001**, *40*, 3237.
- (38)Huh, S.; Wiench, J. W.; Yoo, J.-C.; Pruski, M.; Lin, V. S. Y. *Chemistry of Materials* **2003**, *15*, 4247.
- (39)Ryoo, R.; Jun, S. *The Journal of Physical Chemistry B* **1997**, *101*, 317.
- (40)Ryoo, R.; Hyun Ko, C.; Park, I.-S. *Chemical Communications* **1999**, 1413.
- (41)Kruk, M.; Jaroniec, M.; Kim, J. M.; Ryoo, R. *Langmuir* **1999**, *15*, 5279.
- (42)Jaroniec, M.; Kruk, M.; Shin, H. J.; Ryoo, R.; Sakamoto, Y.; Terasaki, O. *Microporous and Mesoporous Materials* **2001**, *48*, 127.
- (43)Kruk, M.; Jaroniec, M.; Sakamoto, Y.; Terasaki, O.; Ryoo, R.; Ko, C. H. *The Journal of Physical Chemistry B* **1999**, *104*, 292.
- (44)Kruk, M.; Jaroniec, M.; Sayari, A. *Chemistry of Materials* **1999**, *11*, 492.
- (45)Kruk, M.; Jaroniec, M.; Sayari, A. *Langmuir* **1997**, *13*, 6267.
- (46)Sayari, A.; Liu, P.; Kruk, M.; Jaroniec, M. *Chemistry of Materials* **1997**, *9*, 2499.
- (47)Asefa, T.; Kruk, M.; MacLachlan, M. J.; Coombs, N.; Grondy, H.; Jaroniec, M.; Ozin, G. A. *Journal of the American Chemical Society* **2001**, *123*, 8520.
- (48)Brunel, D.; Blanc, A. C.; Galarneau, A.; Fajula, F. *Catalysis Today* **2002**, *73*, 139.

- (49) Calmettes, S.; Albela, B.; Hamelin, O.; Ménage, S.; Miomandre, F.; Bonneviot, L. *New Journal of Chemistry* **2008**, *32*, 727.
- (50) Yoshitake, H.; Yokoi, T.; Tatsumi, T. *Chemistry of Materials* **2002**, *14*, 4603.
- (51) Lei, B.; Li, B.; Zhang, H.; Zhang, L.; Li, W. *The Journal of Physical Chemistry C* **2007**, *111*, 11291.
- (52) Sun, L.-N.; Zhang, H.-J.; Peng, C.-Y.; Yu, J.-B.; Meng, Q.-G.; Fu, L.-S.; Liu, F.-Y.; Guo, X.-M. *The Journal of Physical Chemistry B* **2006**, *110*, 7249.
- (53) Anpo, M.; Yamashita, H.; Ikeue, K.; Fujii, Y.; Zhang, S. G.; Ichihashi, Y.; Park, D. R.; Suzuki, Y.; Koyano, K.; Tatsumi, T. *Catalysis Today* **1998**, *44*, 327.
- (54) Luo, Y.; Lin, J. *Microporous and Mesoporous Materials* **2005**, *86*, 23.
- (55) Zhang, H.; Zhang, Y.; Li, C. *Journal of Catalysis* **2006**, *238*, 369.
- (56) Khatri, P. K.; Singh, B.; Jain, S. L.; Sain, B.; Sinha, A. K. *Chem Commun (Camb)* **2011**, *47*, 1610.
- (57) Liu, Y.-M.; Cao, Y.; Yi, N.; Feng, W.-L.; Dai, W.-L.; Yan, S.-R.; He, H.-Y.; Fan, K.-N. *Journal of Catalysis* **2004**, *224*, 417.
- (58) Trukhan, N. N.; Derevyankin, A. Y.; Shmakov, A. N.; Paukshtis, E. A.; Kholdeeva, O. A.; Romannikov, V. N. *Microporous and Mesoporous Materials* **2001**, *44–45*, 603.
- (59) Lee, C.-H.; Lin, T.-S.; Mou, C.-Y. *The Journal of Physical Chemistry B* **2003**, *107*, 2543.
- (60) Selvam, P.; Dapurkar, S. E. *Applied Catalysis A: General* **2004**, *276*, 257.
- (61) Čapek, L.; Adam, J.; Grygar, T.; Bulánek, R.; Vradman, L.; Košová-Kučerová, G.; Čičmanec, P.; Knotek, P. *Applied Catalysis A: General* **2008**, *342*, 99.
- (62) Hu, S.; Liu, D.; Li, L.; Guo, Z.; Chen, Y.; Borgna, A.; Yang, Y. *Chemical Engineering Journal* **2010**, *165*, 916.
- (63) Kosslick, H.; Lischke, G.; Landmesser, H.; Parlitz, B.; Storek, W.; Fricke, R.

*Journal of Catalysis* **1998**, 176, 102.

(64)Liu, C.; Wang, S.; Rong, Z.; Wang, X.; Gu, G.; Sun, W. *Journal of Non-Crystalline Solids* **2010**, 356, 1246.

(65)Boote, B.; Subramanian, H.; Ranjit, K. T. *Chemical Communications* **2007**, 4543.

(66)Zhang, K.; Yuan, E.-H.; Xu, L.-L.; Xue, Q.-S.; Luo, C.; Albela, B.; Bonneviot, L. *European Journal of Inorganic Chemistry* **2012**, 2012, 4183.

(67)Ryoo, R.; Joo, S. H.; Kim, J. M. *The Journal of Physical Chemistry B* **1999**, 103, 7435.

(68)Zhang, J.; Luz, Z.; Goldfarb, D. *The Journal of Physical Chemistry B* **1997**, 101, 7087.

(69)Regev, O. *Langmuir* **1996**, 12, 4940.

(70)Attard, G. S.; Glyde, J. C.; Goltner, C. G. *Nature* **1995**, 378, 366.

(71)Zana, R.; Frasch, J.; Soulard, M.; Lebeau, B.; Patarin, J. *Langmuir* **1999**, 15, 2603.

(72)Frasch, J.; Lebeau, B.; Soulard, M.; Patarin, J.; Zana, R. *Langmuir* **2000**, 16, 9049.

(73)Patarin, J.; Lebeau, B.; Zana, R. *Current Opinion in Colloid & Interface Science* **2002**, 7, 107.

(74)Ruthstein, S.; Frydman, V.; Kababya, S.; Landau, M.; Goldfarb, D. *The Journal of Physical Chemistry B* **2003**, 107, 1739.

(75)Ruthstein, S.; Schmidt, J.; Kesselman, E.; Talmon, Y.; Goldfarb, D. *Journal of the American Chemical Society* **2006**, 128, 3366.

(76)Flodström, K.; Wennerström, H.; Alfredsson, V. *Langmuir* **2003**, 20, 680.

(77)Bonneviot, L.; Morin, M.; Badiei, A. 2001; Vol. WO 01/55031 A1.

(78)Moller, K.; Bein, T. *Chemistry of Materials* **1998**, 10, 2950.

(79)Goettmann, F.; Sanchez, C. *Journal of Materials Chemistry* **2007**, 17, 24.

- (80)Liu, J.; Shin, Y.; Nie, Z.; Chang, J. H.; Wang, L.-Q.; Fryxell, G. E.; Samuels, W. D.; Exarhos, G. J. *The Journal of Physical Chemistry A* **2000**, *104*, 8328.
- (81)Dufaud, V.; Davis, M. E. *Journal of the American Chemical Society* **2003**, *125*, 9403.
- (82)Margelefsky, E. L.; Bendjériou, A.; Zeidan, R. K.; Dufaud, V. r.; Davis, M. E. *Journal of the American Chemical Society* **2008**, *130*, 13442.
- (83)Abry, S.; Albela, B.; Bonneviot, L. *Comptes Rendus Chimie* **2005**, *8*, 741.
- (84)Katz, A.; Davis, M. E. *Nature* **2000**, *403*, 286.
- (85)Abry, S.; Thibon, A.; Albela, B.; Delichere, P.; Banse, F.; Bonneviot, L. *New Journal of Chemistry* **2009**, *33*, 484.
- (86)Wulff, G.; Heide, B.; Helfmeier, G. *Journal of the American Chemical Society* **1986**, *108*, 1089.
- (87)Hicks, J. C.; Jones, C. W. *Langmuir* **2006**, *22*, 2676.
- (88)Zhou, W.-J.; Albela, B.; Ou, M.; Perriat, P.; He, M.-Y.; Bonneviot, L. *Journal of Materials Chemistry* **2009**, *19*, 7308.
- (89)Jollet, V.; Albela, B.; Senechal-David, K.; Jegou, P.; Kolodziej, E.; Sainton, J.; Bonneviot, L.; Banse, F. *Dalton Transactions* **2013**, *42*, 11607.
- (90)Zhang, K.; Lam, K.-F.; Albela, B.; Xue, T.; Khrouz, L.; Hou, Q.-W.; Yuan, E.-H.; He, M.-Y.; Bonneviot, L. *Chemistry – A European Journal* **2011**, *17*, 14258.
- (91)Sayari, A. *Chemistry of Materials* **1996**, *8*, 1840.
- (92)Laha, S. C.; Kumar, R. *Microporous and Mesoporous Materials* **2002**, *53*, 163.
- (93)Peña, M. L.; Dejoz, A.; Fornés, V.; Rey, F.; Vázquez, M. I.; López Nieto, J. *M. Applied Catalysis A: General* **2001**, *209*, 155.
- (94)Selvam, P.; Dapurkar, S. *Journal of Catalysis* **2005**, *229*, 64.
- (95)Butler, A.; Clague, M. J.; Meister, G. E. *Chemical Reviews* **1994**, *94*, 625.
- (96)Taramasso M, P. G., Notari B. US Patent, **1983**, 4 410 501.

- (97) Keller, D. E.; Visser, T.; Soulimani, F.; Koningsberger, D. C.; Weckhuysen, B. M. *Vibrational Spectroscopy* **2007**, *43*, 140.
- (98) Went, G. T.; Oyama, S. T.; Bell, A. T. *The Journal of Physical Chemistry* **1990**, *94*, 4240.
- (99) Lee, E. L.; Wachs, I. E. *The Journal of Physical Chemistry C* **2008**, *112*, 6487.
- (100) Weckhuysen, B. M.; Jehng, J.-M.; Wachs, I. E. *The Journal of Physical Chemistry B* **2000**, *104*, 7382.
- (101) Wu, Z.; Kim, H.-S.; Stair, P. C.; Rugmini, S.; Jackson, S. D. *The Journal of Physical Chemistry B* **2005**, *109*, 2793.
- (102) Keller, D. E.; de Groot, F. M. F.; Koningsberger, D. C.; Weckhuysen, B. M. *The Journal of Physical Chemistry B* **2005**, *109*, 10223.
- (103) Keller, D. E.; Koningsberger, D. C.; Weckhuysen, B. M. *The Journal of Physical Chemistry B* **2006**, *110*, 14313.
- (104) Gijzeman, O. L. J.; van Lingen, J. N. J.; van Lenthe, J. H.; Tinnemans, S. J.; Keller, D. E.; Weckhuysen, B. M. *Chemical Physics Letters* **2004**, *397*, 277.
- (105) van Lingen, J. N. J.; Gijzeman, O. L. J.; Weckhuysen, B. M.; van Lenthe, J. H. *Journal of Catalysis* **2006**, *239*, 34.
- (106) Mars, P.; van Krevelen, D. W. *Chemical Engineering Science* **1954**, *3*, Supplement 1, 41.
- (107) Magg, N.; Immaraporn, B.; Giorgi, J. B.; Schroeder, T.; Bäumer, M.; Döbler, J.; Wu, Z.; Kondratenko, E.; Cherian, M.; Baerns, M.; Stair, P. C.; Sauer, J.; Freund, H.-J. *Journal of Catalysis* **2004**, *226*, 88.
- (108) Christodoulakis, A.; Machli, M.; Lemonidou, A. A.; Boghosian, S. *Journal of Catalysis* **2004**, *222*, 293.
- (109) Dutoit, D. C. M.; Schneider, M.; Fabrizioli, P.; Baiker, A. *Chemistry of Materials* **1996**, *8*, 734.

- (110) Luan, Z.; Xu, J.; He, H.; Klinowski, J.; Kevan, L. *The Journal of Physical Chemistry* **1996**, *100*, 19595.
- (111) Martínez-Huerta, M. V.; Gao, X.; Tian, H.; Wachs, I. E.; Fierro, J. L. G.; Bañares, M. A. *Catalysis Today* **2006**, *118*, 279.
- (112) Resini, C.; Montanari, T.; Busca, G.; Jehng, J.-M.; Wachs, I. E. *Catalysis Today* **2005**, *99*, 105.
- (113) Zhao, C.; Wachs, I. E. *The Journal of Physical Chemistry C* **2008**, *112*, 11363.
- (114) Gao, X.; Wachs, I. *Topics in Catalysis* **2002**, *18*, 243.
- (115) Gao, X.; Bare, S. R.; Fierro, J. L. G.; Wachs, I. E. *The Journal of Physical Chemistry B* **1999**, *103*, 618.
- (116) Wachs, I. E. *Applied Catalysis A: General* **2011**, *391*, 36.
- (117) Wei, D.; Wang, H.; Feng, X.; Chueh, W.-T.; Ravikovitch, P.; Lyubovsky, M.; Li, C.; Takeguchi, T.; Haller, G. L. *The Journal of Physical Chemistry B* **1999**, *103*, 2113.
- (118) Chao, K. J.; Wu, C. N.; Chang, H.; Lee, L. J.; Hu, S.-f. *The Journal of Physical Chemistry B* **1997**, *101*, 6341.
- (119) Gao, F.; Zhang, Y.; Wan, H.; Kong, Y.; Wu, X.; Dong, L.; Li, B.; Chen, Y. *Microporous and Mesoporous Materials* **2008**, *110*, 508.
- (120) Venkov, T. V.; Hess, C.; Jentoft, F. C. *Langmuir* **2006**, *23*, 1768.
- (121) Roozeboom, F.; Mittelmeijer-Hazeleger, M. C.; Moulijn, J. A.; Medema, J.; De Beer, V. H. J.; Gellings, P. J. *The Journal of Physical Chemistry* **1980**, *84*, 2783.
- (122) Beck, B.; Harth, M.; Hamilton, N. G.; Carrero, C.; Uhlich, J. J.; Trunschke, A.; Shaikhutdinov, S.; Schubert, H.; Freund, H.-J.; Schlögl, R.; Sauer, J.; Schomäcker, R. *Journal of Catalysis* **2012**, *296*, 120.
- (123) Dinse, A.; Ozarowski, A.; Hess, C.; Schomäcker, R.; Dinse, K.-P. *The Journal of Physical Chemistry C* **2008**, *112*, 17664.

- (124) Martínez-Huerta, M. V.; Coronado, J. M.; Fernández-García, M.; Iglesias-Juez, A.; Deo, G.; Fierro, J. L. G.; Bañares, M. A. *Journal of Catalysis* **2004**, 225, 240.
- (125) Rigutto, M. S.; Van Bekkum, H. *Applied Catalysis* **1991**, 68, L1.
- (126) Centi, G.; Perathoner, S.; Trifiro, F.; Aboukais, A.; Aissi, C. F.; Guelton, M. *The Journal of Physical Chemistry* **1992**, 96, 2617.
- (127) Sen, T.; Rajamohanam, P. R.; Ganapathy, S.; Sivasanker, S. *Journal of Catalysis* **1996**, 163, 354.
- (128) Phiriyawirut, P.; Jamieson, A. M.; Wongkasemjit, S. *Microporous and Mesoporous Materials* **2005**, 77, 203.
- (129) Tavolaro, A.; Tavolaro, P.; Drioli, E. *Journal of Crystal Growth* **2006**, 289, 609.
- (130) Guo, B.; Zhu, L.; Hu, X.; Zhang, Q.; Tong, D.; Li, G.; Hu, C. *Catalysis Science & Technology* **2011**, 1, 1060.
- (131) Chien, S.-H.; Ho, J.-C.; Mon, S.-S. *Zeolites* **1997**, 18, 182.
- (132) Anpo, M.; Higashimoto, S.; Matsuoka, M.; Zhanpeisov, N.; Shioya, Y.; Dzwigaj, S.; Che, M. *Catalysis Today* **2003**, 78, 211.
- (133) Ivanova, E.; Hadjiivanov, K.; Dzwigaj, S.; Che, M. *Microporous and Mesoporous Materials* **2006**, 89, 69.
- (134) Tielens, F.; Calatayud, M.; Dzwigaj, S.; Che, M. *Microporous and Mesoporous Materials* **2009**, 119, 137.
- (135) Baran, R.; Millot, Y.; Onfroy, T.; Averseng, F.; Krafft, J.-M.; Dzwigaj, S. *Microporous and Mesoporous Materials* **2012**, 161, 179.
- (136) Sen, T.; Ramaswamy, V.; Ganapathy, S.; Rajamohanam, P. R.; Sivasanker, S. *The Journal of Physical Chemistry* **1996**, 100, 3809.
- (137) Bhaumik, A.; Dongare, M. K.; Kumar, R. *Microporous Materials* **1995**, 5, 173.

- (138) Petras, M.; Wichterlova, B. *The Journal of Physical Chemistry* **1992**, *96*, 1805.
- (139) Zhang, S. G.; Higashimoto, S.; Yamashita, H.; Anpo, M. *The Journal of Physical Chemistry B* **1998**, *102*, 5590.
- (140) Dzwigaj, S.; Ivanova, E.; Kefirov, R.; Hadjiivanov, K.; Averseng, F.; Krafft, J. M.; Che, M. *Catalysis Today* **2009**, *142*, 185.
- (141) Nash, M. J.; Rykov, S.; Lobo, R. F.; Doren, D. J.; Wachs, I. *The Journal of Physical Chemistry C* **2007**, *111*, 7029.
- (142) Datta, S. J.; Yoon, K. B. *Microporous and Mesoporous Materials* **2011**, *143*, 115.
- (143) Luna, F. J.; Ukawa, S. E.; Wallau, M.; Schuchardt, U. *Journal of Molecular Catalysis A: Chemical* **1997**, *117*, 405.
- (144) Reddy, K. M.; Moudrakovski, I.; Sayari, A. *Journal of the Chemical Society, Chemical Communications* **1994**, *0*, 1059.
- (145) Arnold, A. B. J.; Niederer, J. P. M.; Nießen, T. E. W.; Hölderich, W. F. *Microporous and Mesoporous Materials* **1999**, *28*, 353.
- (146) Lim, S.; Haller, G. L. *The Journal of Physical Chemistry B* **2002**, *106*, 8437.
- (147) Mathieu, M.; Van Der Voort, P.; Weckhuysen, B. M.; Rao, R. R.; Catana, G.; Schoonheydt, R. A.; Vansant, E. F. *The Journal of Physical Chemistry B* **2001**, *105*, 3393.
- (148) Baltes, M. *Journal of Catalysis* **2001**, *197*, 160.
- (149) Hess, C.; Hoefelmeyer, J. D.; Tilley, T. D. *The Journal of Physical Chemistry B* **2004**, *108*, 9703.
- (150) Williams, T.; Beltramini, J.; Lu, G. Q. *Microporous and Mesoporous Materials* **2006**, *88*, 91.
- (151) Sudhakar Reddy, J.; Liu, P.; Sayari, A. *Applied Catalysis A: General*

1996, 148, 7.

(152) Chatterjee, M.; Iwasaki, T.; Hayashi, H.; Onodera, Y.; Ebina, T.; Nagase, T. *Chemistry of Materials* **1999**, 11, 1368.

(153) Qiao, Y.; Miao, C.; Yue, Y.; Xie, Z.; Yang, W.; Hua, W.; Gao, Z. *Microporous and Mesoporous Materials* **2009**, 119, 150.

(154) Grubert, G.; Rathouský, J.; Schulz-Ekloff, G.; Wark, M.; Zukal, A. *Microporous and Mesoporous Materials* **1998**, 22, 225.

(155) Dimitrova, R.; Spassova, M.; Kostova, N.; Tsoncheva, T.; Ivanova, L.; Minchev, C. *Applied Catalysis A: General* **2006**, 303, 207.

(156) Shylesh, S.; Singh, A. *Journal of Catalysis* **2005**, 233, 359.

(157) Tsoncheva, T.; Ivanova, L.; Dimitrova, R.; Rosenholm, J. *Journal of colloid and interface science* **2008**, 321, 342.

(158) Chiesa, M.; Meynen, V.; Van Doorslaer, S.; Cool, P.; Vansant, E. F. *Journal of the American Chemical Society* **2006**, 128, 8955.

(159) Luan, Z.; Meloni, P. A.; Czernuszewicz, R. S.; Kevan, L. *The Journal of Physical Chemistry B* **1997**, 101, 9046.

(160) Bastardo-Gonzalez, E.; Jones, W.; Bahranowski, K.; Łabanowska, M.; Serwicka, E. M. *Microporous and Mesoporous Materials* **2001**, 50, 61.

(161) Segura, Y.; Chmielarz, L.; Kustrowski, P.; Cool, P.; Dziembaj, R.; Vansant, E. F. *The Journal of Physical Chemistry B* **2005**, 110, 948.

(162) Yoshitake, H.; Tatsumi, T. *Chemistry of Materials* **2003**, 15, 1695.

(163) Busca, G.; Centi, G.; Marchetti, L.; Trifiro, F. *Langmuir* **1986**, 2, 568.

(164) Hirao, T. *Chemical Reviews* **1997**, 97, 2707.

(165) Xu, T.; Munson, E. J.; Haw, J. F. *Journal of the American Chemical Society* **1994**, 116, 1962.

(166) Chu, C. T. W.; Chang, C. D. *The Journal of Physical Chemistry* **1985**, 89, 1569.

- (167) Mohapatra, S.; Selvam, P. *Catalysis Letters* **2004**, *93*, 47.
- (168) Lee, C.-H.; Lin, T.-S.; Mou, C.-Y. *The Journal of Physical Chemistry C* **2007**, *111*, 3873.
- (169) Blasco, T.; Nieto, J. M. L. *Applied Catalysis A: General* **1997**, *157*, 117.
- (170) Solsona, B.; Blasco, T.; López Nieto, J. M.; Peña, M. L.; Rey, F.; Vidal-Moya, A. *Journal of Catalysis* **2001**, *203*, 443.
- (171) Zhang, Q.; Wang, Y.; Ohishi, Y.; Shishido, T.; Takehira, K. *Journal of Catalysis* **2001**, *202*, 308.
- (172) Zhou, R.; Cao, Y.; Yan, S.; Deng, J.; Liao, Y.; Hong, B. *Catalysis Letters* **2001**, *75*, 107.
- (173) Kondratenko, E. V.; Cherian, M.; Baerns, M.; Su, D.; Schlögl, R.; Wang, X.; Wachs, I. E. *Journal of Catalysis* **2005**, *234*, 131.
- (174) Liu, Y.-M.; Feng, W.-L.; Li, T.-C.; He, H.-Y.; Dai, W.-L.; Huang, W.; Cao, Y.; Fan, K.-N. *Journal of Catalysis* **2006**, *239*, 125.
- (175) Solsona, B.; Lopez Nieto, J. M.; D áz, U. *Microporous and Mesoporous Materials* **2006**, *94*, 339.
- (176) Knotek, P.; Čapek, L.; Bulánek, R.; Adam, J. *Topics in Catalysis* **2007**, *45*, 51.
- (177) Kondratenko, E. V.; Ovsitser, O.; Radnik, J.; Schneider, M.; Kraehnert, R.; Dingerdissen, U. *Applied Catalysis A: General* **2007**, *319*, 98.
- (178) Rozanska, X.; Fortrie, R.; Sauer, J. *The Journal of Physical Chemistry C* **2007**, *111*, 6041.
- (179) Bulánek, R.; Čičmanec, P.; Sheng-Yang, H.; Knotek, P.; Čapek, L.; Setnička, M. *Applied Catalysis A: General* **2012**, *415–416*, 29.
- (180) Mori, K.; Miyamoto, A.; Murakami, Y. *The Journal of Physical Chemistry* **1985**, *89*, 4265.
- (181) Liu, W.; Lai, S.; Dai, H.; Wang, S.; Sun, H.; Au, C. *Catalysis Letters*

**2007**, *113*, 147.

(182) Setnička, M.; Čičmanec, P.; Bulánek, R.; Zukal, A.; Pastva, J. *Catalysis Today* **2013**, *204*, 132.

(183) Feng, H.; Elam, J. W.; Libera, J. A.; Pellin, M. J.; Stair, P. C. *Journal of Catalysis* **2010**, *269*, 421.

(184) De la Rosa, R. I.; Clague, M. J.; Butler, A. *Journal of the American Chemical Society* **1992**, *114*, 760.

(185) Carter-Franklin, J. N.; Butler, A. *Journal of the American Chemical Society* **2004**, *126*, 15060.

(186) Messerschmidt, A.; Prade, L.; Wever, R. In *Biological Chemistry* 1997; Vol. 378, p 309.

(187) Totaro, R. M.; Williams, P. A. M.; Apella, M. C.; Blesa, M. A.; Baran, E. *J. Journal of the Chemical Society, Dalton Transactions* **2000**, 4403.

(188) Moriuchi, T.; Yamaguchi, M.; Kikushima, K.; Hirao, T. *Tetrahedron Letters* **2007**, *48*, 2667.

(189) Kikushima, K.; Moriuchi, T.; Hirao, T. *Tetrahedron* **2010**, *66*, 6906.

(190) Saikia, L.; Rajesh, M.; Srinivas, D.; Ratnasamy, P. *Catalysis Letters* **2010**, *137*, 190.

(191) Rothenberg, G.; Clark, J. H. *Organic Process Research & Development* **2000**, *4*, 270.

## Chapter 3. Chemicals and Characterization

### 3.1 Commercial products

The chemicals used in this study are detailed in the following.

#### 3.1.1 Solvents and gases

Table 1. Solvents utilized in this study.

Solvent	Purity	CAS
EtOH	96%	64-17-5
Acetone	>99,5%	67-64-1
cyclohexane	>99%	110-82-7
methanol	>99.6%	67-56-1
Deionized water		

Table 2. Gases utilized in this study.

Gas	Quality	Utilization
Argon	$\alpha$	Protection gas for synthesis
Nitrogen	U	Working gas for equipment
Air	Industrial	Working gas for equipment
Hydrogen		Working gas for equipment

#### 3.1.2 Reagents

Table 3. Reagents utilized in this study.

Reagents	Purity	Provider	CAS
Ludox HS-40	40%	Sigma-Aldrich	99439-28-8
Sodium hydroxide	>99%	Acros	1310-73-2
Cetyltrimethylammonium tosylate (CTATos)	>99%	Sigma-Aldrich	138-32-9
Tetramethylammonium bromide (TMABr)	>99%	Merck	200-581-2

Hydrochloric acid in water (HCl)	1 N	ACROS	7647-01-1
Aluminum sulfate hydrate	98%	Sigma-Aldrich	66578-72-1
Tetramethylammonium hydroxide in water (TMAOH)	20wt%	ACROS	75-59-2
Titanium(IV) n-butoxide (TBOT)	>98%	Alfa Aesar	5593-70-4
Titanium(IV) isopropoxide (TPOT)	>98%	ACROS	546-68-9
Vanadium(IV) sulfate	99.9%	Alfa Aesar	123334-20-3
Vanadium(V) triisopropoxide (VIP)	96%	Alfa Aesar	5588-84-1
2,2,5,5-tetramethyl-2,5-disila-1-azacyclopentane (TMDSACP)	97%	ABCR	7418-19-1
Tert-butyl hydroperoxide (TBHP) aqueous solution	30%	Alfa Aesar	75-91-2

### 3.2 Characterization method

**XRD:** Low angle powder X-ray powder diffraction (XRD) experiments were accomplished using a Bruker (Siemens) D5005 diffractometer using  $\text{CuK}\alpha$  monochromatic radiation.

**TGA:** Thermogravimetric analyses were carried out by using a DTA-TG Netzsch STA 409 PC/PG instrument. Samples (5-10 mg) placed in 70  $\mu\text{L}$  alumina crucible were heated in air flow (40 ml/min) up to 1000  $^{\circ}\text{C}$  at a heating rate of 10  $^{\circ}\text{C}/\text{min}$  with  $\text{N}_2$  as supporting gas (15 ml/min).

**$\text{N}_2$  sorption:** Nitrogen adsorption-desorption isotherms at 77 K were measured at BELSORPmax (BEL Japan, INC.). The pretreatment of samples were carried out by degassing at 130  $^{\circ}\text{C}$  for overnight to the samples without organic groups and for 2h to the samples possessing organic groups. The specific surface area was calculated according to the BET method in the 0.05-0.25 range of relative pressure. The

mesopore diameter evaluated by the pressure of the mesopore filling step of the nitrogen isotherm at 77 K ( $D_{\text{BdB}}(A) = 14.60994 + 74.67812 * X + 81.96198 * X^2 + 155.8457 * X^3$ ,  $X = p/p^0$  ( $0.11 \leq p/p^0 \leq 0.50$ )).<sup>1,2</sup>

**FT-IR:** Fourier transform infrared spectra (FT-IR) were recorded using a JASCO FT/IR-4200 (JASCO) spectrometer with ATR PRO470-H accessory, on which about 1 mg sample was measured by reflectance (%R).

**EPR:** Electron paramagnetic resonance (EPR) spectra were recorded using a Bruker Elexsys e500 X-band (9.4 GHz) spectrometer with a standard cavity.

**Solid NMR:** <sup>29</sup>Si NMR measurements were collected on a Bruker AVANCE III 500 spectrometer at 99.362 MHz. Solid samples were analyzed in a 4 mm zirconia rotor and spectra were recorded by magic angle spinning (MAS) at 5 kHz. Chemical shifts ( $\delta$ ) of <sup>29</sup>Si were externally referred to tetramethylsilane ( $\delta = 0.0$  ppm).

**UV-visible:** Solid UV-visible spectra were recorded using a JASCO V-670 (JASCO) spectrophotometer in the diffuse reflectance mode.

**Raman:** Unpolarized Raman spectra were excited with 514.5 nm and 244 nm of an argon-ion laser and recorded by the Horiba Jobin-Yvon Labram HR800 visible spectrometer in backscattering mode at room temperature.

**GC:** GC analyses were performed on a Varian GC-3800 chromatograph equipped with a FID detector, a DB-Wax GC column (30 m \* 0.25 mm \* 0.25  $\mu$ m). Nitrogen was used as carrier gas.

**H<sub>2</sub>-TPR:** Temperature Programmed Reduction measurements were run from room temperature to 800 degrees under H<sub>2</sub> flow.

### 3.3 References

- (1) Galarneau, A.; Desplantier, D.; Dutartre, R.; Di Renzo, F. *Microporous and Mesoporous Materials* **1999**, 27, 297.
- (2) Broekhoff, J. C. P.; De Boer, J. H. *Journal of Catalysis* **1967**, 9, 15.

## Chapter 4. Effect of Al(III) and Ti(IV) additives on vanadium dispersion in MCM-41 type silicas

### 4.1 Introduction

The transition metal supported material plays an important role in catalytic oxidation. Vanadium(V) peroxo complexes was considered as a catalyst for various oxidation reaction such as epoxidation and hydroxylation of alkene,<sup>1</sup> oxidation of aromatic,<sup>2,3</sup> alkane<sup>4,5</sup> and alcohol<sup>6</sup>. In heterogeneous catalysis the most regarded metal is titanium since the discovery of titanium silicalite-1 and 2 aluminum free structural analogues of ZSM-5 and ZSM-11 zeolites of MFI and MEL framework type, respectively. These microporous systems exhibit remarkable performance in catalytic oxidation of hydrocarbons in the selective oxidation for small molecules using H<sub>2</sub>O<sub>2</sub> as a green oxidant. For larger molecules, a lot of efforts have been devoted to Ti-MCM-41, Ti-SBA and other metals including vanadium since these systems possesses much larger pores (> 2 nm) than zeolites (< 1.2 nm). The vanadium equivalent were highly regarded owing to the specificity of this metal to catalyze direct oxidation of alkanes into primary alcohols, a highly relevant reaction for industry not feasible using supported titanium catalyst. In the case of epoxidation, the titanium catalyst gave mainly epoxidation of the double bond, whereas the vanadium catalyst favored oxidation of the alcohol moiety.<sup>7</sup> The first direct hydrothermal synthesis of V-MCM-41 was proposed by Reddy et al. showing its potential to catalyze the selective oxidation of cyclododecane and 1-naphthol by H<sub>2</sub>O<sub>2</sub>.<sup>8</sup> From then on, V-MCM-41 was synthesized by other method such as impregnation<sup>9-11</sup>, grafting<sup>2,3,12</sup> and chemical vapor deposition<sup>11</sup>, and was applied in the oxidation catalysis. Vanadium chemistry presents also another originality as an oxidant in the present of bromide evidenced by the discovery of the bromo peroxidase vanadium(V) enzyme of marine algae.<sup>13</sup>

Like in the case of titanium, it appears that the active sites in supported vanadium catalysts are unsaturated and isolated V(V) since the highest activity per vanadium is obtained for the lowest metal content.<sup>14</sup> Indeed, it is often invoked that the active sites are supported peroxo species analogue to the peroxo complexes active in homogeneous catalysis. Nonetheless, it is shown that the V-O-support covalent linkage is critical for the catalytic oxidation reaction particularly in the case of the selective oxidation of methanol to formaldehyde. This observation seems to hold true also in many other catalytic oxidation reaction though a systematic study.<sup>14</sup> Since V-O-V bridge are not so determinant while V-O-support binding seems necessary, it is important to improve the vanadium-support interaction to the detriment of vanadium pairs or oligomers. In other words, catalysts with the best vanadium dispersion are those with the highest potential for catalytic activity.

Unfortunately, the incorporation of vanadium into the framework of zeolites or inside mesoporous silica network and also its grafting on the surface of non porous silica has always been critical issue regarding the weakness of the V-O-Si bridges. Indeed, poor vanadium dispersion and high metal leaching under reaction condition are often observed.<sup>3,5</sup> The leaching depends on the nature of the substrate, the solvent and the oxidant.<sup>15</sup> Introduction of complexing amino groups nearby grafted (VO)<sup>2+</sup> species stabilizes the vanadium ions during the catalytic oxidation of benzene.<sup>12</sup> However, changing the nature of the oxides is a simpler solution. Considering reactivity, it was found that the best oxide can be ranked as follows: SiO<sub>2</sub> < Al<sub>2</sub>O<sub>3</sub> < Nb<sub>2</sub>O<sub>5</sub> < Ta<sub>2</sub>O<sub>5</sub> < TiO<sub>2</sub> < ZrO<sub>2</sub> < CeO<sub>2</sub>.<sup>14</sup> The authors concluded that higher TOF values corresponded to lower electronegativity of the support cation.<sup>14</sup> In other words, the more basic oxygen the better for grafting, site isolation and metal retention; this not surprising for vanadium IV or V, which are both strong and oxophilic Lewis acids. Accordingly vanadium supported on TiO<sub>2</sub> would be more active than on SiO<sub>2</sub>. However, it is much

easier to develop high surface area with SiO<sub>2</sub> than TiO<sub>2</sub> with a much larger versatility in pore design and morphology control and a much higher thermal stability useful for recyclability. This is the rationale for the high interest for hybrid support such as TiO<sub>2</sub>/SiO<sub>2</sub> systems where vanadium can bind on TiO<sub>2</sub> patches stabilized in a silica matrix.<sup>16</sup>

To better probe the dispersion of vanadium on silica, R. Bulánek *et al.* have recently proposed a method based on the quantification of the charge transfer bands measured by diffuse reflectance UV-visible spectroscopy.<sup>17</sup> It is proposed here to show that this method based on a Gaussian deconvolution of the band applies to MCM-41 type of silicas and to study the effect of aluminium and titanium heteroatoms on the vanadium dispersion. EPR spectroscopy is applied here to show that there is a correlation with the dispersion of the V(IV) ions which are oxidized into V(V) species.<sup>18</sup> Raman spectroscopy is used to reveal the bonding of Ti-O-V.

## 4.2 Experimental

### 4.2.1 Synthesis of 2D hexagonal mesoporous silica:<sup>19-21</sup>

pure silica LUS, this MCM-41 type mesoporous silica was prepared as follows: sodium hydroxide (32.0 g) was dissolved in distilled water (800 mL), then Ludox (187 mL) was added. Precipitation happened immediately when the mixture was formed after stirring the mixture at 40 °C for 24 h to form Na<sub>2</sub>SiO<sub>3</sub> solution. A second solution of CTATos (12.8 g) in distilled water (462 mL) was stirred for 1 h at 60 °C until the surfactant was dissolved completely. Na<sub>2</sub>SiO<sub>3</sub> solution (320 mL) was stirred for 1 h at 60 °C, and then added dropwise into the CTATos solution. The mixture was stirred for 2 h at 60 °C. The final parent gel was transferred into autoclave to be heated at 130 °C for 20 h. The resulting product was filtered and washed with distilled water. The as-synthesized solid was dried at 80 °C overnight.

Al-LUS was prepared in the similar way except that aluminium sulfate was added into the CTATos solution before it was mixed with  $\text{Na}_2\text{SiO}_3$  solution.

Ti-LUS was synthesized by TEOS as silica source, TMAOH as base source and TBOT as titanium source. The procedure is following: TEOS (83.3 g) was hydrolyzed by TMAOH (51.0 g) in the distilled water (179.2 g) at room temperature until the solution was clear. TBOT (6.8 g) dissolved in the isopropanol (50 mL) was added into the hydrolysed TEOS solution. The mixture was stirred at 0 °C until it turns into clear solution. A second solution of CTATos (16.4 g) in distilled water (358.5 g) was prepared the same way as LUS. The titania-silica solution was added dropwise into the CTATos solution at 60 °C and the mixture was stirred for 2 h at 60 °C. The mixture was transferred into the autoclave and was heated at 130 °C for 20 h. The resulting product was treated as LUS.

The surfactant contained in the as-synthesized product was removed by calcination at 550 °C for 10h. The calcined sample was used as support in the next impregnation preparation of vanadium-containing silica.

#### **4.2.2 Preparation of vanadium-containing materials:**

The vanadium species were incorporated using the incipient wetness impregnation method. The support was first dried and evacuated at 130 °C to remove air and other adsorbates. Then an “aqueous” solution of  $\text{VO}_2$  equivalent to the pore volume was added and mixed with the support under vacuum (incipient wetness technique). The powder was transferred to a Petri dish and dried in ambient air. This vanadium (IV)-containing product was calcined at 550 °C for 6 h in air flow. The products were named as LUS-V (x) where x (= 1.25, 2.5, 5) is the mole percentage of vanadium amount obtained from element analyst, Al (y)-LUS-V(x) where y (= 2.9, 5, 8) which

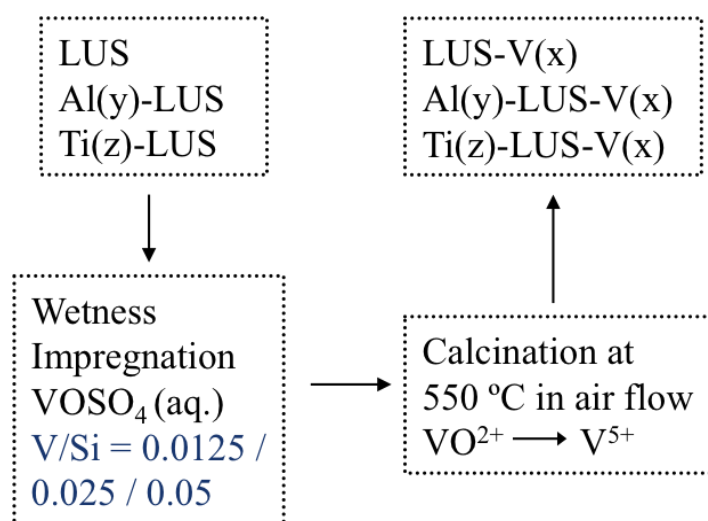
is the mole percentage of aluminium amount obtained from element analysis, Ti (z)-LUS-V(x) where z (= 2.8, 7, 12.5) which is the mole percentage of titanium amount obtained from element analyst.

### 4.3 Results and discussion

#### 4.3.1 Synthesis of materials and textural characterization

##### 4.3.1.1 Preparation of the materials

LUS support (MCM-41 type silica) was synthesized using CTATos as surfactant.<sup>21</sup> Supports containing heteroatoms were synthesized in similar conditions with an addition of heteroatom precursors during the preparation of parent gels. The support was calcined at 550 °C to remove the surfactant. The vanadium species were introduced by wetness impregnation of an aqueous solution of  $\text{VOSO}_4$  (Scheme 1). The sample was calcined again at 550 °C to oxidize the  $\text{VO}^{2+}$  to  $\text{V}^{5+}$ . All the samples were denoted as LUS-V(x), Al(y)-LUS-V(x) and Ti(z)-LUS-V(x). The x, y, z in the parenthesis are the content of the elements obtained from elementary analysis.



Scheme 1. Preparation process of impregnated vanadium containing materials.

### 4.3.1.2 Textural characterization

The MCM-41 hexagonal structure of the supports was characterized by low-angle XRD. The diffraction powder pattern of LUS (Figure 1a) showed readily distinguished bands indexed as (100), (110) and (200) of the 2D hexagonal point group. The patterns of Al(5)-LUS (Figure 1b) and Ti(7)-LUS (Figure 1c) showed a similar pattern with a decrease of the bands of (110) and (200) bands resulted from the incorporation of the heteroatom. The mesoporous structure was maintained during the vanadium incorporation and oxidation from vanadium (IV) to vanadium (V) (Figure 2) although the Al(5)-LUS and Ti(7)-LUS were not as perfect as the pure silica one.

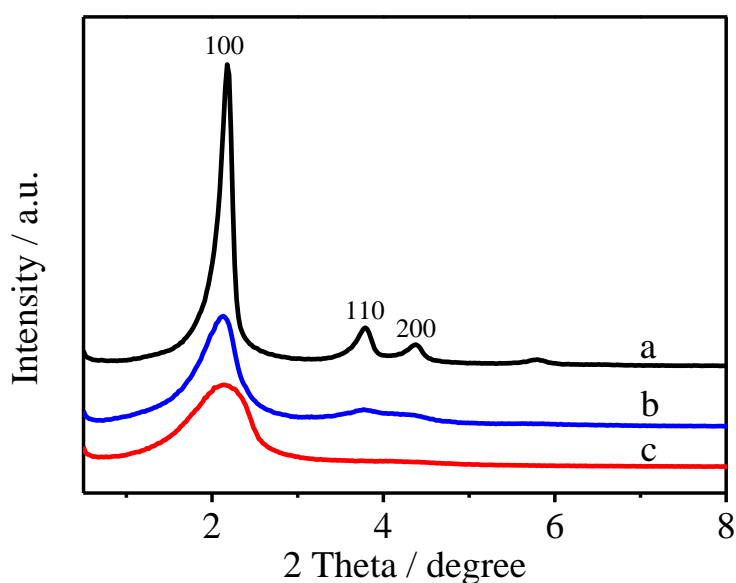


Figure 1. Low-angle XRD powder pattern of a.LUS, b. Al(5)-LUS, and c. Ti(7)-LUS.

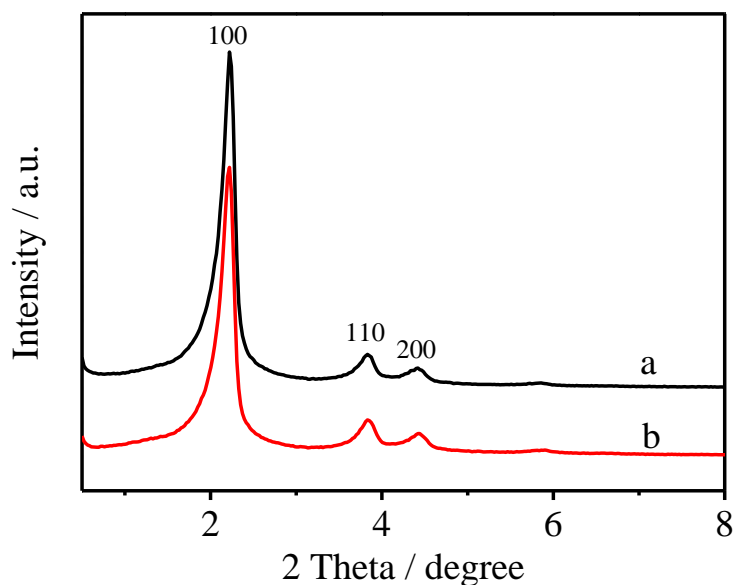


Figure 2. Low angle powder XRD of a. LUS-V(2.5) before calcination, and b. LUS-V(2.5) after calcination.

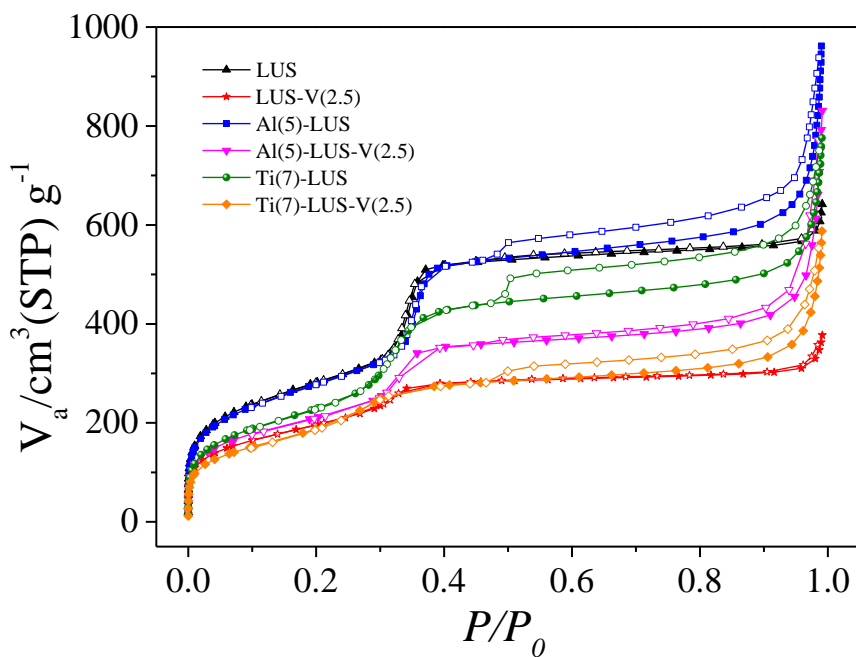


Figure 3.  $\text{N}_2$  adsorption-desorption isotherms of LUS (black up-triangle), LUS-V(2.5) (red star), Al(5)-LUS (blue square), Al(5)-LUS-V(2.5) (pink down-triangle), Ti(7)-LUS (green sphere) and Ti(7)-LUS-V(2.5) (orange diamond).

Nitrogen sorption isotherms at 77K were measured on samples evacuated at 130 °C (Figure 3). All the isotherms showed typical type (IV) isotherm according to IUPAC classification, which suggested all the series of samples possessed long-range order channels with opening pores of typical MCM-41 type silica. The specific BET surface of LUS and Al-LUS are around 1000 m<sup>2</sup>g<sup>-1</sup>, while the one of Ti-LUS is lower (839 m<sup>2</sup>g<sup>-1</sup>). The pore size of all the samples is 3.7 nm according to the BdB model. With the incorporation of vanadium species, the specific surface and the pore volume decreased due to partial degradation of the solid caused by the acidity of the VOSO<sub>4</sub> solution. Concomitantly, the BET constant C decreased for all the series after incorporation of vanadium species, which indicates that the surface was less polar, indicating the presence of vanadium species on the surface of the pores. (Table 1)

Table 1. Textural analysis of supports and materials with vanadium.

	Heteroatoms content <sup>a</sup>			S <sub>BET</sub> <sup>b</sup> (m <sup>2</sup> g <sup>-1</sup> )	V <sub>total</sub> <sup>c</sup> (cm <sup>3</sup> g <sup>-1</sup> )	D <sub>BdB</sub> <sup>d</sup> (nm)	C <sup>e</sup>
	V (mol %)	Al (mol %)	Ti (mol %)				
LUS	-	-	-	1018	0.86	3.7	99
LUS-V(2.5)	2.5	-	-	888	0.74	3.7	87
Al(5)-LUS	-	4.8	-	1011	0.94	3.8	86
Al(5)-LUS-V(2.5)	2.5	4.8	-	806	0.67	3.7	71
Ti(7)-LUS	-	-	7.1	839	0.78	3.7	72
Ti(7)-LUS-V(2.5)	2.5	-	7.1	810	0.62	3.6	51

[a] Results from elementary analysis.

[b] S<sub>BET</sub> calculated by using the Brunauer-Emmett-Teller (BET) equation over a range of relative pressure from 0.05 to 0.35.

[c] Total pore volume measured at P/P<sub>0</sub> = 0.90.

[d] Pore size diameter obtained from Broekhoff and de Boer method (BdB).

[e] BET parameter.

### 4.3.2 Vanadium state during the preparation

The preparation of the vanadium-supported material was performed with the  $\text{VOSO}_4$  salt corresponding to +4 oxidation state of vanadium. This  $3d^1$  ion possesses a  $S = 1/2$  spin state and is active in EPR as revealed by its very typical multiline spectrum. Indeed, it is expected that each eigenvalues of the  $g$  factor exhibits a splitting of eight lines due to the hyperfine structure of the  $I=7/2$   $^{51}\text{V}$  nuclei (natural abundance

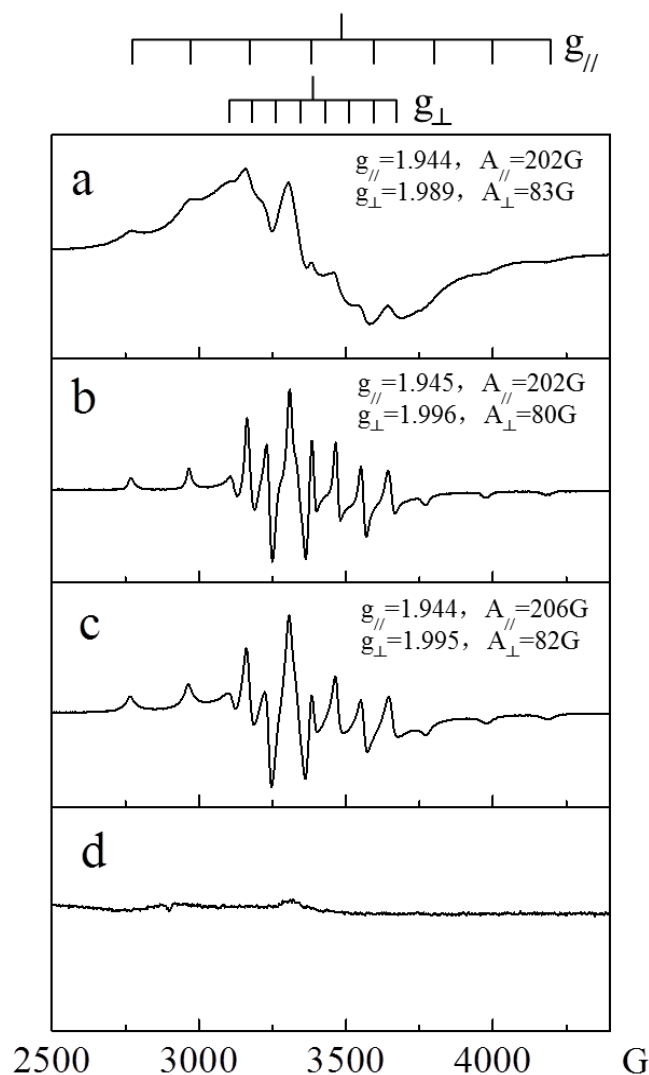


Figure 4. EPR spectra of a. LUS-V(2.5) before calcination, b. Al(5)-LUS-V(2.5) before calcination, c. Ti(7)-LUS-V(2.5) before calcination and d. Si-LUS-V(2.5) after calcination.

99.8%).(Figure 4) The paramagnetic parameters are  $g_{//} = 1.944 \pm 0.001$ , and  $A_{//} = 202 \pm 4\text{G}$ , where  $A$  is the hyperfine coupling constant. The perpendicular component parameters are  $g_{\perp} = 1.995 \pm 0.006$  and  $A_{\perp} = 82 \pm 2\text{G}$ . The signal was disappeared after calcination treatment. (Figure 4d) It is interesting to note that the hyperfine patterns of Al-LUS-V(2.5) (Figure 4b) and Ti-LUS-V(2.5) (Figure 4c) are better resolved than the one of LUS-V(2.5) (Figure 4a), indicating that V-V distance is closer in LUS-V(2.5) than those in the other two samples.<sup>22</sup>

Diffuse reflectance UV-visible spectroscopy is a simple, effective and very accessible experimental technique to provide information about the different oxidation states and coordination states of solid materials. Herein, the UV-visible spectra of LUS-V(2.5) before and after calcination are shown in Figure 5 as an example to understand the effect of calcination on the state of vanadium species. In the spectra of the sample before calcination(Figure 5a), the peaks at about  $13000\text{ cm}^{-1}$  and  $16000\text{ cm}^{-1}$  were attributed to the d-d transitions of V(IV), which is generally 30 times lower than the charge transfer band.<sup>23,24</sup> The signal on the high energy side was attributed to the charge transfer transition from oxygen to vanadium. After the oxidation (Figure 5b), the peaks of d-d transitions disappeared, and a complex multiple signal appeared in the region from  $20000\text{ cm}^{-1}$  to  $47000\text{ cm}^{-1}$  (500 nm to 200 nm). These bands are attributed to oxygen to V(V) charge transfer bands which are known to occur a much lower energies for V(V) than V(IV).<sup>25</sup> These data reveals that oxidation transformed all V(IV) into V(V) species. This is also confirmed by the disappearance of the EPR signal. (Figure 4d)

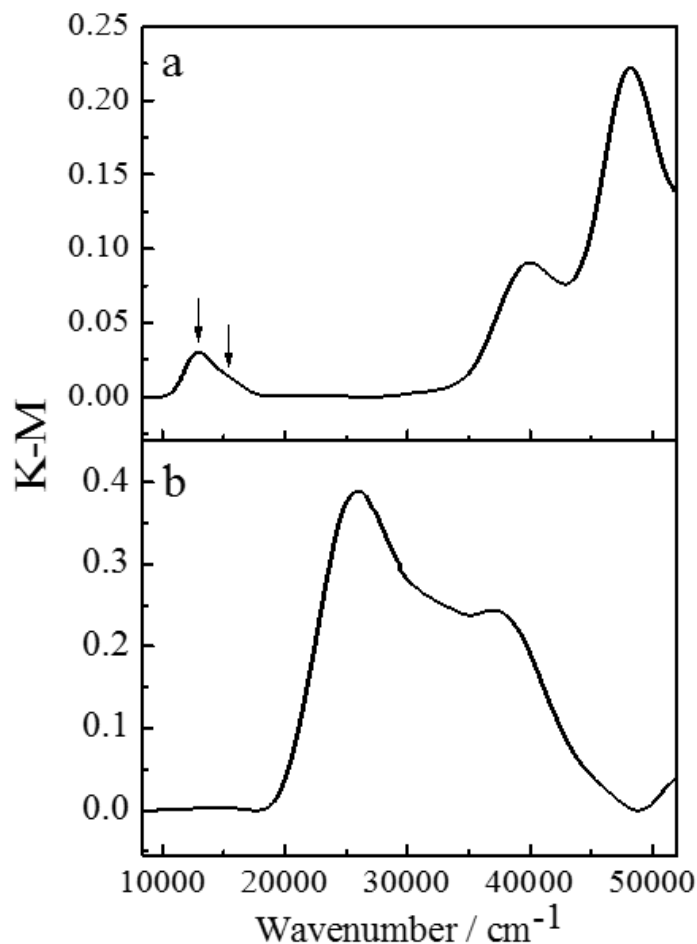


Figure 5. DR UV-visible spectra of a. LUS-V(2.5) before calcination, and b. LUS-V(2.5) after calcination.

#### 4.3.3 Analysis of vanadium species polymerization based on Tauc's plot.

UV-visible spectroscopy is considered as a simple and efficient method to understand the state of transition metals in heterogeneous catalysts. However, the raw data came from spectra were always obscure and hard to obtain direct information in the case of vanadium (V)-containing materials. Herein, we introduced a method related to the edge energies to compare the states of vanadium species in all samples.

There were several contributions to develop and apply to derive  $E_g$  values of solid materials from optical absorption spectra and diffuse reflectance spectra. Davis and Mott developed a general power law form as early as 1970. (Equation 1)

$$\alpha h\omega \propto (h\omega - E_g)^n \quad \text{Equation 1}$$

where  $\alpha$  is the absorption coefficient,  $h\omega = hv$  is the photon energy,  $n = 2, 3, 1/2$  and  $3/2$  for indirect allowed, indirect forbidden, direct allowed, and direct forbidden transitions, respectively. In fact, the  $n$  value for the specific transition was generally determined by the linear fit in the lower absorption region.<sup>26</sup> A similar equation was developed by Tauc via which the results was quite close to Davis and Mott's equation when  $n = 2$ . R. Bulanek *et al.* applied this method to compare the various UV-vis spectra of V-HMS displaying in the  $[F(R_\infty) hv]^2$  vs.  $hv$ . The comparison of the values of edge energies led to the conclusion of different distribution of vanadium species in all the samples.<sup>27</sup>

The DR UV-visible spectra of LUS-V(x), Al(5)-LUS-V(x) and Ti(7)-LUS-V(x) were transformed into Tauc's plot in Figure 6 and the edge energies of these samples were listed in Table 2. The ranking of edge energies is: Al(5)-LUS-V(5) < LUS-V(5) < LUS-V(2.5) = LUS-V(1.25) < Al(5)-LUS-V(2.5) < Al(5)-LUS-V(1.25) < Ti(7)-LUS-V(5) < Ti(7)-LUS-V(2.5) < Ti(7)-LUS-V(1.25), indicating the particle sizes of largest vanadium clusters or oligomers in the samples decreased in this order.

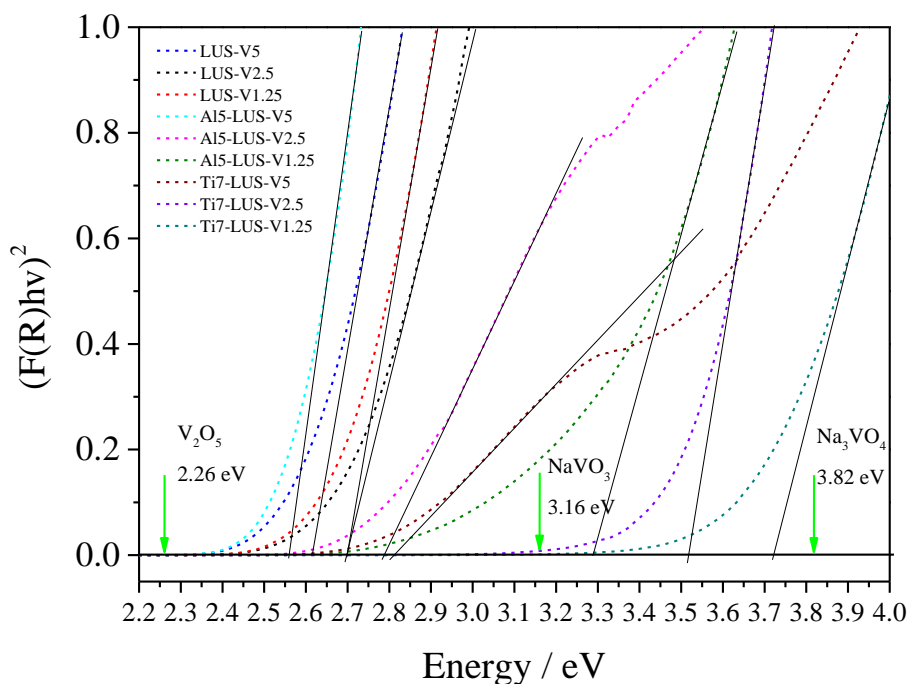


Figure 6. Tauc's plot based on UV-visible spectra of LUS-V(x), Al(5)-LUS-V(x) and Ti(7)-LUS-V(x).

It is noted that the sizes of largest vanadium species reduced with decreasing of vanadium contents in the samples. The possibility of forming clusters is reduced by decreasing the loading of vanadium. On the other hand, the sizes of vanadium species also decrease in the support with foreign atoms especially in the case of Ti-LUS. Three values of edge energies are marked as reference of 3D crystalline polymer vanadium oxide ( $V_2O_5$ ) (2.26 eV), linear oligomer ( $NaVO_3$ ) (3.16 eV) and monomer ( $Na_3VO_4$ ) (3.82 eV). Compared to reference, the largest particles in all three LUS-V(x) are small than crystalline cluster  $V_2O_5$ , but larger than linear polymer. Only in the case of Al(5)-LUS-V(1.25), Ti(7)-LUS-V(2.5) and Ti(7)-LUS-V(1.25), the largest particles in the samples are smaller than linear species, indicating that the well-dispersed vanadium species need more than twice in content of foreign atoms. All the edge energies are less than the value of monomer, which reveals that the presence of oligomers in all the samples.

Table 2. Edge energies of obtained from Tauc's plot of LUS-V(x), Al(5)-LUS-V(x), and Ti(7)-LUS-V(x).

	Edge energy (eV)
LUS-V(5)	2.61
LUS-V(2.5)	2.70
LUS-V(1.25)	2.70
Al(5)-LUS-V(5)	2.56
Al(5)-LUS-V(2.5)	2.79
Al(5)-LUS-V(1.25)	3.29
Ti(7)-LUS-V(5)	2.81
Ti(7)-LUS-V(2.5)	3.52
Ti(7)-LUS-V(1.25)	3.72

Considering that the introduction of Al and Ti affected the dispersion of vanadium species, different contents of foreign atoms were incorporated into the supports. The Tauc's plot of Al(y)-LUS-V(2.5) and Ti(z)-LUS-V(2.5) are compared with LUS-V(2.5) in Figure 7, and their values of edge energies are listed in Table 2. The increasing of aluminium contents in the samples doesn't change the state of the largest particles of vanadium species shown as the similar energies of Al(2.9)-LUS-V(2.5), Al(5)-LUS-V(2.5) and Al(8)-LUS-V(2.5). Differently, titanium atoms affect strongly on the polymerization of vanadium species which is suggested by the change of titanium contents in the supports. Energies increase with the increasing of titanium contents, which indicated that the vanadium species dispersed better in the samples with high concentrated titanium samples. The polymerization of titanium species increases with the contents in the samples.(Figure 8) As a consequence, the better dispersed vanadium species relates to the state of titanium in

the supports. The larger particles of titanium oxides contribute more to the dispersion of vanadium species.

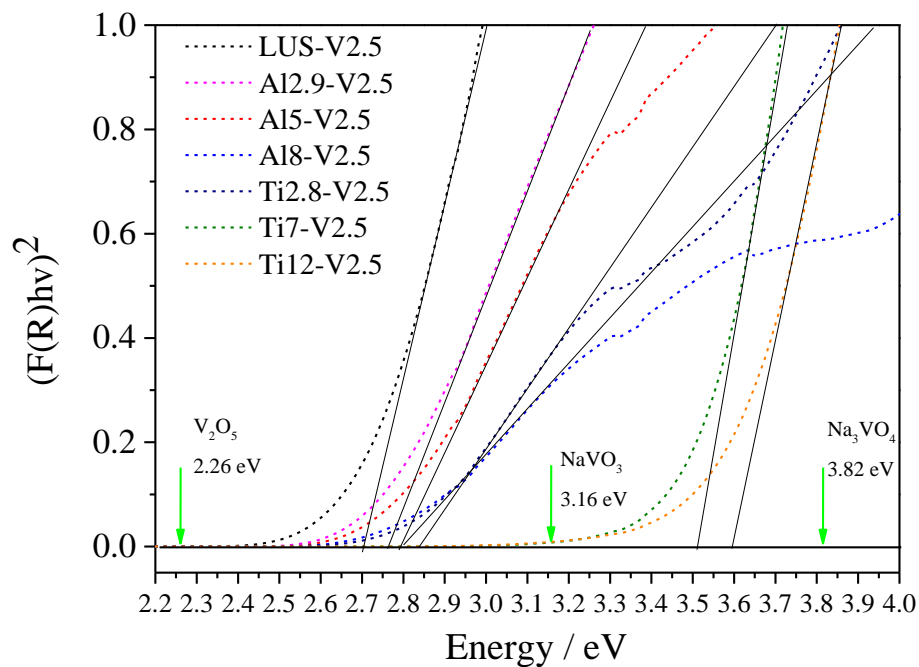


Figure 7. Tauc's plot based on UV-visible spectra of LUS-V(2.5), Al(y)-LUS-V(2.5), Ti(z)-LUS-V(2.5).

Table 3. Edge energies of obtained from Tauc's plot of LUS-V(2.5), Al(y)-LUS-V(2.5), and Ti(y)-LUS-V(2.5).

	Edge energy (eV)
LUS-V(2.5)	2.70
Al(2.9)-LUS-V(2.5)	2.76
Al(5)-LUS-V(2.5)	2.79
Al(8)-LUS-V(2.5)	2.79
Ti(2.8)-LUS-V(2.5)	2.84
Ti(7)-LUS-V(2.5)	3.52
Ti(12.5)-LUS-V(2.5)	3.59

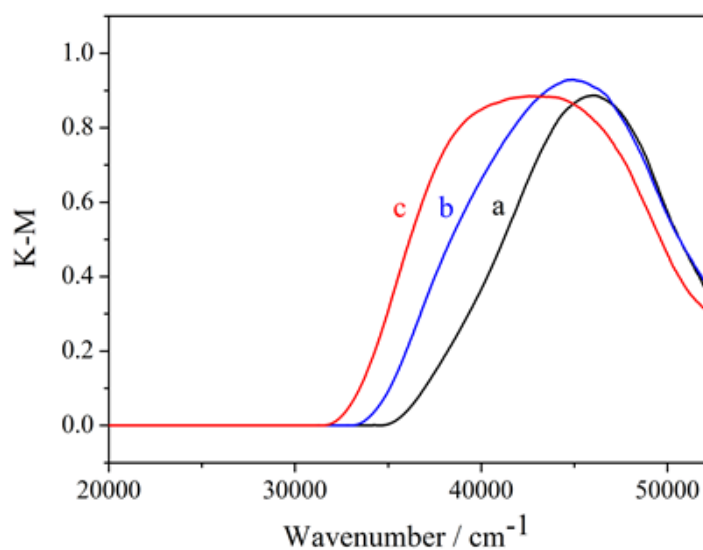


Figure 8. DR UV-visible spectra of a. Ti(2.8)-LUS, b. Ti(7)-LUS, and c. Ti(12.5)-LUS.

#### 4.3.4 Quantitative investigation of vanadium state on the different supports by DR UV-visible spectroscopy

The broad and overlapped UV-visible bands of the vanadium (V) spectra needed to be analysed more accurately. After being fitted by Gaussian curve, the multiple peaks attributed to vanadium (V) were clearly separated. Three or four peaks were necessary to fit the complex UV-visible band depending on the sample. The peak at  $25000\text{ cm}^{-1}$  (orange peak in Figure) is attributed to polymeric vanadium species. The one at  $30000\text{ cm}^{-1}$  (green peak in Figure) is attributed to oligomer and the two last at  $38000\text{ cm}^{-1}$  and  $35000\text{ cm}^{-1}$  (blue and violet peak in Figure) are attributed to monomer with different coordination environment.<sup>17</sup> In the case of Ti-LUS as support, it cannot be avoided that charge transfer transition of O-Ti contribute to the intensity of the adsorption band at  $38000\text{ cm}^{-1}$  and  $45000\text{ cm}^{-1}$ .

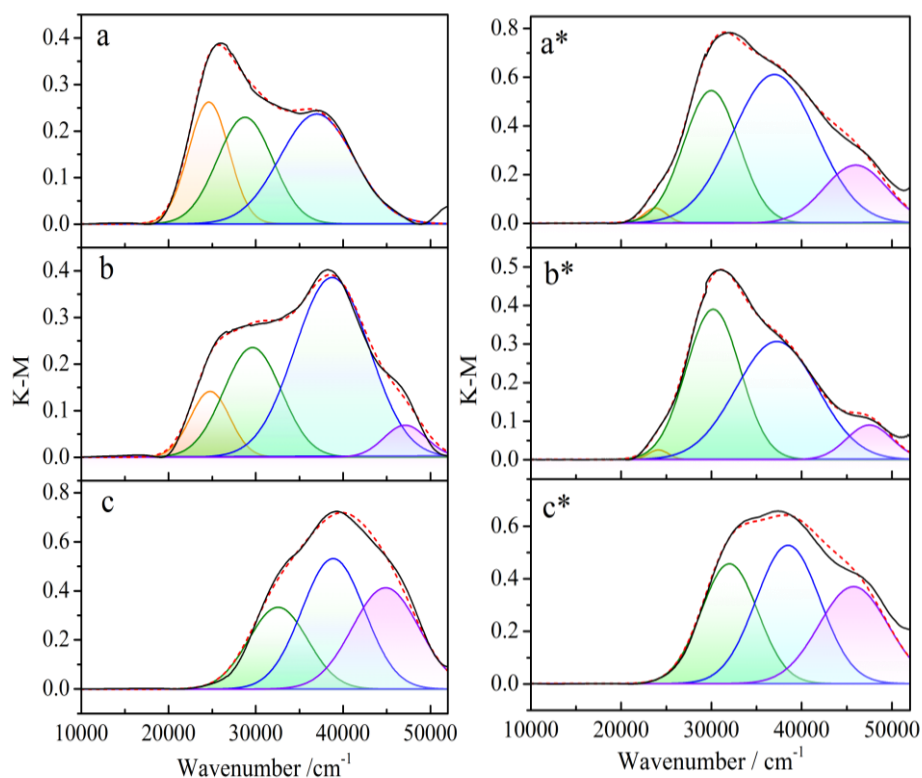


Figure 9. DR UV-visible spectra fitted by Gaussian curve of a. LUS-V(2.5), b. Al(5)-LUS-V(2.5), c. Ti(7)-LUS-V(2.5) and a\*. dehydrated LUS-V(2.5), b\*. dehydrated Al(5)-LUS-V(2.5), c\*. dehydrated Ti(7)-LUS-V(2.5)

It is noted that, there exists a clear blue shift of bands in the spectrum of Al(5)-LUS-V(2.5) (Figure 9b) compared to LUS-V(2.5) (Figure 9a), and even more in the spectrum of Ti(7)-LUS-V(2.5) (Figure 9c). That blue shift indicates that the particles of vanadium species are smaller in the Al-LUS as support. The lack of peaks at  $25000\text{ cm}^{-1}$  suggested that there existed no polymeric vanadium in Ti(7)-LUS-V(2.5), that is to say, there is less or no clusters in Ti(7)-LUS-V(2.5). The spectrum of dehydrated LUS-V(2.5) (Figure 9a\*) showed different bands while the one of Ti(7)-LUS-V(2.5) (Figure 9c\*) didn't change a lot. Meanwhile, the colour of LUS-V(2.5) powder changed from orange to light yellow after dehydration, and it turned back when the powder exposed in atmospheric condition. The intensity of the

band of LUS-V(2.5) shifted to higher energy after the dehydration, which suggested that the coordination state changed from high to low. It means that the polymeric species in LUS-V(2.5) were aggregated in the ambient condition with trace of water and were dispersed during the dehydration. The mechanism of the formation of vanadium cluster during the hydration was reported a lot in the literature.<sup>28-30</sup> This phenomenon was also found in the other transition metal supported materials such as Mo/SiO<sub>2</sub>.<sup>31-33</sup> This also proved that the vanadium species in the LUS-V(2.5) were immobilized.

To shed new light on the effect of heteroatom on the dispersion of vanadium ion on siliceous network, a series of silica LUS with or without Al(III) or Ti(IV) were impregnated with VOSO<sub>4</sub> salt. Furthermore, the supports with different heteroatom content were synthesized. All the samples were fitted by Gaussian curve via the same way as LUS-V(2.5), Al(5)-LUS-V(2.5) and Ti(7)-LUS-V(2.5). The coefficient R<sup>2</sup> of all fitting curve are over 0.99, which means the fitted curve is very close to the original spectra curve. (Table 4) The results of fitting were concluded in the Figure 10. Compared LUS with different vanadium content, it was easy to find out that the content of polymeric vanadium species increased with the increasing of vanadium content in the sample. The sample LUS-V(5) contained the most clusters of V<sub>2</sub>O<sub>5</sub> (orange column in the Figure 10). The same phenomena also happened in the Al-LUS and Ti-LUS as support. On the other hand, the effects of different heteroatom-containing supports were studied by comparing the LUS-V series with Al-LUS-V series and Ti-LUS-V series. It was widely observed that the Al-LUS-V series contained less polymeric vanadium species and more monomeric species (blue and violet column in Figure 10). Considered that the O-Ti charge-transfer transition was overlapped in the region of 38000 cm<sup>-1</sup> and 45000 cm<sup>-1</sup> (220-260nm),<sup>34,35</sup> the results after fitting were only compared the bands of polymers among all the samples.

It was still surprising that the Ti-LUS-V series contained less clusters than the other two series. When the vanadium content was decreased till 2.5 wt% and 1.25 wt%, there even didn't exist the clusters in the sample. Compared the Ti(2.8)-LUS-V(2.5), Ti(7)-LUS-V(2.5) and Ti(12.5)-LUS-V(2.5), it was also interesting that the clusters phase appeared when the titanium content in the support was decreased while the same phenomena didn't appear in the case of Al-LUS-V series. The UV-visible spectra of Ti-LUS (Figure 8) gave the information of titanium state in the Ti-LUS. With increasing of titanium content, the bands of Ti-O charge transfer shift to low energy region, which revealed the increasing of coordination number of titanium and formation of clusters in the samples. Combined the titanium state in Ti-LUS supports and the vanadium state introduced into these Ti-LUS supports, it was found that the vanadium species were easier to be immobilized on the larger particles of TiO<sub>2</sub>.

The results obtained from UV-visible spectra indicated that the heteroatoms were introduced into supports affected the formation of clusters of vanadium species. In the case of LUS, the V-O-Si was not strong enough which led to the vanadium species prefer to aggregate and form the cluster. When the Al and Ti atom existed on the surface of materials, the vanadium preferred to form V-O-Al and V-O-Ti firstly. Hence, the fact that Al-LUS-V and Ti-LUS-V were better dispersed than LUS-V suggested that the V-O-Al bond were stronger than V-O-Si, and V-O-Ti is the strongest one.

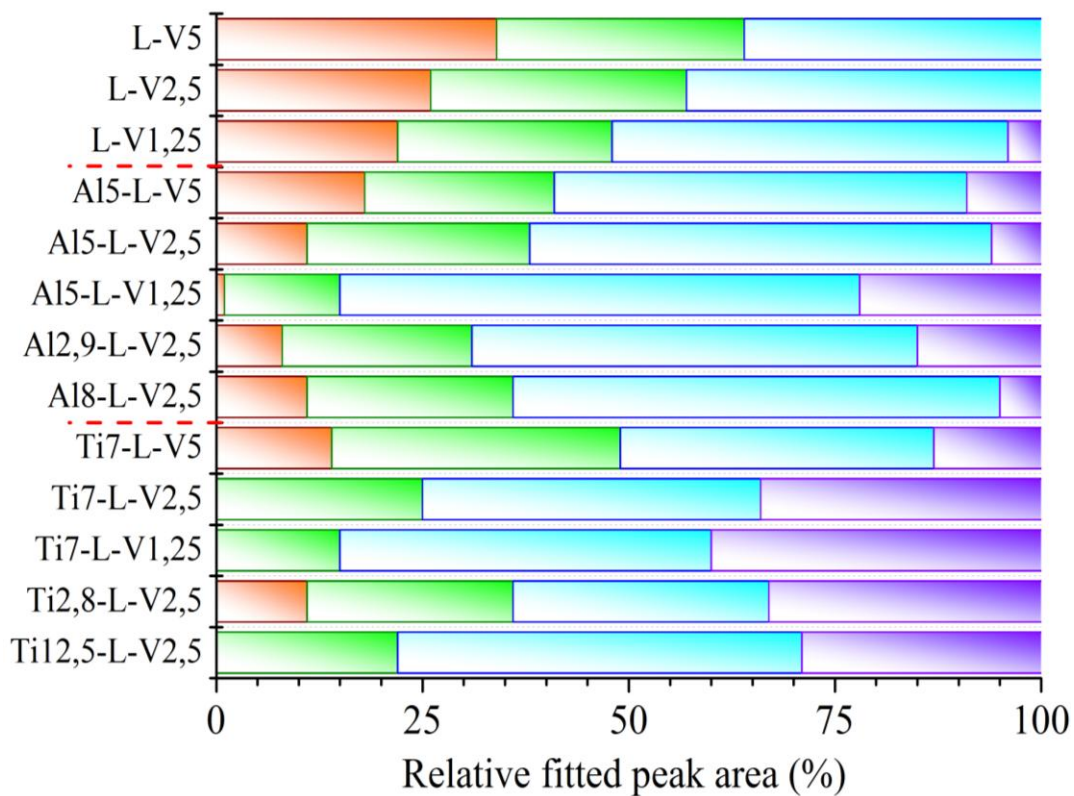


Figure 10. Relative fitted peak area of LUS-V series, Al-LUS-V series and Ti-LUS-V series.

Table 4. The detail of fitting Gaussian curve of all the sample.

	$R^2$	Peak A			Peak B			Peak C			Peak D		
		$X_c$ ( $\text{cm}^{-1}$ )	FWHM	A (%)	$X_c$ ( $\text{cm}^{-1}$ )	FWHM	A (%)	$X_c$ ( $\text{cm}^{-1}$ )	FWHM	A (%)	$X_c$ ( $\text{cm}^{-1}$ )	FWHM	A (%)
LUS-V1.25	0.999			22			26			48			4
LUS-V2.5	0.999	24610	5442	26	28762	7481	31	36986	9990	43	46169	3986	-
LUS-V5	0.992			34			30			36			-
Al5-LUS-V1.25	0.991			1			14			63			22
Al5-LUS-V2.5	0.998			11			27			56			6
Al5-LUS-V5	0.995	24758	5316	18	29622	7791	23	38745	10041	50	47105	5705	9
Al2.9-LUS-V2.5	0.999			8			23			54			15
Al8-LUS-V2.5	0.996			11			25			59			5
Ti7-LUS-V1.25	0.999			-			15			45			40
Ti7-LUS-V2.5	0.998			-			25			41			34
Ti7-LUS-V5	0.994	25332	4965	14	32557	7957	35	38865	8459	38	44874	9014	13
Ti2.8-LUS-V2.5	0.994			11			25			31			33
Ti12.5-LUS-V2.5	0.998			-			22			49			29

### 4.3.5 Investigation the Ti-O-V bonds based on Raman spectroscopy.

The investigation of V-O-Ti bonds was realized by Raman spectroscopy measurement, which is widely used in lots of work to discover the structural information of vanadium species.<sup>36-38</sup> The samples LUS, Ti(7)-LUS, LUS-V(2.5), Ti(7)-LUS-V(2.5) were measured under two different exciting wavelength: 244 nm and 514 nm.

Figure 11 showed Raman spectra of Ti(7)-LUS-V(1.25) compared with pure silica LUS, Ti(7)-LUS and LUS-V(2.5) as blank samples under 514 nm as exciting wavelength. The bands at 485, 605, 800  $\text{cm}^{-1}$  are attributed to the vibration of  $\text{SiO}_2$ . The 970  $\text{cm}^{-1}$  band which is assigned to Si-OH stretching intensified after Si-O-Ti forming. The existence of bands at around 1100  $\text{cm}^{-1}$  in the samples containing titanium or vanadium atoms is also resulted from the formation bonds of Si-O-Ti or Si-O-V. The strong bands located at 1030  $\text{cm}^{-1}$  come from terminal V=O of isolated

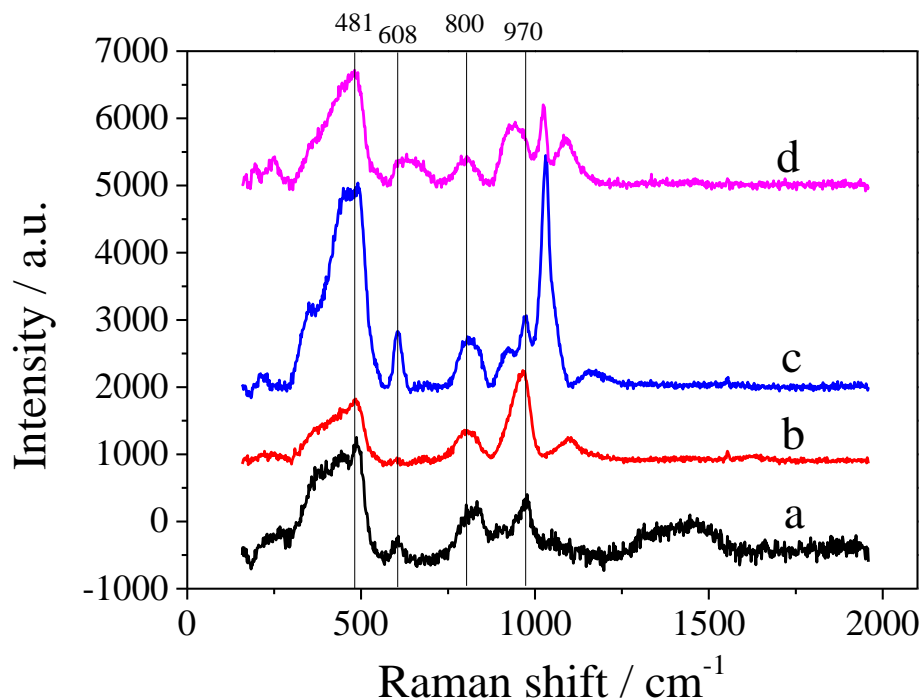


Figure 11. Raman spectra (exciting wavelength: 514 nm) of a. LUS, b. Ti(7)-LUS c. LUS-V(2.5), and d. Ti(7)-LUS-V(2.5).

$\text{VO}_4$  species. The absence bands at  $994\text{ cm}^{-1}$  reveals that no crystalline  $\text{V}_2\text{O}_5$  existed in vanadium containing samples.

The raw Raman spectra are not evident enough to show the difference of Ti(7)-LUS-V(2.5) from Ti(7)-LUS and LUS-V(2.5) due to various bands coming from vibration of silica. Transformation of Ti(7)-LUS + LUS-V(2.5) (Figure 12d) was carried out to identify the characteristic bands comparing to Ti(7)-LUS-V(2.5) (Figure 12a). The obvious difference appeared at 245, 640, 930 and  $1089\text{ cm}^{-1}$ . The 245 and  $640\text{ cm}^{-1}$  bands are assigned to bending and stretching modes of Ti-O-V bonds respectively<sup>16</sup>, which is an evidence of the Ti-O-V bonds forming. The change of 930 and  $1089\text{ cm}^{-1}$  is resulted from the change of Si-O-X bonds. Besides, there is a slight shift of V=O bands from  $1029$  to  $1023\text{ cm}^{-1}$  in the Ti(7)-LUS-V(2.5) also demonstrate the interaction between dispersed vanadium species and titanium species.<sup>16</sup>

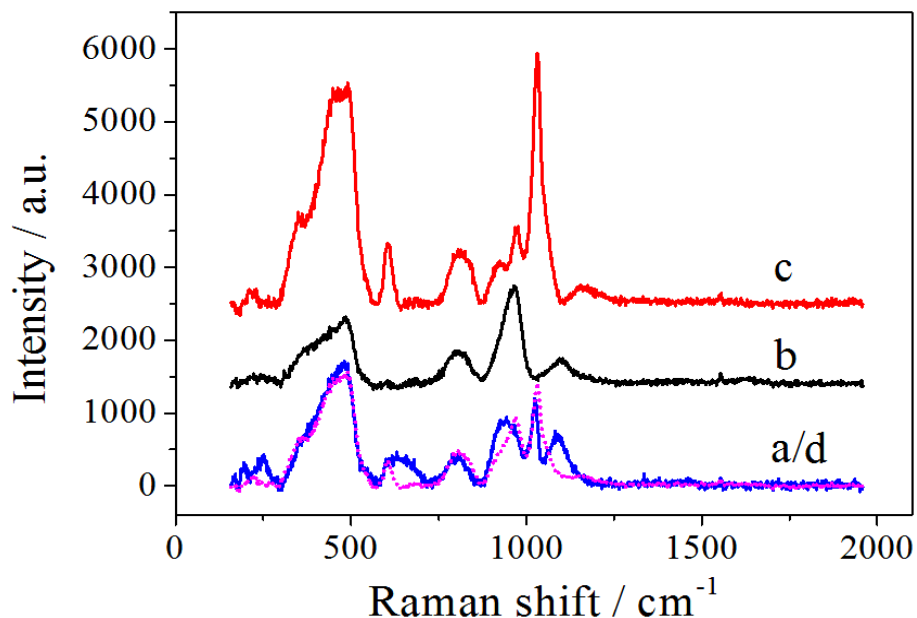


Figure 12. Raman spectra (exciting wavelength: 514 nm) of a. Ti(7)-LUS-V(2.5) (blue solid line), b. Ti(7)-LUS, c. LUS-V(2.5), and d.  $[\text{LUS-V}(2.5)+\text{Ti}(7)\text{-LUS}]*0.4$  (pink dash line).

The samples were also measured under 244 nm exciting wavelength which is close to the charge-transfer absorption of isolated titanium and vanadium species. In the spectra of pure silica LUS (Figure 13a), the bands at 490, 610  $\text{cm}^{-1}$  are attributed to vibration of 3, 4 siloxane rings respectively, while those one at 810 and 980  $\text{cm}^{-1}$  are assigned to Si-O-Si bonds and surface silanol groups Si-OH.<sup>38</sup> The bands at 1100  $\text{cm}^{-1}$  is ascribed to asymmetric stretching of Si-O bonds,<sup>35</sup> and its intensity increases after introduction of titanium atoms due to the formation of Si-O-Ti bonds (Figure 13b). This bands are also intensified in the spectra of LUS-V(2.5) (Figure 13c) and shift to low frequency (1070  $\text{cm}^{-1}$ ) because the Si-O-V bonds are weaker than Si-O-Ti. The bands at 1035  $\text{cm}^{-1}$  is attributed to the V=O bonds of monomer  $\text{VO}_4$ . The weak bands at 925  $\text{cm}^{-1}$  was believed by G. Xiong *et al.* to be assigned to V=O bonds in the

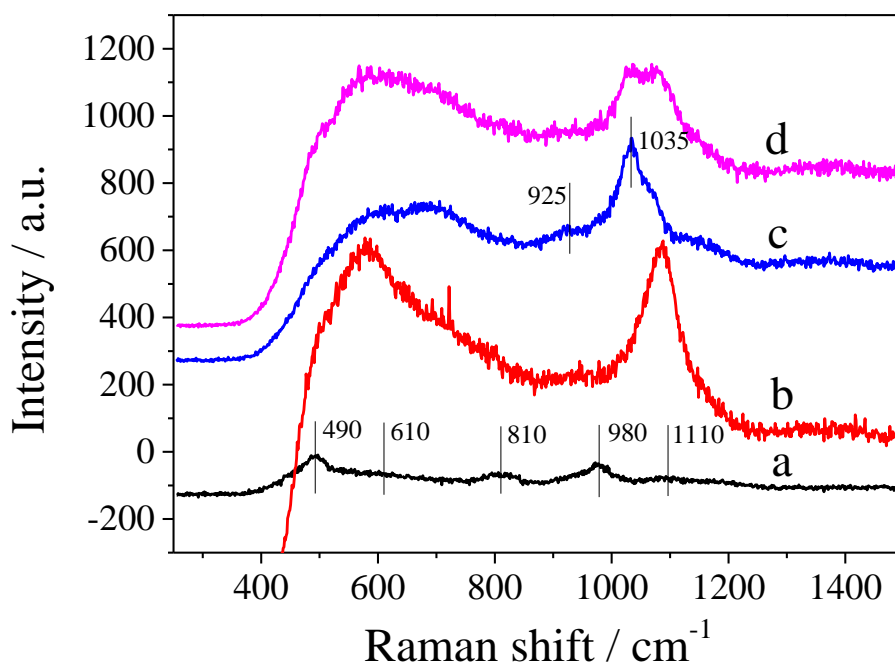


Figure 13. Raman spectra (exciting wavelength: 244 nm) of a. LUS, b. Ti(7)-LUS, c. LUS-V(2.5), and d. Ti(7)-LUS-V(2.5).

polymeric vanadium species. The spectra of Ti(7)-LUS-V(2.5) (Figure 13d) showed integrated bands of Ti(7)-LUS and LUS-V(2.5). A simple transformation as the way used in the spectra measured under 514 nm exciting wavelength was applied again in Figure 12. The difference is obvious at 1070  $\text{cm}^{-1}$  bands ascribed to asymmetric stretching mode of Si-O bonds connect to the Ti or V, while other bands are overlapped. This band in the Ti(7)-LUS-V(2.5) is less intense than the simulated LUS-V(2.5)+Ti(7)-LUS. It is believed that the decreasing of intensity is caused by the formation of Ti-O-V, which reduce the influence of titanium atoms to Si-O bonds. This slight difference is considered as an evidence of the presence of Ti-O-V bonds in the samples Ti(z)-LUS-V(x).

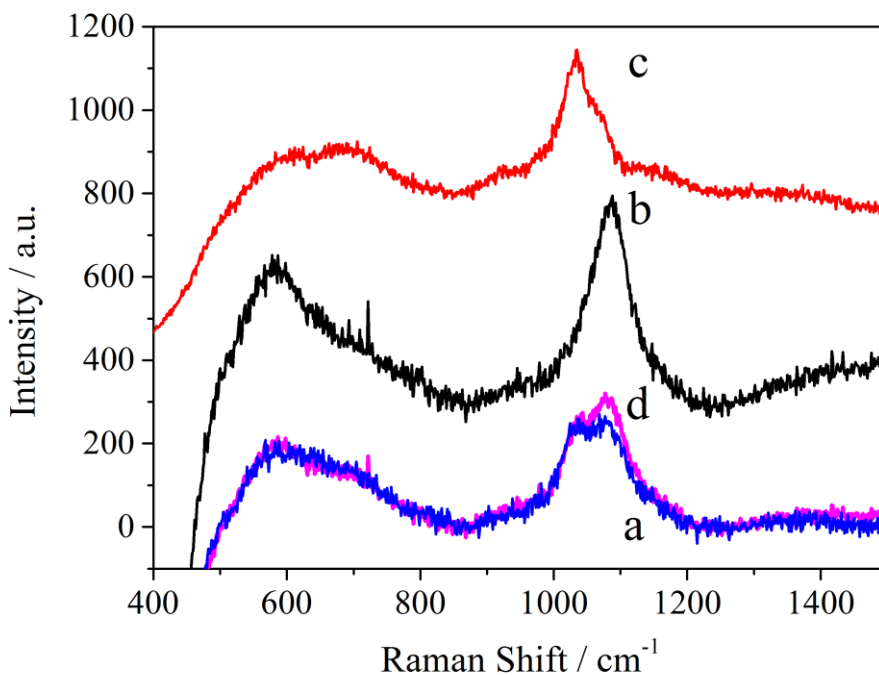


Figure 14. Raman spectra (exciting wavelength: 244 nm) of a. Ti(7)-LUS-V(2.5), b. Ti(7)-LUS, c. LUS-V(2.5), and d. [LUS-V(2.5)+Ti(7)-LUS]\*0.5 (pink line).

## 4.4 Conclusion

A series of vanadium supported on pure siliceous and Al or Ti modified MCM-41 type of materials and denoted LUS-V, Al-LUS-V and Ti-LUS-V were synthesized and investigated by EPR before calcination and diffuse reflectance UV-visible spectroscopy (DR UV-Visible) after calcination. The structural array of the channel as well as the porosity of the Ti and Al modified supports were checked using XRD powder pattern and nitrogen adsorption desorption isotherms showing that the general characteristics were close to that of the pure silica system. The vanadium species deposited by incipient wetness impregnation of the support using an aqueous solution of  $\text{VO}_2\text{SO}_4$  exhibited the classical  $S = 1/2$  eight lines spectra ( $I = 7/2$ ,  $^{51}\text{V}$  nuclei of natural abundance 99.8%) of isolated  $\text{V}^{4+}$  ( $d^1$  ion). Also before calcination, the EPR line broadening indicated that the species were much closer one to another on the pure silica system than in the Al and Ti modified ones. The V(IV) precursors were totally oxidized into V(V) species after calcination according to the complete disappearance of the V(IV) EPR signals concomitantly with the disappearance of all the d-d electronic transitions in the visible region of the DR UV-Visible spectra. The absorption band in the UV region of the spectra were consistent with a composite charge transfer bands of V(V) species. Their profound shape evolution and overall blue shift in the presence of Al or Ti additives in the supports were consistent with a higher vanadium dispersion, i.e., a distribution of smaller clusters hydrated oxo-hydroxo V(V) species. These charge transfer bands of the 13 different hydrated samples were fitted with only four different Gaussian functions defined by their line width and position while varying only their relative intensity. These Gaussian were very close to that of a Ti-LUS-V series obtained the best dispersion of vanadium species, Al-LUS-V series came second, and the Si-LUS-V contained the most polymeric vanadium species. Raman spectra provided some evidence to support the formation of Ti-O-V bonds in the samples.

## 4.5 Reference

- (1) Laha, S. C.; Kumar, R. *Microporous and Mesoporous Materials* **2002**, *53*, 163.
- (2) Shylesh, S.; Singh, A. *Journal of Catalysis* **2004**, *228*, 333.
- (3) George, J.; Shylesh, S.; Singh, A. P. *Applied Catalysis A: General* **2005**, *290*, 148.
- (4) Pe ña, M. L.; Dejoz, A.; Forn és, V.; Rey, F.; V ázquez, M. I.; López Nieto, J. M. *Applied Catalysis A: General* **2001**, *209*, 155.
- (5) Selvam, P.; Dapurkar, S. *Journal of Catalysis* **2005**, *229*, 64.
- (6) Butler, A.; Clague, M. J.; Meister, G. E. *Chemical Reviews* **1994**, *94*, 625.
- (7) Arends, I. W. C. E.; Sheldon, R. A.; Wallau, M.; Schuchardt, U. *Angewandte Chemie International Edition in English* **1997**, *36*, 1144.
- (8) Reddy, K. M.; Moudrakovski, I.; Sayari, A. *Journal of the Chemical Society, Chemical Communications* **1994**, *0*, 1059.
- (9) Berndt, H.; Martin, A.; Brückner, A.; Schreier, E.; Müller, D.; Kosslick, H.; Wolf, G. U.; Lücke, B. *Journal of Catalysis* **2000**, *191*, 384.
- (10) Solsona, B.; Blasco, T.; López Nieto, J. M.; Pe ña, M. L.; Rey, F.; Vidal-Moya, A. *Journal of Catalysis* **2001**, *203*, 443.
- (11) Grubert, G.; Rathouský, J.; Schulz-Ekloff, G.; Wark, M.; Zukal, A. *Microporous and Mesoporous Materials* **1998**, *22*, 225.
- (12) Lee, C.-H.; Lin, T.-S.; Mou, C.-Y. *The Journal of Physical Chemistry B* **2003**, *107*, 2543.
- (13) Butler, A.; Walker, J. V. *Chemical Reviews* **1993**, *93*, 1937.
- (14) Muylaert, I.; Van Der Voort, P. *Physical chemistry chemical physics : PCCP* **2009**, *11*, 2826.
- (15) Sudhakar Reddy, J.; Liu, P.; Sayari, A. *Applied Catalysis A: General* **1996**, *148*, 7.

- (16)Gao, X.; Bare, S. R.; Fierro, J. L. G.; Wachs, I. E. *The Journal of Physical Chemistry B* **1999**, *103*, 618.
- (17)Bulánek, R.; Čapek, L.; Setnička, M.; Čičmanec, P. *The Journal of Physical Chemistry C* **2011**, *115*, 12430.
- (18)Luan, Z.; Kevan, L. *The Journal of Physical Chemistry B* **1997**, *101*, 2020.
- (19)Bonnevot, L.; Morin, M.; Badiei, A. 2001; Vol. WO 01/55031 A1.
- (20)Calmettes, S.; Albela, B.; Hamelin, O.; Ménage, S.; Miomandre, F.; Bonneviot, L. *New Journal of Chemistry* **2008**, *32*, 727.
- (21)Zhang, K.; Albela, B.; He, M. Y.; Wang, Y.; Bonneviot, L. *Physical chemistry chemical physics : PCCP* **2009**, *11*, 2912.
- (22)Lee, C.-H.; Lin, T.-S.; Mou, C.-Y. *The Journal of Physical Chemistry C* **2007**, *111*, 3873.
- (23)Dutoit, D. C. M.; Schneider, M.; Fabrizioli, P.; Baiker, A. *Chemistry of Materials* **1996**, *8*, 734.
- (24)Chao, K. J.; Wu, C. N.; Chang, H.; Lee, L. J.; Hu, S.-f. *The Journal of Physical Chemistry B* **1997**, *101*, 6341.
- (25)Lever, A. B. P. *Inorganic Electronic Spectroscopy*; Elsevier: Amsterdam, 1984.
- (26)Gao, X.; Wachs, I. E. *The Journal of Physical Chemistry B* **2000**, *104*, 1261.
- (27)Bulánek, R.; Čičmanec, P.; Sheng-Yang, H.; Knotek, P.; Čapek, L.; Setnička, M. *Applied Catalysis A: General* **2012**, *415–416*, 29.
- (28)Gao, X.; Bare, S. R.; Weckhuysen, B. M.; Wachs, I. E. *The Journal of Physical Chemistry B* **1998**, *102*, 10842.
- (29)Xie, S.; Iglesia, E.; Bell, A. T. *Langmuir* **2000**, *16*, 7162.
- (30)Keller, D. E.; Visser, T.; Soulimani, F.; Koningsberger, D. C.; Weckhuysen, B. M. *Vibrational Spectroscopy* **2007**, *43*, 140.
- (31)Marcinkowska, K.; Rodrigo, L.; Kaliaguine, S.; Roberge, P. C. *Journal of*

*Molecular Catalysis* **1985**, *33*, 189.

(32) Marcinkowska, K.; Rodrigo, L.; Kaliaguine, S.; Roberge, P. C. *Journal of Catalysis* **1986**, *97*, 75.

(33) Stencel, J. M.; Diehl, J. R.; D'Este, J. R.; Makovsky, L. E.; Rodrigo, L.; Marcinkowska, K.; Adnot, A.; Roberge, P. C.; Kaliaguine, S. *The Journal of Physical Chemistry* **1986**, *90*, 4739.

(34) Koyano, K. A.; Tatsumi, T. *Microporous Materials* **1997**, *10*, 259.

(35) Yu, J.; Feng, Z.; Xu, L.; Li, M.; Xin, Q.; Liu, Z.; Li, C. *Chemistry of Materials* **2001**, *13*, 994.

(36) Luan, Z.; Meloni, P. A.; Czernuszewicz, R. S.; Kevan, L. *The Journal of Physical Chemistry B* **1997**, *101*, 9046.

(37) Gao, X.; Wachs, I. E. *Journal of Catalysis* **2000**, *192*, 18.

(38) Xiong, G.; Li, C.; Li, H.; Xin, Q.; Feng, Z. *Chemical Communications* **2000**, 677.

## Chapter 5. Improvement of vanadium dispersion using molecular surface engineering

### 5.1 Introduction

According to the results reported in the last chapter, the addition of foreign ions such as Al(III) or Ti(IV) to the supports improve the dispersion of vanadium species. A quantitative treatment of the UV visible spectra and vanadium leaching tests let us to propose that Ti(IV) has a more beneficial effect than Al(III) on dispersion. This is attributed to the chemical anchoring role of titanium or aluminum through oxo bridges with the following ranking of stability  $V-O-Ti > V-O-Al > V-O-Si$ . Noteworthy, the aluminum or titanium species were distributed all through the bulk of the siliceous matrix of the pore wall since the MCM-41 mesophase was prepared directly by mixing both the foreign ions and silica precursors into the sol-gel synthesis. It is likely that a fair fraction of the aluminum or titanium ions were not accessible to vanadium species, leading to anchoring effect of poor efficiency. A better approach consists to locate by design the anchoring function exclusively on the surface to ensure a better potentiality for direct bonding to the vanadium ion. This is the purpose of this chapter.

On the advantage of grafting is to start with a well-controlled pure silica phase as a support. The anchoring may be obtained from a ligand tethered to the silica surface. This is the approach adopted by P. K. Khatri and his colleagues to fix an oxo-vanadium Schiff base on MCM-41 silica for hydroxylation of benzene with  $H_2O_2$ . Cyclotriphosphazene groups were grafted at first to immobilize the oxo-vanadium Schiff base. The catalytic materials showed magnificent performance in catalytic oxidation.<sup>1</sup> However, the synthesis of precursors i.e. cyclotriphosphazene and

oxo-vanadium Schiff base is complicated, difficult and too expensive for any industrial application. It is preferable to simplify the synthesis and use cheap commercial vanadium precursor such as  $\text{VO}(\text{SO}_4)_2$  and eventually triisopropoxyvanadium (V) oxide. Meanwhile, other functional groups can be introduced to create a proper environment for active sites.

Molecular Stencil Patterning (MSP) is a technique developed in our group to control the dispersion of metal ion, their molecular vicinity and the hydrophobicity in the nano channel of MCM-41 type silica.<sup>2-6</sup> Then, multiple functional sites can co-exist together in a nano-confined space while maintaining accessibility. Organosilane are grafted to surface silanol groups not only to tune the hydrophobic of the surface but also to dilute and isolate the second functional sites.<sup>2,6</sup> This is technique based on a sequential transformation of the surface. The surfactant used as a molecular masking agent is partially removed to provide vacancy for the first functional groups that is grafted at second. The masking surfactant is removed at the third step for the introduction of the second functional groups processed at fourth. The self-repulsion of positive charge of the surfactant head ensures a regular patterned mask and consequently a homogeneous dispersion of the grafted groups. In the work of S. Abry,<sup>2</sup> Trimethylsilyl groups (TMS) provided a hydrophobic environment and the vacancy for the second functions. Bromopropylsilyl tripod tethers were introduced following in order to connect a tetradentate ligand ( $\text{N,N}'$ -bis(2-pyridinylmethyl)ethane-1,2-diamine). The target copper ions coordinated to the ligands to form final materials. The trimethylsilyland diamine groups created a bio-mimic environment for the copper ions which was inspired from bio-catalysis. Hence, this technique opened a wide range of possibilities to design new types of heterogeneous catalysts with high molecular definition.<sup>2</sup>

In this chapter, novel vanadium-containing materials are prepared by grafting vanadium ions as well as anchoring titanium (IV) ions using the MSP technique described above. Cheap and simple commercial vanadium were used and the more robust organosilane (2,2,5,5-tetramethyl-2,5-disila-1-azacyclopentane) was used because of its potential double grafting functions instead of the monopodal trimethylsilyl used by Abry et al. (see above). Therefore, the purpose is to demonstrate that combining the MSP technique to the anchoring effect of Ti lead not only to a better dispersion, a stronger linkage and a higher catalytic activity. To proceed and generate blanks for comparison, four series of vanadium-containing MCM-41 type silicas with different environments were developed: V grafted only, V and organic pattern, V plus Ti anchors, V plus Ti anchors and organic patterning. Their textual characteristic properties and the states of vanadium species were studied to characterize the nature of the vanadium sites in final materials. UV-visible spectroscopy, a simple and inexpensive characteristic technique, was utilized to quantify as much as possible the relative distribution between the vanadium species on different modified surfaces.

## 5.2 Experimental

### 5.2.1 Synthesis of 2D hexagonal mesoporous silica<sup>7</sup>.

Pure silica LUS, this MCM-41 type mesoporous silica was prepared as follows: sodium hydroxide (32.0 g) was dissolved in distilled water (800 mL), then Ludox (187 mL) was added. Precipitation happened immediately when the mixture was formed after stirring the mixture at 40 °C for 24 h to form Na<sub>2</sub>SiO<sub>3</sub> solution. A second solution of CTATos (12.8 g) in distilled water (462 mL) was stirred for 1 h at 60 °C until the surfactant was dissolved completely. Na<sub>2</sub>SiO<sub>3</sub> solution (320 mL) was stirred for 1 h at 60 °C, and then added dropwise into the CTATos solution. The mixture was

stirred for 2 h at 60 °C. The final parent gel was transferred into autoclave to be heated at 130 °C for 20 h. The resulting product was filtered and washed with distilled water. The as-synthesized solid was dried at 80 °C overnight.

## 5.2.2 Preparation of vanadium-containing silica catalysts.

The preparation process of LUS-V(x), LUS-Ti(y)-V(x), LUS-E-V(x) and LUS-E-Ti(x)-V(x) is shown in Scheme 1.

### 5.2.2.1 Preparation of LUS-V(x)

(x=1.25, 2.5, 5, which represented the mol% to SiO<sub>2</sub> of vanadium content in the preparation process).

**Step 1.** Removal of surfactant. 1 g LUS powder was dispersed in 40 mL ethanol (tech) following the addition of 1.1 eq. HCl to the moles of CTA ions in the channel which was quantified via Thermo Gravimetric Analysis (TGA). The solution was stirred at 40 °C for 1 h. The powder was filtered, washed by EtOH and acetone for 3 times, and dried in the room ambience. This process was repeated 3 times. The final powder was dried at 80 °C overnight.

**Step 2.** Grafting of vanadium species. 1 g LUS powder without surfactant was activated in the round bottom flask under vacuum at 130 °C for 2 h. The round bottom flask was filled with Ar after activation of silica powder. 40 mL cyclohexane was added as a solvent following the addition of vanadium precursors triisopropoxyvanadium (V) oxide (VIP). The mixture was refluxed at 80 °C for 16 h. The final products was filtered, washed by cyclohexane for 3 times and dried at 80 °C overnight.

### 5.2.2.2 Preparation of LUS-Ti(y)-V(x)

( $x=1.25, 2.5, 5$  and  $y=5$ , which represented the mol% to  $\text{SiO}_2$  of vanadium and titanium content respectively in the preparation process).

**Step 1.** Removal of surfactant. This procedure was same as Step 1 in the preparation of LUS-V(x).

**Step 2.** Grafting of titanium species. The procedure was same as the grafting of vanadium species except that the precursor was replaced by titanium isopropoxide (TPOT).

**Step 3.** Grafting of vanadium species. The procedure was same as Step 1 in the preparation of LUS-V(x) except that the silica was replaced by titanium-containing silica obtained in last step.

### 5.2.2.3 Preparation of LUS-E-V(x)

( $x=1.25, 2.5, 5$ , which represented the mol% to  $\text{SiO}_2$  of vanadium content in the preparation process).

**Step 1.** Ion exchange of CTA by TMA cations. TMABr (3 eq. to CTA) was mixed with 40mL EtOH at 40 °C following the addition of 1 g LUS as-made powder. The mixture continued to be stirred at 40 °C for 45 min. The ion-exchanged samples were filtered, washed by EtOH and acetone for 3 times, dried at room ambience. This process was repeated for 3 times.

**Step 2.** Partial removal of TMA ions used as masked agent. 1 g ion-exchanged silica powder was dispersed in 40 mL EtOH with 0.5 eq. HCl to TMA moles contents (quantified via TGA). The mixture was stirred at 40 °C for 1h. The powder was filtered, washed by EtOH and acetone for 3 times and dried at 80 °C overnight.

**Step 3.** Grafting of functional groupethyl-1,2-bis(dimethylsilyl) (EBDMS). 1 g silica obtained in the last step was mixed with 40 mL cyclohexane and 3 eq. 2,2,5,5-tetramethyl-2,5-disila-1-azacyclopentane(TMDSACP) to the moles of half

Si-OH on the surface which was qualified by  $^{29}\text{Si-NMR}$ . The mixture was stirred at  $80\text{ }^{\circ}\text{C}$  for 16 h. The powder was filtered, washed by EtOH and acetone for 3 times and dried at  $80\text{ }^{\circ}\text{C}$  overnight. The final product was named as LUS-E.

**Step 4.** Grafting of vanadium species. The procedure was same as Step 1 in the preparation of LUS-V(x) except that the silica was replaced by LUS-E.

#### **5.2.2.4 Preparation of LUS-E-Ti(y)-V(x)**

( $x=1.25, 2.5, 5$  and  $y=5$ , which represented the mol% to  $\text{SiO}_2$  of vanadium and titanium content respectively in the preparation process).

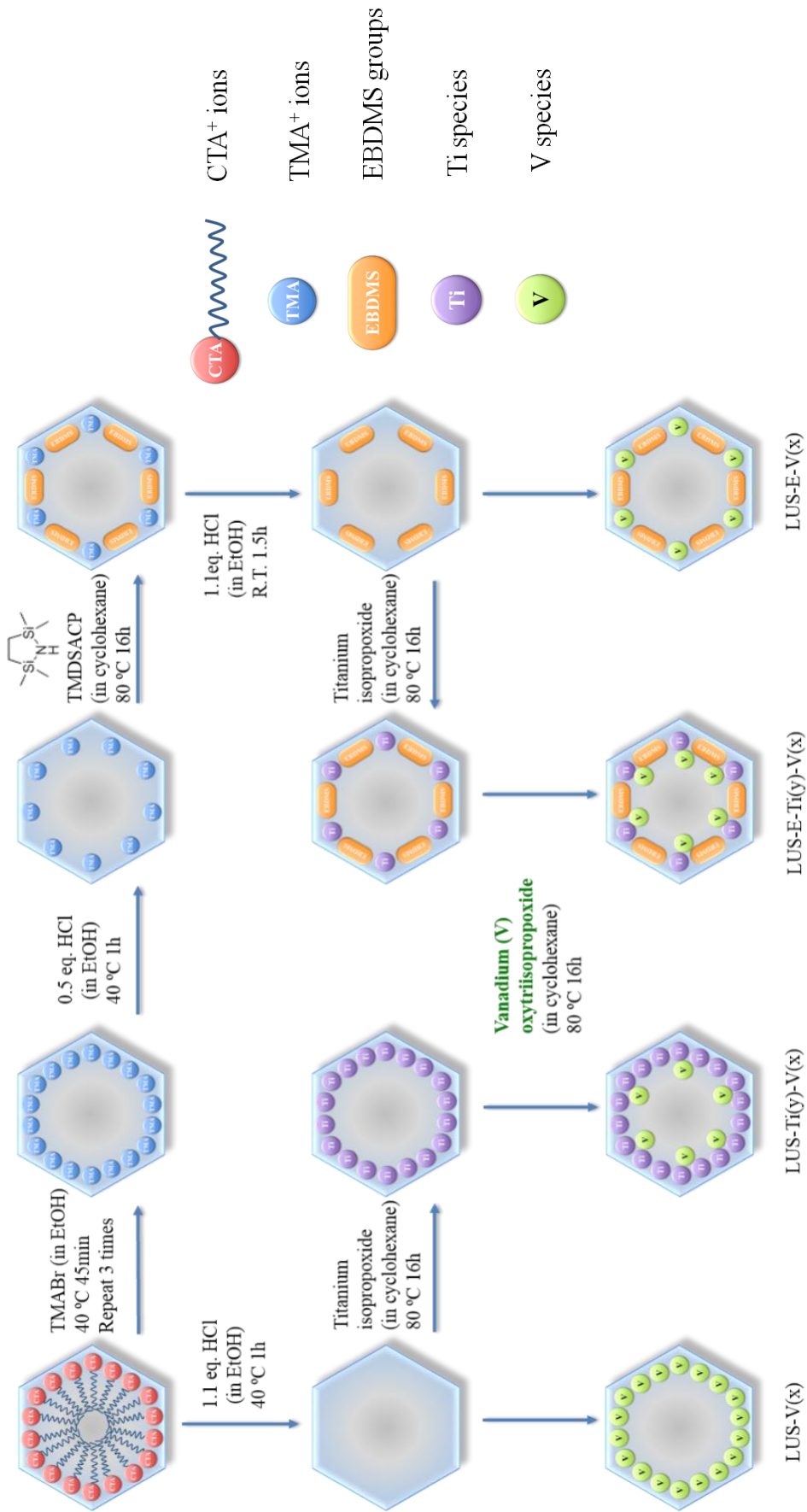
**Step 1 to Step 3.** These three steps were similar to those first steps of preparation of LUS-E-V(x).

**Step 4.** Grafting of titanium species. This procedure was same as the grafting of titanium species (step 2) in the Preparation of LUS-Ti(y)-V(x).

**Step 5.** Grafting of titanium species. The procedure was same as Step 1 in the preparation of LUS-V(x) except that the silica was replaced by the LUS-E-Ti(y) obtained in the last step.

The calcination of samples underwent in the condition of  $550\text{ }^{\circ}\text{C}$  for 6 h in air flow.

The calcined samples have -cal in the names.



Scheme 1. Preparation procedure of LUS-V(x), LUS-Ti(y)-V(x), LUS-E-Ti(y)-V(x) and LUS-E-V(x).

## 5.3 Results and discussion

### 5.3.1 Synthesis of materials and textural characterization

#### 5.3.1.1 Preparation of samples

Four series samples synthesized in this work provided four different environments of vanadium species. In the LUS-V(x) series, vanadium species were incorporated into pure MCM-41 type silica surface without any vicinal species. In the samples of LUS-Ti(y)-V(x), titanium species were grafted first onto the surface of silica following by the incorporation of vanadium species. The EBDMS organic groups were grafted firstly which was supposed to restrict the aggregation of vanadium species or titanium species in the series of LUS-E-V(x) and LUS-E-Ti(y)-V(x). The final elements contents are listed in the Table 1.

Table 1. Elemental analysis of samples.

	Si (wt%)	Ti (wt%)	V (wt%)	C (wt%)	Si/Ti	Si/V	Ti (mol%)	V (mol %)
LUS-V(5)	35.77	-	4.35	-	-	15	-	6.7
LUS-V(2.5)	36.48	-	1.69	-	-	39	-	2.6
LUS-V(1.25)	36.16	-	1.09	-	-	60	-	1.6
LUS-E-V(5)	34.95	-	3.42	9.95	-	18	-	5.5
LUS-E-V(2.5)	37.59	-	1.49	10.61	-	45	-	2.2
LUS-E-V(1.25)	37.51	-	1.01	10.35	-	67	-	1.5
LUS-Ti(5)-V(5)	32.88	2.96	3.15	-	19	19	5.2	5.2
LUS-Ti5-V(2.5)	32.89	3.19	1.36	-	18	44	5.2	2.3

LUS-Ti(5)-V(1.25)	34.22	3.11	1.03	-	20	61	5.0	1.6
LUS-E-Ti(5)-V(5)	40.98	2.29	3.90	10.34	30	19	3.3	5.2
LUS-E-Ti(5)-V(2.5)	34.80	2.09	1.91	10.77	29	33	3.4	3.0
LUS-E-Ti(5)-V(1.25)	36.99	2.12	1.08	8.54	30	62	3.3	1.6

### 5.3.1.2 Textural characterization

The MCM-41 hexagonal structure of the supports was characterized by low-angle XRD. The diffraction powder patterns of LUS-V(5), LUS-E-V(5), LUS-Ti(5)-V(5), LUS-E-Ti(5)-V(5) are shown in Figure 1A. All the patterns show readily distinguished bands indexed as (100), (110) and (200) of the 2D hexagonal point group, which indicates the mesoporous structure of MCM-41 type was maintained

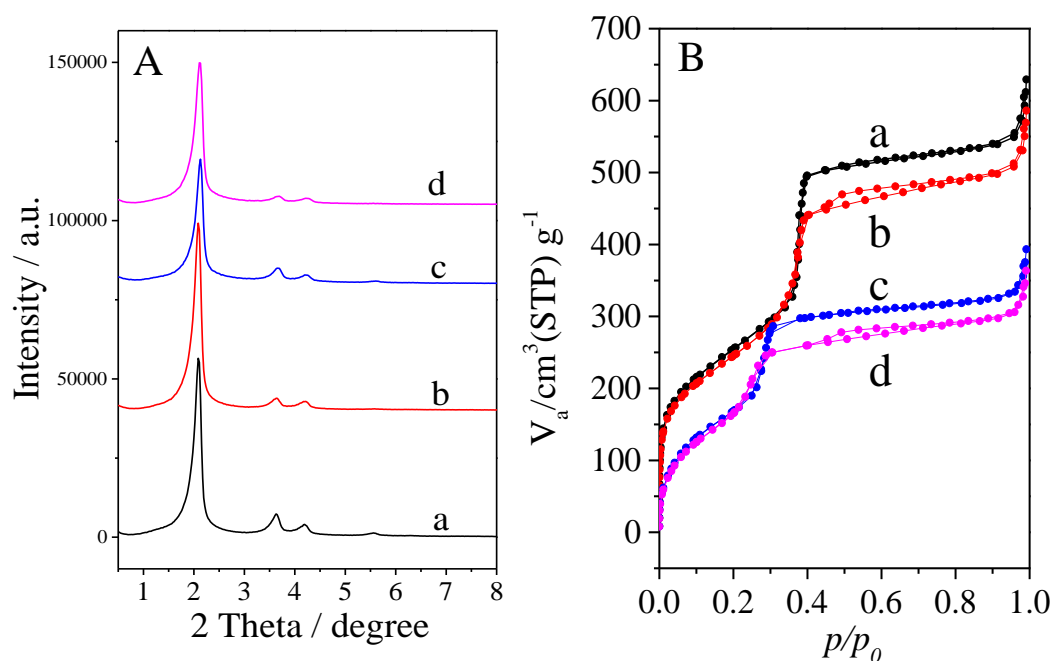


Figure 1. Low angle power XRD patterns (A) and N<sub>2</sub> adsorption-desorption isotherms (B) of a. LUS-V(5), b. LUS-E-V(5), c. LUS-Ti(5)-V(5), and d. LUS-E-Ti(5)-V(5).

during the modification of silica surface upon the introduction of EBDMS groups, titanium and vanadium species.

Nitrogen sorption isotherms at 77 K were measured on samples evacuated at 130 °C for overnight or 2 h (for the samples containing organic EBDMS groups). All the isotherms show typical type (IV) isotherm according to IUPAC classification (Figure 1B), which suggests that all the series of samples possessed long-range order channels with open pores typical of MCM-41 type silica. Compared the specific BET surface of LUS-V(x) series to pure silica LUS (Table 2), the specific surface and pore volume decrease slightly with increasing content of incorporated vanadium species, while the pore size changed little. This phenomenon is slightly more pronounced in LUS-Ti(5)-V(5) due to the increasing amount of incorporated heteroatoms. The difference is more obvious between the series with and without EBDMS groups. All the specific surface area, pore volume and pore size decreased when the organic groups were introduced. Concomitantly, the BET constant C, which probes the polarity of the surface, decreased from around 120 to 30. This drastic trend was consistent with the high hydrophobicity generated by grafted EBDMS groups. In contrast, the grafted heteroatoms had little influence on C nor on the pore diameter.

As a conclusion, the specific area and pore size were maintained and the slight decreases of surface area, pore diameter, pore volume and C parameter are consistent with modification occurring in the nano-channels of the mesoporous MCM-41 support.

Table 2. Textural properties of samples analyzed by N<sub>2</sub> sorption.

	BET plot			BdB
	S <sub>BET</sub> (m <sup>2</sup> g <sup>-1</sup> ) <sup>a</sup>	C <sup>b</sup>	V <sub>total</sub> (cm <sup>3</sup> g <sup>-1</sup> ) <sup>c</sup>	d (nm) <sup>d</sup>
LUS	1033	120	0.93	4.0
LUS-V(1.25)	988	119	0.91	4.0
LUS-V(2.5)	921	115	0.84	4.0
LUS-V(5)	919	106	0.83	3.9
LUS-Ti(5)-V(5)	895	89	0.77	3.9
LUS-E	730	34	0.57	3.3
LUS-E-V(5)	654	34	0.50	3.2
LUS-E-Ti(5)-V(5)	648	29	0.46	3.1
LUS-E-Ti(5)-V(2.5)	649	28	0.47	3.1
LUS-E-Ti(5)-V(1.25)	645	28	0.47	3.1

[a] S<sub>BET</sub> calculated by using the Brunauer-Emmett-Teller (BET) equation over a range of relative pressure from 0.05 to 0.35.

[b] BET parameter.

[c] Total pore volume measured at P/P<sub>0</sub> = 0.90.

[d] Pore size diameter obtained from Broekhoff and de Boer method (BdB).

### 5.3.1.3 Organic groups in the LUS-E-V(x) and LUS-E-Ti(y)-V(x) series.

The presence of the organic functional groups was characterized by TGA, FT-IR and  $^{29}\text{Si}$  solid NMR besides  $\text{N}_2$  sorption. The TGA curves (Figure 2) shows that the samples containing EBDMS groups exhibited typical weight loss between 360 and 540  $^\circ\text{C}$ , which assigned to the composition of the EBDMS groups. The very sharp decrease around 500  $^\circ\text{C}$  (see the peak at 520  $^\circ\text{C}$  in the derivative curve) is likely due to the condensation of the silanol groups left behind the last loss of organic species. It is noted that the DTG peaks around 100  $^\circ\text{C}$  of LUS-V(5) and LUS-Ti(5)-V(5) are much stronger than those one in LUS-E-Ti(5)-V(5) and LUS-E-V(5). Considering that this weight loss is attributed to the  $\text{H}_2\text{O}$  adsorbed by the surface silanols, it can be concluded that the samples with organic groups are much more hydrophobic than the other two, which is consistent with the BET parameter C.

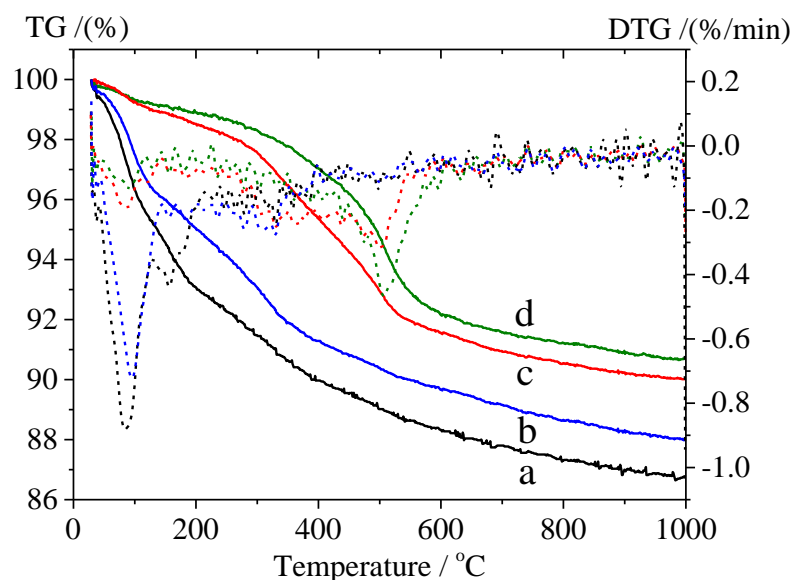


Figure 2. TG-DTG curves of a. LUS-V(5), b. LUS-Ti(5)-V(5), c. LUS-E-Ti(5)-V(5), and d. LUS-E-V(5).

The ATR-FTIR was utilized to characterize the appearance or the modification of vibration modes of that are assigned to chemical bonds in the materials. Note that the ATR mode for IR absorption measurements produces a strong attenuation of the bands in the region  $2000 - 4000 \text{ cm}^{-1}$  where usually the OH and CH stretching modes are easily observed in the transmission mode. Indeed, these peaks are very weak here and therefore to be commented. One difficulty resides in the overlap of bands, particularly those of the bulk or the surface that remain unchanged from one step to the other in the different sequences of the synthesis. Of course, this is worse in the region  $900$  to  $1300 \text{ cm}^{-1}$  of the Si-O stretching modes as shown in Figure 3.

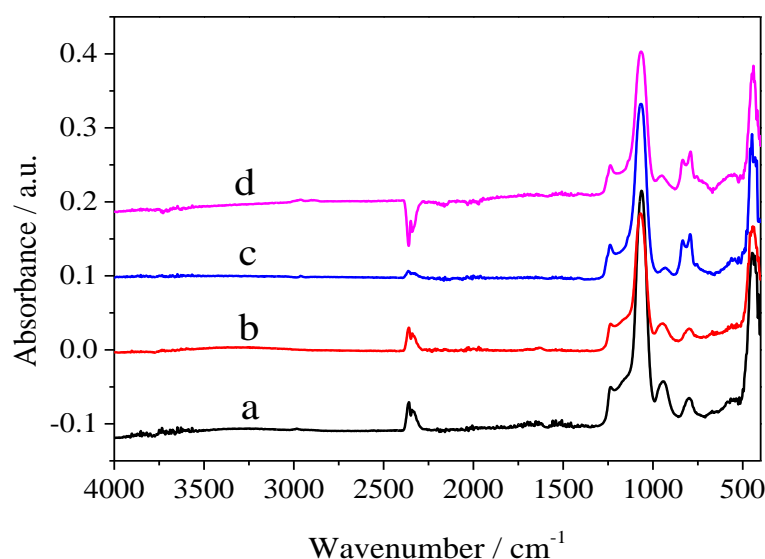


Figure 3. ATR-IR spectra of a. LUS-V(5), b. LUS-Ti(5)-V(5), c. LUS-E-V(5), and d. LUS-E-Ti(5)-V(5).

To exacerbate the appearing and disappearing features before and after grafting, difference between spectra were calculated and shown between  $400$  and  $1500 \text{ cm}^{-1}$ . To do so, the intensity was normalized using as an internal reference the narrow peak  $450 \text{ cm}^{-1}$ . It belongs to weakly coupled valence bond angle vibration mode of the  $[\text{SiO}_4]$  units of the siliceous matrix,  $\delta_{\text{O-Si-O}}$ . Then, the spectra of pure LUS was subtracted to

that of LUS-V(5), LUS-Ti(5)-V(5), LUS-E-V(5) and LUS-E-Ti(5)-V(5). These difference spectra are depicted for direct grafting of V or Ti plus V on either extracted pure SiO<sub>2</sub> LUS (Figure 4a and b) or for LUS the surface of which was partially covered by EBDMS moieties according to the MSP technique (Figure 4c and d), respectively. The grayish region corresponds to the zone used for intensity normalization where residual intensity of the reference peak can be seen showing the quality of the subtraction process. Indeed, this peak appears more than 6 times smaller after subtraction in the absence of EBDMS moieties (residue <18%). In the presence of EBDMS, this region exhibits an up and down signal residue of the  $\delta_{\text{O-Si-O}}$  vibrational modes of pure silica that is reminiscent of wavenumbers shift towards of about 10 cm<sup>-1</sup> accounting for about 20 % of the total intensity of the symmetric mode [SiO<sub>4</sub>] units. This is consistent with surface silanol groups the majority of which are engaged in grafting either EBDMS ([SiOC<sub>3</sub>] instead of [SiO<sub>4</sub>] units). Note also as a relatively satisfactory information about the quality of the subtraction, the peak at 800 cm<sup>-1</sup> assigned to the symmetrical stretching vibrational modes  $\nu_{\text{as}}$  of [SiO<sub>4</sub>] units is nearly cancelled. These remarks point out that the normalization-subtraction process was is reliable enough to extract reasonable information on appearing and disappearing species.

Figure 4a exhibits mostly two intense peaks at 1050 and 943 cm<sup>-1</sup>. The former is usually assigned to a local vibrational mode mostly due to the oxovanadyl function, V=O. The second one fall in the region expected for the asymmetrical stretching vibrational modes  $\nu_{\text{asym}}$  of [SiO<sub>4</sub>] units and, particularly to the Si-OM local stretching mode where M stands for Cr, V, Ti or H as often observed in silicalite-1 and its metal modification equivalents.<sup>8,9</sup> Furthermore, TiO<sub>2</sub>-SiO<sub>2</sub> hybrid glasses shows that these vibration modes are expected in the range 928 to 940 depending on the number of Si-O-bonds around Ti.<sup>10</sup> In fact, this mode which is triply degenerated may upon

orthorhombic distortion generate three new vibrational states. This has been evidence first time in 1994 for  $\nu_{as}$  of  $[O_3SiOTi]$  using difference of IR spectra in titanium silicalite, TS-1 with three resonances at 965, 1080 and 1200  $cm^{-1}$ .<sup>11</sup> In the present case, the second local mode may be hidden below the strong peak of V=O at 1050  $cm^{-1}$ . Then, the third local mode could be represented by the broad peak at 1170 or the narrower one at 1240  $cm^{-1}$ .

When titanium was grafted in the first place and vanadium in the second place, the peak at 943  $cm^{-1}$  remained, though about twice less intense indicating a lower number of V-O-Si bridges (Figure 4b). Strikingly, where lied only one strong peak due to the V=O local mode, there is now two peaks at 1030 and 1090  $cm^{-1}$ . This could indicate that the presence of titanium (IV) ions on the support strongly affects the nature of the vanadium species. Another noticeable information lies in the low IR wavenumber region 500 - 700  $cm^{-1}$  where bands show up that could be due to Ti-O-Ti, V-O-V and Ti-O-V bridges. In fact, in bulk  $TiO_2$  (brookite, anatase and rutile) the IR spectra is mainly located below 800  $cm^{-1}$  due to mainly  $A_u$  and  $E_u$  vibrational modes strongly influenced by the shape of the crystal.<sup>12,13</sup> The rutile spectrum that should arise at 388 and 500  $cm^{-1}$  for both modes, respectively, may shift up to 800  $cm^{-1}$  for plate like crystals.<sup>14</sup> In  $TiO_2$ - $SiO_2$  glasses, the Ti-O-Ti are also observed at 342, 550  $cm^{-1}$ .<sup>15</sup> In bulk  $V_2O_5$ , the amorphous phases is mainly represented by three peaks: one relatively narrow at 1018  $cm^{-1}$  mainly due to terminal V=O oxo bond and like in  $TiO_2$  systems two other relatively broad at 820 and 500  $cm^{-1}$ .<sup>16</sup> In Figure 4b, the peaks arose at 560 and 690  $cm^{-1}$ . The former peak evidences the formation of Ti-O-Ti including most likely Ti-O-V bridges. The second peak though less blue shifted than in the bulk could be still related to a flat shape of the (Ti, V) $O_x$  grafted clusters. This question remains open.

In samples LUS-E-V(5) and LUS-E-Ti(5)-V(5), the surface was partly covered by EBDMS organic species using the MSP technique that are characterized by narrow IR peaks at 755 (weak), 790 (strong), 834 (strong), 1090 (strong) and 1256  $\text{cm}^{-1}$ (weak). The assignment to the normal stretching modes of the  $[\text{SiOC}_3]$  units of EBDMS has been proposed previously (Figure 4c and 4d).<sup>17</sup> In addition to these novel features, in Figure 4c in absence of Ti, there is a negative peak at 960  $\text{cm}^{-1}$  that is due to a strong utilization of the surface silanol groups engaged into grafting either metal ions or EBDMS. Noticeably, when Ti is present this loss of intensity is compensated by the formation of Si-O-Ti bridges that arose at about the same wavenumber. Finally, the absorption in the 500-700  $\text{cm}^{-1}$  range is much smaller than in Figure 4a and 4b suggesting an improvement of vanadium dispersion in presence of the organic surface masking agent. This will be confirmed below using UV-Visible spectroscopy.

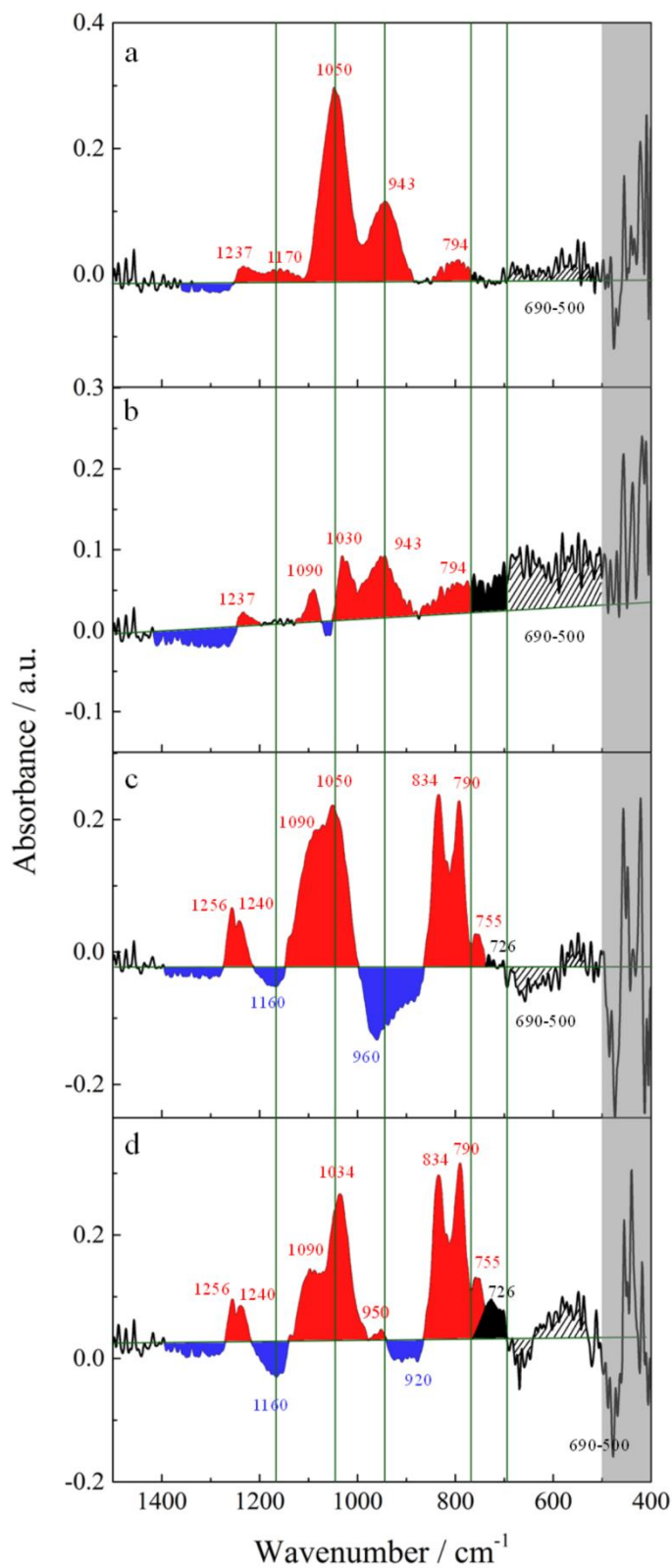


Figure 4. Difference spectra obtained by normalization and substraction of the spectrum of genuine LUS, to a. LUS-V(5), b. LUS-Ti(5)-V(5), b. LUS-E-V(5) and c. LUS-E-Ti(5)-V(5).

The deconvoluted  $^{29}\text{Si}$  NMR spectra (Figure 5) indicate the different silicon environment in the samples. (Table 3) The signals at -94, -101, -110 ppm assigned to the  $Q_2$ ,  $Q_3$ ,  $Q_4$  respectively, which are dominant in the spectra of the samples without organic groups. The appearance of  $M_n$  signals reveals the presence of grafted dipodal of EBDMS. The signal at 14 ppm is assigned to the silicon links to three carbons and -O-Si-O<sub>3</sub> (blue balls in the scheme 2) which was represented as  $M_1$  silicon.<sup>18</sup> The signals of  $M_1$ - $M_1$  (8 ppm) and  $M_0$  (19 ppm) are deduced to the presence of the mono-grafted and grafted dimeric species as the second and third structure shown in scheme 2.

Table 3. Percentage of  $Q_n$ ,  $M_n$  obtained from  $^{29}\text{Si}$  NMR

		$M_1$ - $M_1$	$M_0$	$M_1$	$\text{Si}_{(\text{org})}$	$Q_2$	$Q_3$	$Q_4$	$\text{Si}_{(\text{inorg})}$
	ppm	8	19	14	-	-94	-101	-110	-
LUS	%	-	-	-	-	4	31	65	100
LUS-V(1.25)	%	-	-	-	-	7	37	56	100
LUS-V(5)	%	-	-	-	-	5	34	61	100
LUS-Ti(5)-V(1.25)	%	-	-	-	-	4	33	63	100
LUS-E	%	3	3	13	19	4	18	59	81
LUS-E-V(1.25)	%	3	1	13	17	2	16	65	84
LUS-E-V(5)	%	3	2	14	19	1	13	66	81
LUS-E-Ti(5)	%	4	2	14	20	1	11	68	80
LUS-E-Ti(5)-V(1.25)	%	2	2	14	18	3	18	61	82

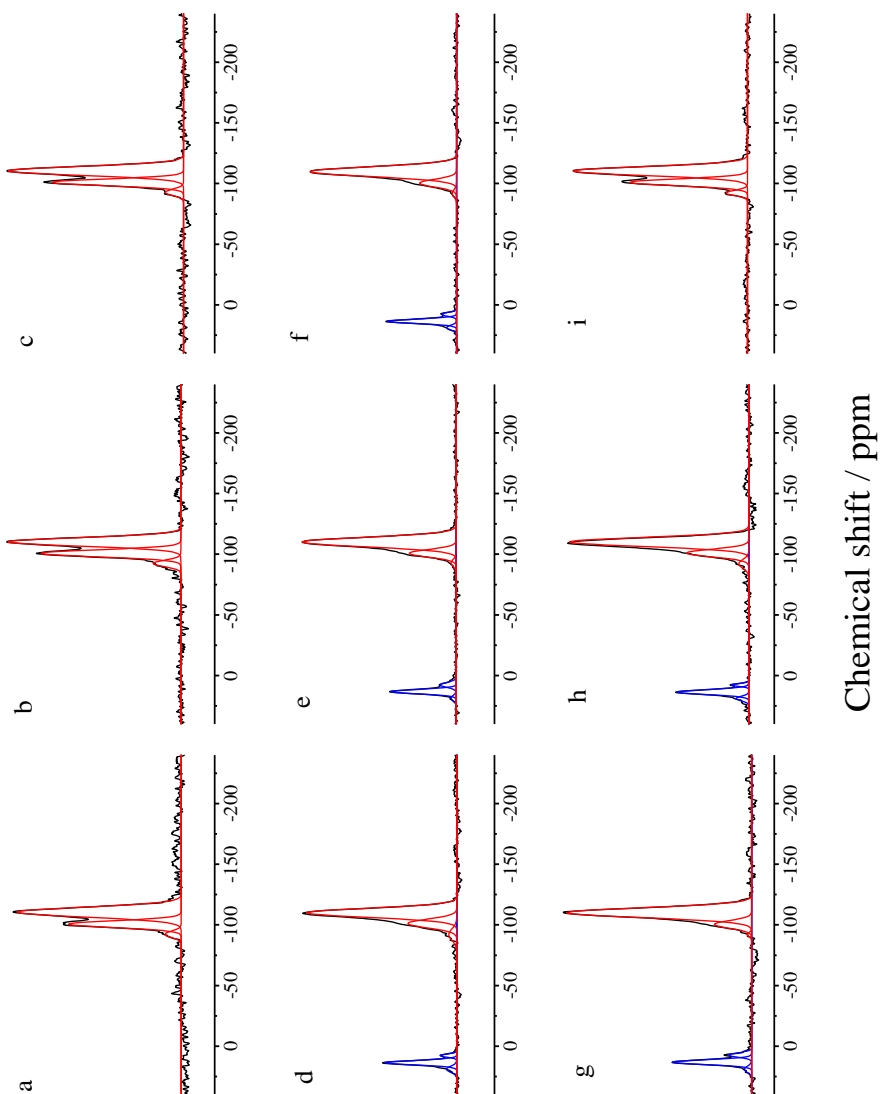
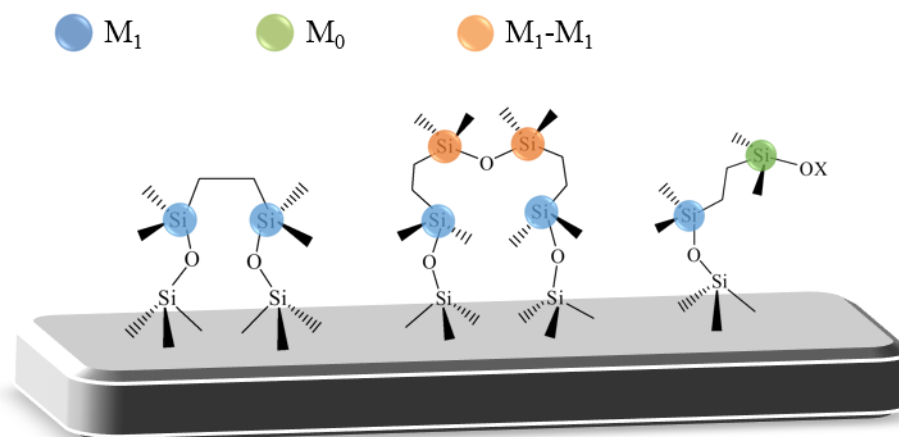


Figure 5.  $^{29}\text{Si}$  solid NMR spectra of a. LUS, b. LUS-V(1.25), c. LUS-V(5), d. LUS-E, e. LUS-E-V(1.25), f. LUS-E-V(5), g. LUS-E-Ti(5), h. LUS-E-Ti(5)-V(1.25) and i. LUS-Ti(5)-V(5).



Scheme 2. Possible structures of EBDMS surface species in the samples.

### 5.3.2 The influence of EBDMS groups on dispersion of vanadium species.

The dispersion of vanadium species in the samples was collected by UV-visible spectroscopy, which is a simple and direct way to understand the nature of target transition metal in the heterogeneous catalyst. Two multiple bands in the region  $10000\text{ cm}^{-1}$  -  $20000\text{ cm}^{-1}$  and  $20000\text{ cm}^{-1}$  -  $50000\text{ cm}^{-1}$  are attributed to d-d transition of V(IV) and charge transfer of V(V) or V(IV) respectively. (Figure 6) The presence of V(IV) was confirmed by a typical multiline signal in EPR spectra (Figure 7) that disappeared upon calcination concomitantly with the elimination of the d-d absorption bands below  $20000\text{ cm}^{-1}$  in the UV-visible spectra (Figure 8). Reminding that vanadium was grafted using the vanadium (V) oxytriisopropoxide that evolved isopropanol known to be a reductants for V(V), the formation of V(IV) is not surprising. Besides, it has been noticed that the EPR spectra of LUS-V(x) were more resolved than that of LUS-E-V(x). Indeed, the broad signal due to dipolar broadening and underlying below the characteristic hyperfine structure suggests that a larger fraction of V(IV) atoms are closer in the LUS-E-V(x) than in the LUS-V(x).

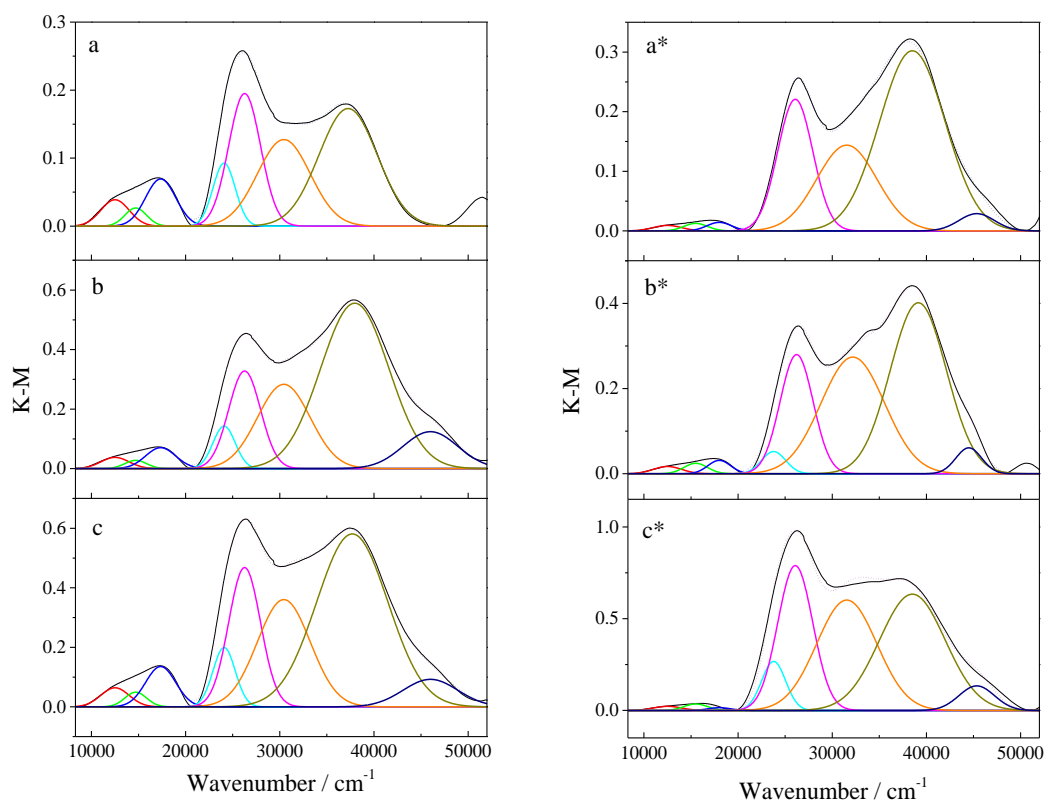


Figure 6. UV-vis spectra of non-calcined samples: a. LUS-V(1.25), b. LUS-V(2.5), c. LUS-V(5), a\*. LUS-E-V(1.25), b\*. LUS-E-V(2.5), and c\*. LUS-E-V(5).

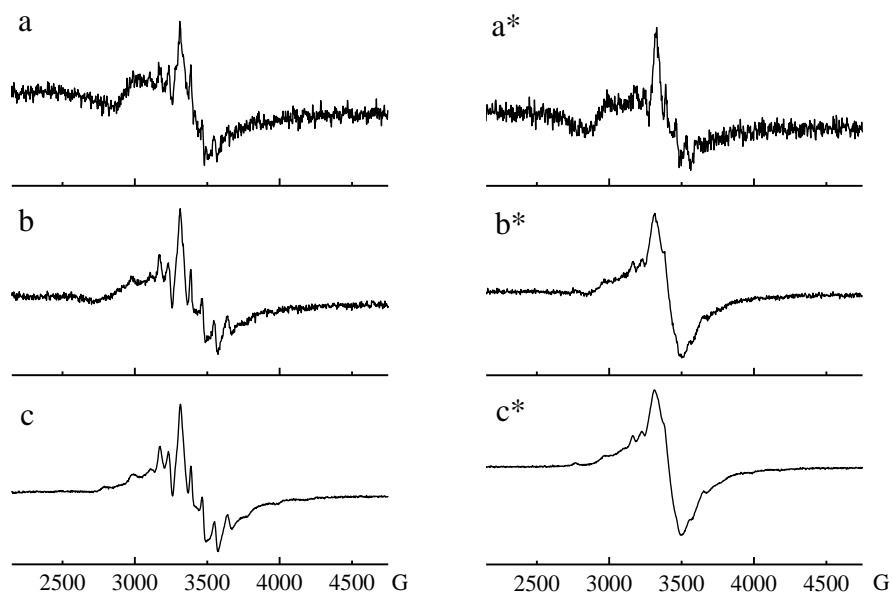


Figure 7. EPR spectra of a. LUS-V(1.25), b. LUS-V(2.5), c. LUS-V(5), a\*. LUS-E-V(1.25), b\*. LUS-E-V(2.5), and c\*. LUS-E-V(5).

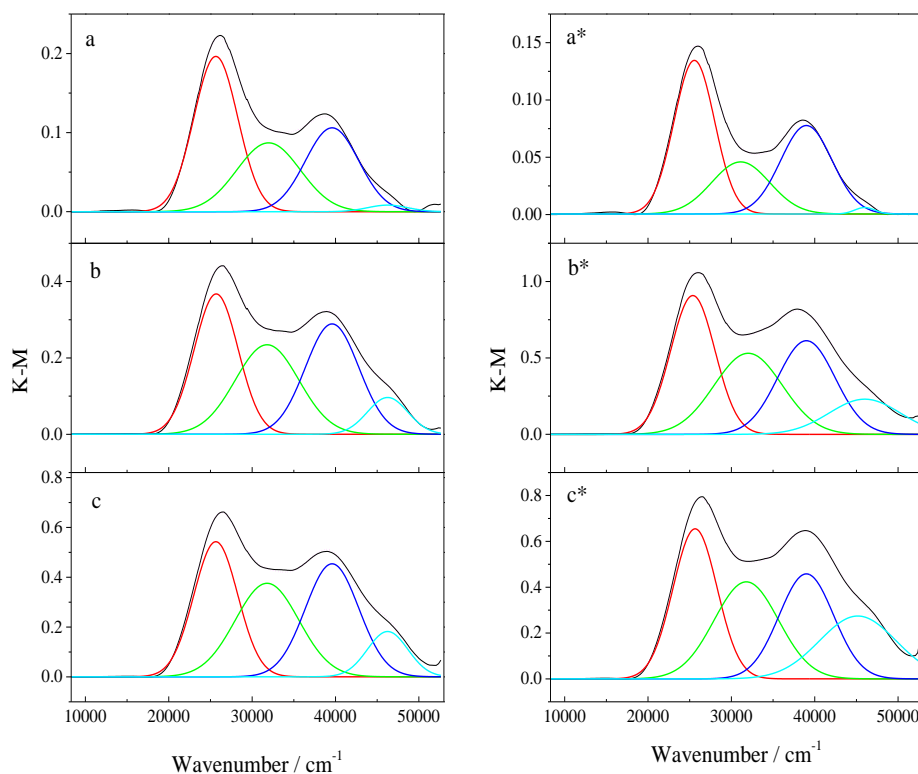


Figure 8. UV-vis spectra of a. LUS-V(1.25)-cal, b. LUS-V(2.5)-cal, c. LUS-V(5)-cal, a\*. LUS-E-V(1.25)-cal, b\*. LUS-E-V(2.5)-cal, and c\*. LUS-E-V(5)-cal.

All the samples showed bands in the region of  $20000\text{ cm}^{-1}$  -  $25000\text{ cm}^{-1}$ , which are attributed to polymeric vanadium species.<sup>20</sup> Tauc's plot<sup>19</sup> were drawn to extract the energy gap and estimate the level of aggregation. This value obtained from the adsorption energy edge will decreased for larger polymeric vanadium species giving in the actual series the following ranking (Figure 9): LUS-E-V(5) ( $2.68\text{ eV}$ ) < LUS-V(5) ( $2.79\text{ eV}$ ) < LUS-V(2.5) ( $2.85\text{ eV}$ ) < LUS-V(1.25) ( $2.86\text{ eV}$ ) < LUS-E-V(2.5) ( $2.90\text{ eV}$ ) < LUS-E-V(1.25) ( $2.92\text{ eV}$ ). The energy edges of crystalline  $\text{V}_2\text{O}_5$  ( $2.26\text{ eV}$ ) and  $\text{NaVO}_3$  ( $3.16\text{ eV}$ ) were provided as reference for 3D "infinite" clusters and linear vanadium polymers. The energy gap of the polymeric vanadium species in all the present samples falls in between that of these two references, though

much closer to the 1D  $\text{NaVO}_3$ . This strongly suggested that the polymeric V species were grafted as 2D clusters of varying size depending on the surface treatment and the loading. Logically for a given surface the lowest loading produces the smallest clusters. Note that for the organically modified surface, the vanadium (V) clusters are smaller for 1.25 and 2.5 V mol%. This is only for the 5 mol% that the available surface left for grafting is saturated and produces larger clusters than the non-modified surface. This clearly demonstrate the beneficial effect of the organic patterning on the dispersion of vanadium during grafting as far as the loading does not exceed the capacity of the uncovered surface to host grafted species. The progressive evolution of the gap in this series shows that we are dealing with different populations of clusters of various sizes. A more synthetic view can be obtained with the analysis of the full signal using deconvoluted into several Gaussian as proposed in the previous chapter.

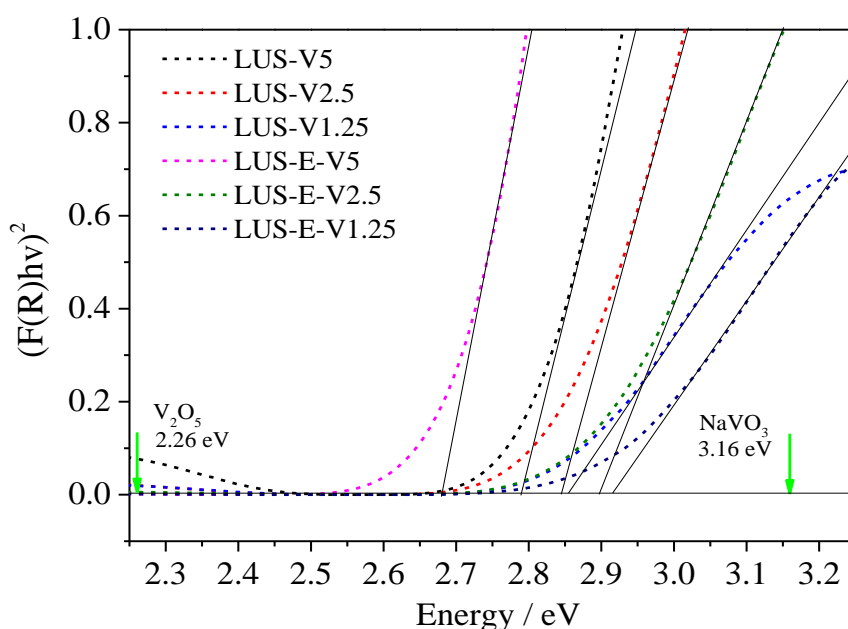


Figure 9. Tauc's plot  $([F(R)hv]^2$  vs.  $hv$  for both LUS-V(x) and LUS-E-V(x) series

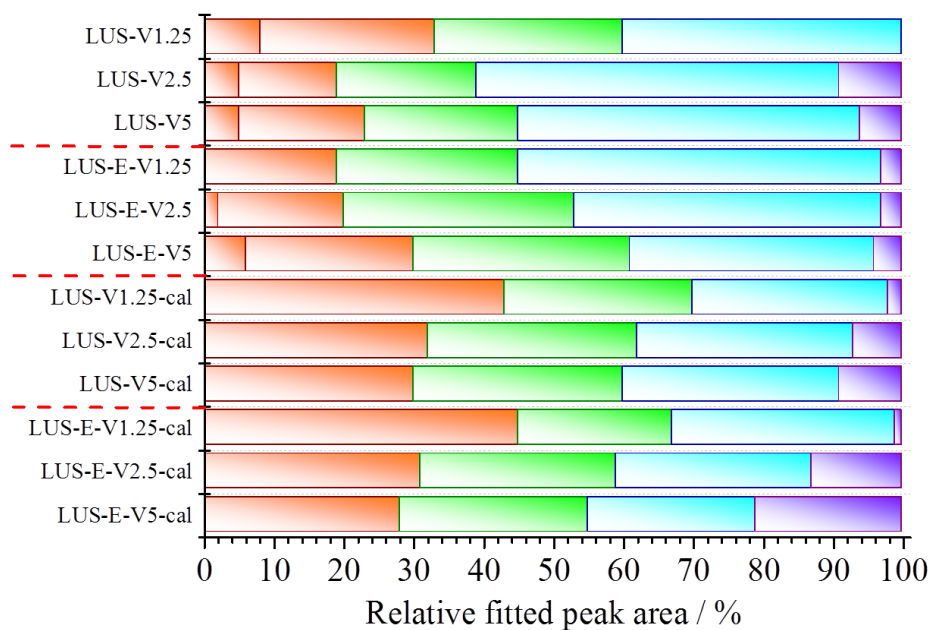


Figure 10. Relative fitted peak area LUS-V(x), LUS-E-V(x), LUS-V(x)-cal and LUS-E-V(x)-cal. Orange bar represented the bands at  $20000\text{ cm}^{-1} - 25000\text{ cm}^{-1}$  (polymer) Green bar represented the bands at  $30000\text{ cm}^{-1}$  (oligomer) ; Blue bar represented the bands at  $38000\text{ cm}^{-1}$  (monomer); Violet bar represented the bands at  $46000\text{ cm}^{-1}$  (monomer).

Table 4. Data of deconvolution for LUS-V(x), LUS-E-V(x), LUS-V(x)-cal and LUS-E-V(x)-cal.

	R <sup>2</sup>	Peak A				Peak B				Peak C				Peak D				Peak E					
		Xc (cm <sup>-1</sup> )	FWHM	A(%)	Xc (cm <sup>-1</sup> )	FWHM	A(%)	Xc (cm <sup>-1</sup> )	FWHM	A(%)	Xc (cm <sup>-1</sup> )	FWHM	A(%)	Xc (cm <sup>-1</sup> )	FWHM	A(%)	Xc (cm <sup>-1</sup> )	FWHM	A(%)	Xc (cm <sup>-1</sup> )	FWHM	A(%)	
LUS-V(1.25)	0.995			8			25					27			40								-
LUS-V(2.5)	0.999	24090	2790	4	26265	3991	15	30430	6605	20	37259	8539	52	46000	6829	9							9
LUS-V(5)	0.999			5			18			22			49			6							6
LUS-E-V(1.25)	0.999			-			19			26			52			3							3
LUS-E-V(2.5)	0.997	23775	3002	3	26075	4380	18	31545	7512	33	38508	8211	43	45344	4434	3							3
LUS-E-V(5)	0.998			5			24			31			36			4							4
LUS-V(1.25)-cal	0.999			-			43			27			28			2							2
LUS-V(2.5)-cal	1.000			-	25649	6203	32	31795	8975	30	39592	7547	31	46253	5702	7							7
LUS-V(5)-cal	0.999			-			30			30			31			9							9
LUS-E-V(1.25)-cal	0.999			-			45			22			33			1							1
LUS-E-V(2.5)-cal	1.000			-	25487	6010	31	31594	8926	28	39000	7681	27	45746	7847	13							13
LUS-E-V(5)-cal	0.999			-			27			28			25			20							20

Figure 8 with the Gaussian component used for the deconvolution as well as the bar diagrams of Figure 10 show that the trend is the same before and after calcination. In addition, the non-calcined samples exhibits an obvious mixture of V(IV) and V(V) oxidation states and the composite charge transfer, which is hardly resolved become non-exploitable for discussion. Therefore, the following discussion is based on the charge transfer band of the calcined samples only. The bar diagram of Figure 10 is particularly useful to drawn the trends. In fact, the logical rule on loading found from the Tauc's plots appears inverted here not only for the polymeric V species but also for the smallest clusters. Indeed, the number of isolated species provided by the most blue shifted peak is higher for the highest V loadings (light and dark blue bars in Figure 10 or Gaussian curves in Figure 8). These conclusions are fully at odd with those drawn for grafted titanium, which exhibit a logical behavior of higher distribution for lower loading and in the presence of an organic masked silica surface. The contradiction between the Tauc's plot and the full deconvoluted signal come from the limitation of 4 Gaussian curves for the fit that hides a lot of information particularly for populations of polymeric (brown curves) and small clusters (green curves). Though the information obtained from the Tauc's plot does not help us concerning the small clusters in this series of samples, it helps for the case of polymeric species. Combining information from both sources now, it appears that increasing the vanadium loading increase the size of the polymer (Tauc) but it decreases the number of polymers. It clearly evidences that vanadium is highly mobile on the surface during grafting allowing the growth of the polymeric species at the expense of the smallest polymers. Consequently, the vanadium concentration decreases on the rest of the surface where well dispersed species can remains as represented in Scheme 3.



Scheme 3. Possible model of vanadium species distribution in the LUS-V(x) and LUS-E-V(x).

### 5.3.3 The influence of Titanium species on dispersion of vanadium species.

The role of titanium shown to improve the fixation of vanadium should invert the trend observe when vanadium in grafted directly on silica. Herein, titanium species was incorporated in between EBDMS groups system to favor the direct interaction of vanadium species with grafted Ti species. The first striking information is the much weaker absorption in the region of  $10000 - 20000 \text{ cm}^{-1}$  and  $20000 - 25000 \text{ cm}^{-1}$  assigned to V (IV) species. This clearly indicate that vanadium interacting with titanium is more difficult to reduce than vanadium linked to silica directly (Figure 11 left). This is more pronounced for lower V loadings, up to the point that there is no V(IV) observed for LUS-E-Ti(5)-V(1.25) and only minute amount in LUS-Ti(5)-V(1.25). Anyhow, V(IV) species are oxidized into V(V) species after calcination as observed previously without the presence of titanium. (Figure 12) Such a lower reductibility of vanadium species on titanium dioxide was described previously.<sup>21,22</sup> The resistance to reduction can be explained by a better dispersion (less V-O-V bridges). Indeed, there is a much lower absorption in the region  $25000 \text{ cm}^{-1}$  assigned to polymeric V species in LUS-Ti(5)-V(x) or LUS-E-Ti(5)-V(x) than in

the titanium free counterparts LUS-V(x) or LUS-E-V(x). In addition, the dispersion follows now a logical trend of higher dispersion for lower V loading with or without organic patterning using EBDMS.

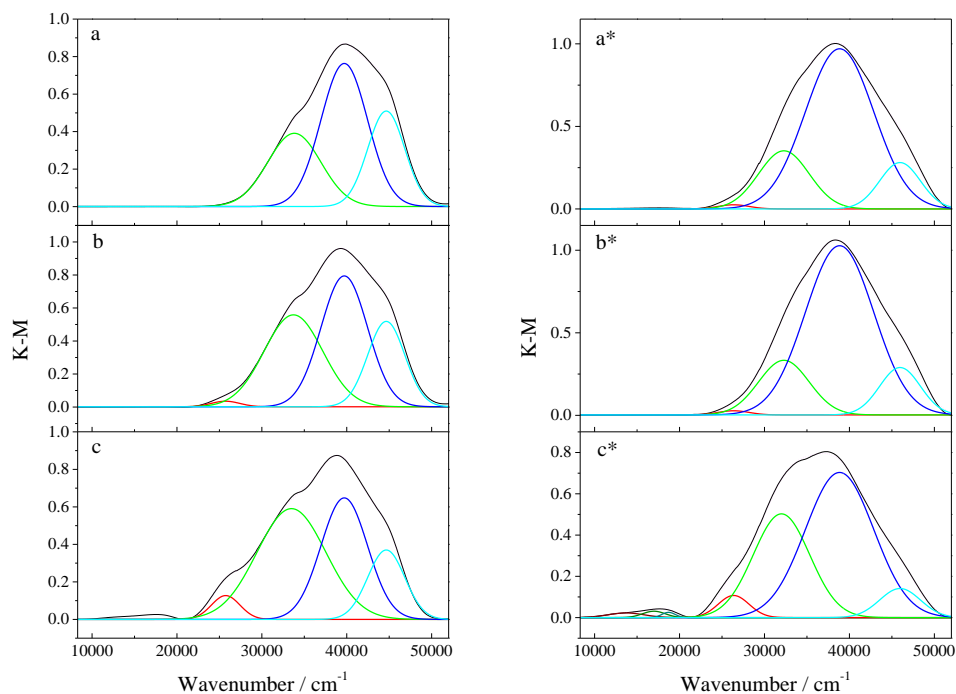


Figure 11. UV-vis spectra of a. LUS-E-Ti(5)-V(1.25), b. LUS-E-Ti(5)-V(2.5), c. LUS-E-Ti(5)-V(5), a\*. LUS-Ti(5)-V(1.25), b\*. LUS-Ti(5)-V(2.5), and c\*. LUS-Ti(5)-V(5).

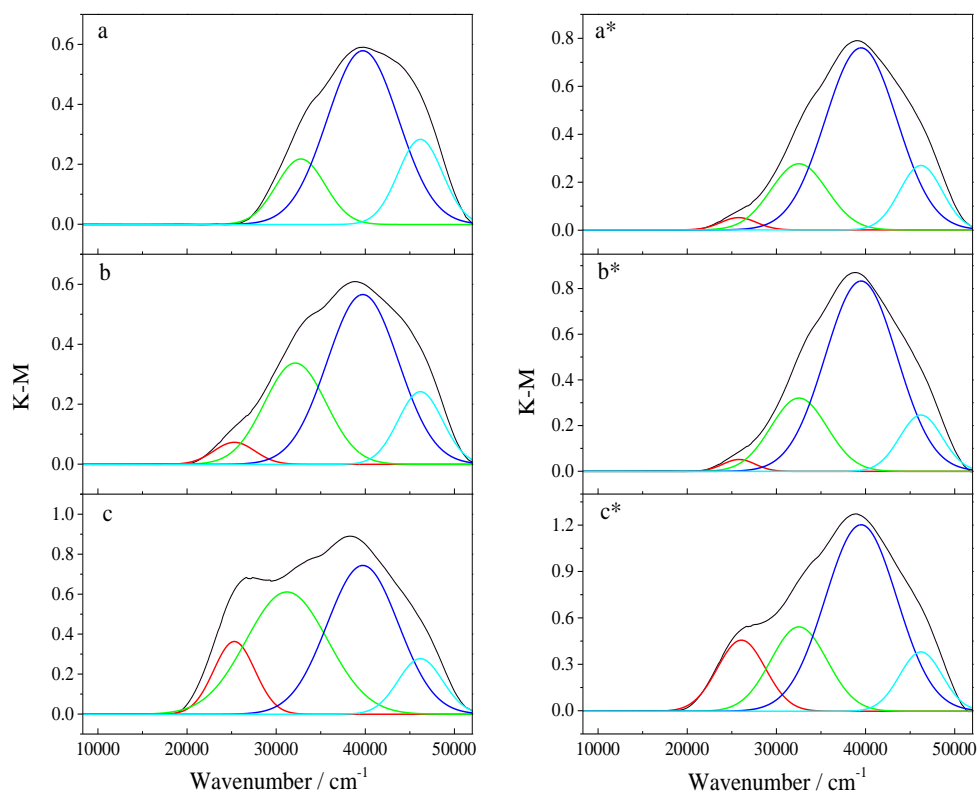


Figure 12. UV-vis spectra of a. LUS-E-Ti(5)-V(1.25)-cal, b. LUS-E-Ti(5)-V(2.5)-cal, c. LUS-E-Ti(5)-V(5)-cal, a\*. LUS-Ti(5)-V(1.25)-cal, b\*. LUS-Ti(5)-V(2.5)-cal, and c\*. LUS-Ti(5)-V(5)-cal.

At first sight, the effect of the organic masking agent seems relatively weak. Nonetheless, at low loading the organic mask improved slightly the dispersion (less the polymeric species, red line) while by contrast at 5 mol% V, aggregation is favored. The saturation effect describe for vanadium alone takes place also in the presence of titanium.

The dispersion of vanadium was further documented using the energy gap that focused the information on the most aggregated species as explained above. (Figure 13) Then, the Tauc'plot provides the followng ranking was obtained towards from the

worse to the best dispersion: LUS-E-Ti(5)-V(5) (2.94 eV) < LUS-Ti(5)-V(5) (3.07 eV) < LUS-Ti(5)-V(2.5) (3.43 eV) < LUS-Ti(5)-V(1.25) (3.44 eV) < LUS-E-Ti(5)-V(2.5) (3.52 eV) < LUS-E-Ti(5)-V(1.25) (3.63 eV). Note at first that the energy gap were higher than those of any of the previous samples where Ti was absent. This strongly illustrate the drastic anti-polimerization effect of Ti acting as an anchor. Furthermore, the polymer or the small clusters that now intervene here in the energy gap are obviously smaller for lower loading and when the organic mask is present.

Note that the trend before or after calcination is the same since the V(IV) species are relatively marginal. Nonetheless, calcination yielded polmeric V (V) species not present in the non-calcined sample in higher proportion for higher V loading.

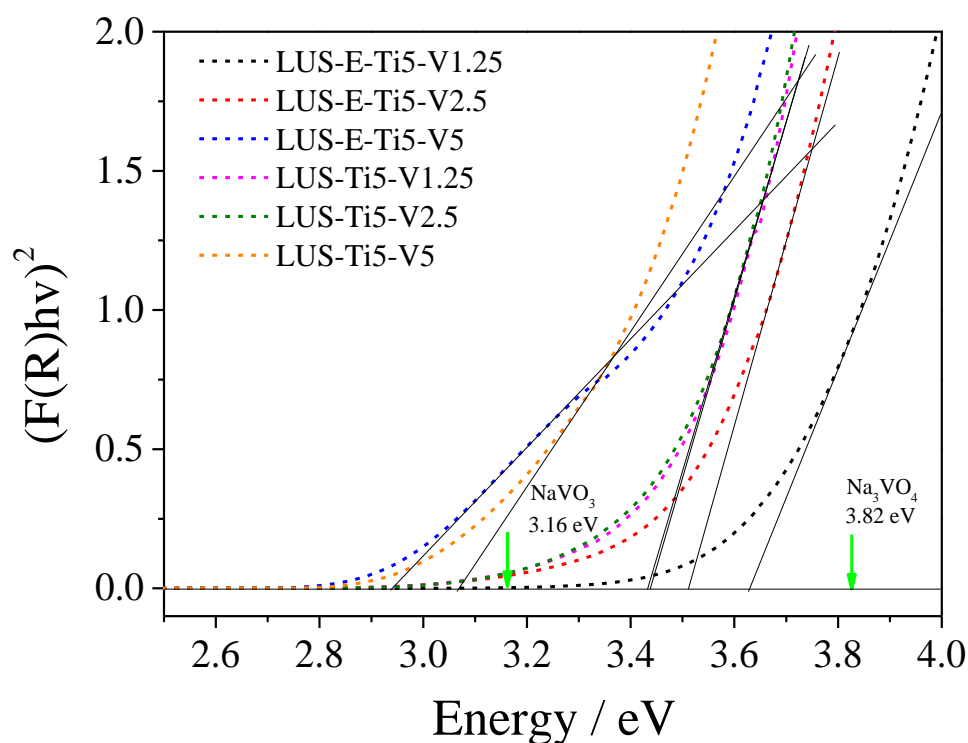


Figure 13. Tauc's plot ( $[F(R_\infty) hv]^2$  vs.  $hv$ ) of LUS-E-Ti(5)-V(x) and LUS-Ti(5)-V(x).

Table 5 and Figure 14 gathered the data and summarizes into a bar diagram all the trends, respectively. The loss of dispersion started to be noticeable for  $V/Ti = 1/2$  and obvious for  $V/Ti = 1$ . The molecular masking effect of EBDMS on the surface appeared rather subtle since it does not change much the population of polymeric or small clusters versus isolated species. However, it affects the population inside the polymeric species by decreasing the degree of polymerization, i. e., the size of the polymers. The degree of aggregation of the Ti clusters is another concern. It can be seen from the UV-visible diffuse reflectance spectra that we are dealing mainly with a mixture of monomeric, dimeric and trimeric species (Figure 15). The neat blue shift in the presence of EBDMS revealing that there is less clusters and more monomers. In fact, the question remains on the optimal nuclearity of the Ti clusters to efficiently anchor V on  $SiO_2$ . According to the previous chapter with framework Ti used as anchors, a ratio  $V/Ti$  of  $1/3$  was suggested. Here, the number of 2 Ti per V seems sufficient. This is not incompatible with the data of the previous chapter since some Ti species were embedded in the wall and not all accessible to V contrary to the grafted one used in the present chapter. To further complete the picture of the anchored V site, one has to remind that the presence of Ti does not fully suppress the formation of  $Vi-O-Si$  bridges (see above the IR study on LUS-Ti(5)-V(x) and LUS-E-Ti(5)-V(x) series). In addition, the high mobility of vanadium precursors on the surface leading in absence of Ti to large polymeric species, favors the fixation of each of the V species onto a Ti cluster (see the titanium free LUS-V(x) and LUS-E-V(x) series). Then, it is likely that V species remains anchored to the silica while binding the Ti cluster via a mixture of  $Vi-O-Si$  and  $V-O-Ti$  bridges.(Scheme 4) Assuming a tripodal site, an average proportion of 1 for 2, would be reasonable, respectively.

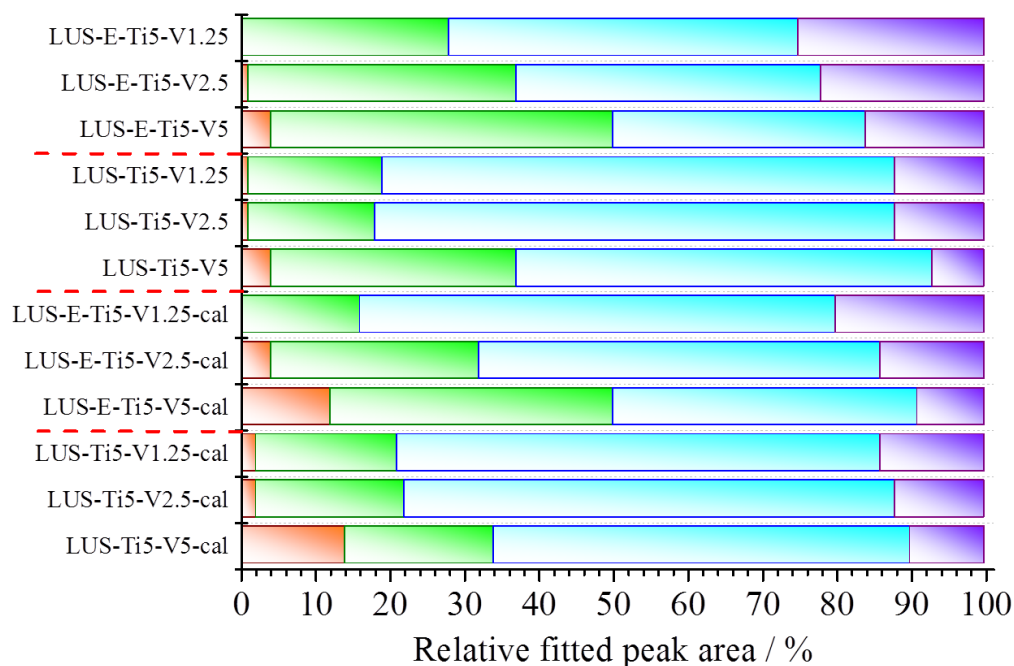


Figure 14. Relative fitted peak area LUS-E-Ti(5)-V(x), LUS-Ti(5)-V(x), LUS-E-Ti(5)-V(x)-cal and LUS-Ti(5)-V(x)-cal. Orange bar represented the bands at  $20000\text{ cm}^{-1} - 25000\text{ cm}^{-1}$  (polymer) Green bar represented the bands at  $30000\text{ cm}^{-1}$  (oligomer) ; Blue bar represented the bands at  $38000\text{ cm}^{-1}$  (monomer); Violet bar represented the bands at  $46000\text{ cm}^{-1}$  (monomer).

Table 5. Data of deconvolution for LUS-E-Ti(5)-V(x), LUS-Ti(y)-V(x), LUS-E-Ti(y)-V(x)-cal and LUS-Ti(y)-V(x)-cal.

	Peak A				Peak B				Peak C				Peak D			
	R <sup>2</sup>	X <sub>c</sub> (cm <sup>-1</sup> )	FWHM A(%)													
LUS-E-Ti(5)-V(1.25)	0.998		0		28		47		25							
LUS-E-Ti(5)-V(2.5)	1.000	25726	3949	1	33675	8353	36	39706	6464	41	44651	5145	22			
LUS-E-Ti(5)-V(5)	0.997		4		46		34		16							
LUS-Ti(5)-V(1.25)	1.000		1		18		69		12							
LUS-Ti(5)-V(2.5)	1.000	26365	4276	1	32187	7274	17	38839	9488	70	45956	5645	12			
LUS-Ti(5)-V(5)	1.000		4		33		56		7							
LUS-E-Ti(5)-V(1.25)-cal	0.999		0		16		64		20							
LUS-E-Ti(5)-V(2.5)-cal	1.000	25303	5434	4	32041	8443	28	39724	9424	54	46176	5868	14			
LUS-E-Ti(5)-V(5)-cal	1.000		12		38		41		9							
LUS-Ti(5)-V(1.25)-cal	1.000		2		19		65		14							
LUS-Ti(5)-V(2.5)-cal	1.000	25941	5304	2	32527	7422	20	39498	9462	66	49207	5628	12			
LUS-Ti(5)-V(5)-cal	1.000		14		20		56		10							

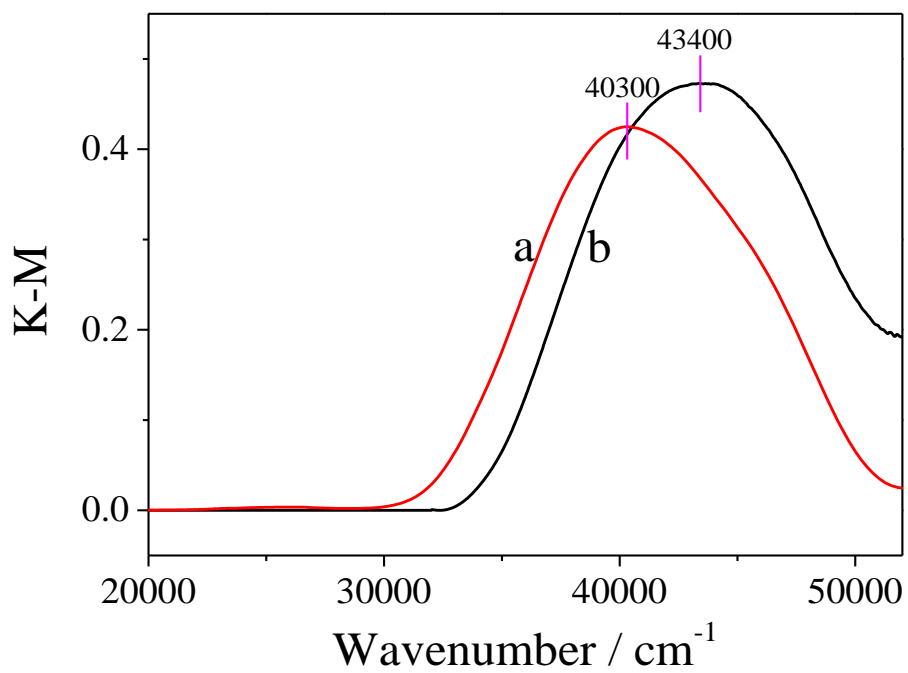
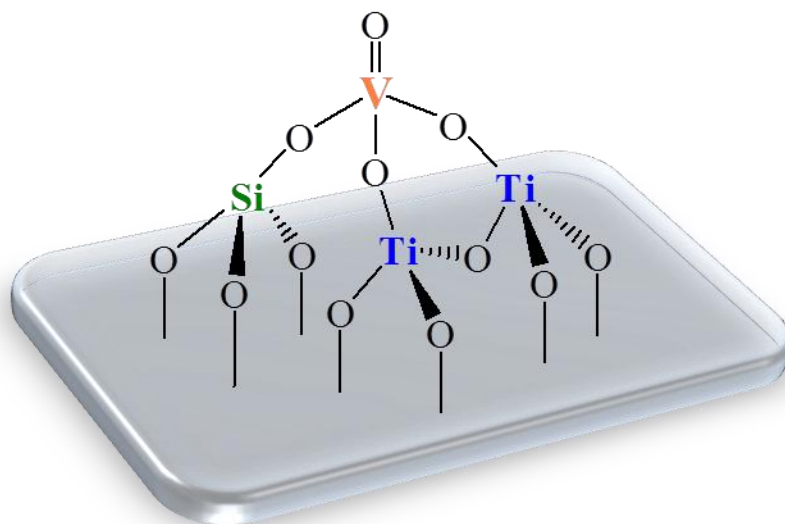


Figure 15. UV-visible spectra of a. LUS-Ti(5) and b. LUS-E-Ti(5).



Scheme 4. The ideal anchored V species moieties with a single V=O species linked to the silica support by one V-O-Si and 2 V-O-Ti on a dimeric Ti site.

## 5.4. Conclusion

In the previous chapter, a characterization methodology particularly based on the exploitation of the UV-visible diffuse reflectance spectroscopy was developed to evidence the anchoring effect of heteroions like  $\text{Al}^{3+}$  and  $\text{Ti}^{4+}$  on the dispersion of grafted V (V) ions on silica silica. In this chapter, the focus was made on Ti, which is better than Al and the heteroion was introduced by grafting on the surface of the as-made MCM-41 instead of a direct synthesis that locates  $\text{Ti}^{4+}$  statistically on the surface or inside the wall. In addition, the molecular stencil patterning technique was applied to decorate the surface with organic moieties and block some anchoring sites to improve the dispersion. X-ray diffraction patterns proved that the long-range order channels of MCM-41 silicas were maintained after multiple steps preparation process. The information obtained from  $\text{N}_2$  sorption measurement suggested the decrease of pore size and the polarity change after introduction of dipodal organosilyl groups. The presence of EBDMS groups was evidenced using TG Analysis and quantitative Infrared and Solid  $^{29}\text{Si}$  NMR revealing three different states of absorption.

The states of vanadium species were investigated using a deconvolution into four Gaussian curves of UV-visible spectra assigned to polymeric, small clusters and isolated vanadium species. Tauc's plots were exploited to rank the samples by the size of the polymeric species in all the samples. When vanadium was grafted alone, the formation of large clusters was favored while the remaining species could remain isolated showing a large mobility and equilibrium between aggregates. The introduction of EBDMS groups using the MSP technique favors the formation of aggregate but smaller than without EBDMS at low loading. Conversely at high loading, the polymeric species are larger than without EBDMS and the remaining species are better dispersed. This is consistent with the nanobead effect produced by the organic masking pattern. The incorporation of titanium changed completely the

picture by fixing the vanadium species, blocking mobility and inhibiting polymeric growth. This is the confirmation of the anchoring role of Ti that immobilizes the vanadium for a better efficiency at  $V/Ti \leq 1/2$ . The introduction of organic EBDMS groups by the MSP technique decreases slightly the size of the anchoring Ti clusters at least for low loading ( $\leq 2.5$  mol V %). At higher loading, the effect is reverse with a worse V dispersion, consistent with a saturation of the nanobead volume. The data suggest that the average anchoring of an isolated  $V=O$  species is tripodal with 2 V-O-Ti and 1 V-O-Si bridges.

## 5.5. References

- (1) Khatri, P. K.; Singh, B.; Jain, S. L.; Sain, B.; Sinha, A. K. *Chem Commun (Camb)* **2011**, *47*, 1610.
- (2) Abry, S.; Thibon, A.; Albela, B.; Delichere, P.; Banse, F.; Bonneviot, L. *New Journal of Chemistry* **2009**, *33*, 484.
- (3) Zhou, W.-J.; Albela, B.; Ou, M.; Perriat, P.; He, M.-Y.; Bonneviot, L. *Journal of Materials Chemistry* **2009**, *19*, 7308.
- (4) Calmettes, S.; Albela, B.; Hamelin, O.; Menage, S.; Miomandre, F.; Bonneviot, L. *New Journal of Chemistry* **2008**, *32*, 727.
- (5) Zhang, K.; Albela, B.; He, M. Y.; Wang, Y.; Bonneviot, L. *Physical chemistry chemical physics : PCCP* **2009**, *11*, 2912.
- (6) Abry, S.; Albela, B.; Bonneviot, L. *Comptes Rendus Chimie* **2005**, *8*, 741.
- (7) Bonneviot, L.; Morin, M.; Badiei, A. **2001**; Vol. WO 01/55031 A1.
- (8) Khouw, C. B.; Davis, M. E. *Journal of Catalysis* **1995**, *151*, 77.
- (9) Lee, E. L.; Wachs, I. E. *The Journal of Physical Chemistry C* **2007**, *111*, 14410.
- (10) Fraile, J. M.; Garcia, J. I.; Mayoral, J. A.; Vispe, E. *Journal of Catalysis* **2005**, *233*, 90.
- (11) On, D. T.; Denis, I.; Lortie, C.; Cartier, C.; Bonneviot, L. *Studies in Surface Science and Catalysis* **1994**, *83*, 101.
- (12) Iliev, M. N.; Hadjiev, V. G.; Litvinchuk, A. P. *Vibrational Spectroscopy* **2013**, *64*, 148.
- (13) Gonzalez, R. J.; Zallen, R.; Berger, H. *Physic Reviews B* **1997**, *55*, 7014.
- (14) Ocana, M.; Serna, C. J. *Spectrochimica Acta* **1991**, *47*, 765.
- (15) Murashkevich, A. N.; Lavitskaya, A. S.; Barannikova, T. I.; Zharskii, I. M. *Journal of Applied Spectroscopy* **2008**, *75*, 730.
- (16) Sanchez, C.; Livage, J.; Lucazeau, G. *Journal of Raman Spectroscopy* **1982**,

12, 68.

(17) Fang, L. thesis: Surface Engineering in Mesoporous Silica for Ti-Based Epoxidation Catalysts. Ecole Normale Supérieure de Lyon & East China Normal University, **2012**.

(18) Shimojima, A.; Umeda, N.; Kuroda, K. *Chemistry of Materials* **2001**, *13*, 3610.

(19) Bulánek, R.; Čičmanec, P.; Sheng-Yang, H.; Knotek, P.; Čapek, L.; Setnička, M. *Applied Catalysis A: General* **2012**, *415–416*, 29.

(20) Bulánek, R.; Čapek, L.; Setnička, M.; Čičmanec, P. *The Journal of Physical Chemistry C* **2011**, *115*, 12430.

(21) Luan, Z.; Kevan, L. *The Journal of Physical Chemistry B* **1997**, *101*, 2020.

(22) Luan, Z.; Meloni, P. A.; Czernuszewicz, R. S.; Kevan, L. *The Journal of Physical Chemistry B* **1997**, *101*, 9046.

## Chapter 6. Investigation of catalytic application of vanadium containing mesoporous silica

### 6.1 Introduction

Catalysis is an important application of transition metals, particularly in heterogeneous catalysis, in which they are often at the head of the active phase and most of the time, supported on oxides. Vanadium-containing heterogeneous catalysts provides edifying examples for oxidation reactions<sup>1-16</sup> or lately for bromination processes<sup>17-19</sup>. Among them, vanadium-containing MCM-41 type silicas are particularly interesting since they combine high surface area, accessibility for large molecules through the mesopores and control on the vanadium phase dispersion as shown in the two preceding chapters.

In comparison to titanium-containing materials, vanadium-containing heterogeneous catalysts were much less exploited as catalysts for oxidation reaction. One of the main reasons is the poor stability of vanadium species, which unfortunately tend to leach out particularly in the liquid phase type of reactions. In the earlier 1996, J. S. Reddy *et al.* reported claimed that the leaching problem was related with the nature of the substrates, the solvents and even the oxidants.<sup>20</sup> This is of course right but incomplete since it eludes the problem on which we now have a hand on, the strengthening of the vanadium interaction with the support. Though we have mostly focus our investigation on the effect on the dispersion and site isolation, it should also impact on the retention of vanadium in the support during reaction. However, there is few study reported about the details of the leaching process. Vanadium dispersion and leaching will be treated in parallel in this chapter.

Besides, it is necessary to choose a proper reaction to probe the catalytic performance and the leaching problem. Considering the potentiality of vanadium in selective oxidation reaction of alkanes, our choice went to oxidation of cyclohexane, a useful industrial production process. Two main products of this reaction i.e. cyclohexanone and cyclohexanol often called in industry KA oil. Ring opening and deeper oxidation into adipic acid is a strategic industrial intermediate for the Nylon industry. This process included two steps: 1) cyclohexane was oxidized to cyclohexyl hydroperoxide (CHHP) non-catalytically, 2) deperoxidation of CHHP to products catalyzed by transition metal containing materials.<sup>21,22</sup> In traditional procedure, the catalyst is Co(II) homogeneous catalyst which is hard to be recovered and recycled. The traditional protocol also produced amounts of alkaline solution during the production. These drawbacks drove the researchers to look for greener processes using heterogeneous materials. W-J Zhou *et al.* evaluated the catalytic activities of titanium-containing silicate zeolites in the oxidation reaction of cyclohexane. The oxyl species was firstly detected and proved to be helpful for the proposal of mechanism.<sup>22</sup>

Vanadium-containing silica was once applied in the oxidation of cyclohexane as a heterogeneous catalyst in literature. P. Selvam *et al.*<sup>23</sup> studied the effect of vanadium sources on the synthesis of V-MCM-41, and the oxidation of cyclohexane and cyclododecane was taken as probe reaction to evaluate the catalytic abilities of samples. The main product is cyclohexanol with less amounts of cyclohexanone. In comparison to titanium-containing catalysts there is trace of side-products, mainly cyclohexyl acetate showing that vanadium revealed a too strong catalyst. In addition, the V-MCM-41 showed high capacity for regeneration and nonetheless serious leaching problem. A pre-washing treatment was advocated to avoid the vanadium leaching during reaction and allow the recycling of the catalysts.

Here the use of catalysts prepared in Chapters 4 and 5 provides a variety of vanadium dispersion with and without polymeric vanadium species weakly bound to the support. In this Chapter, the redox properties of these materials were investigated by temperature programmed reduction, TPR. Washing by methanol was used to probe vanadium leaching and catalytic performance was tested on the oxidation of cyclohexane including recyclability in relation to the leaching limitation.

## **6.2 Experimental**

Both series of samples prepared in Chapter 4 and Chapter 5 were investigated. The former series is denoted as by the suffix “-I” for impregnation from the V(IV) precursor while the latter by the “-G” for grafting from the V(V) alkoxides.

### **6.2.1 Leaching test**

30 mg catalyst was dispersed in 15 mL methanol (>99.6%) and stirred at room temperature for 30 minutes. The solid was separated from liquid phase by filtration and dried at 80 °C overnight. The solid after washing and the liquid phase was characterized by UV-visible spectroscopy, and elemental analysis.

### **6.2.2 Oxidation reaction of cyclohexane**

100 mg catalyst was dispersed in cyclohexane solution with 7.5 wt % tert-butyl hydroperoxide (TBHP). The mixture was refluxed under 80 °C for 1h. The reactant was cooled down to room temperature and filtrated to separate the catalyst and reactant. The products were analyzed by gas chromatography (GC) using 0.05 g chlorobenzene as external standard. Cyclohexane conversion was calculated from the molar ratio of cyclohexanol plus cyclohexanone over the initial concentration of

cyclohexane. TBHP conversion was obtained from titration by an iodometric method. TBHP efficiency is obtained from the concentration of cyclohexanol and cyclohexanone divided by the concentration of converted TBHP. K/A is the molar ratio of cyclohexanone over cyclohexanol at the end of the reaction. The turn over number, TON, is based on the cyclohexane conversion per V atom obtained from elemental analysis. For mere recycling, the solid was separated by filtration, dried at 80 °C overnight and used in the following run. The calcined samples were heated at 550 °C for 6 h in a flow of dry air for a second type of recycling.

## **6.3 Results and discussion**

### **6.3.1 Redox behaviors of vanadium-containing silica.**

The H<sub>2</sub>-TPR patterns of LUS-V(x)-I were depicted in Figure 1. It is shown that the main peak of LUS-V(x)-I located at the region of 550 °C - 650 °C with a shoulder at around 515 °C, while the support pure silica showed no signal of H<sub>2</sub> consumption. The low temperature shoulder was assigned to the reduction of monomeric vanadium species. The higher reduction temperature was assigned to the reduction oligomers and polymers. A progressive shifts to higher temperature corresponding to lower vanadium dispersion in complete agreement with the results from UV-visible spectroscopy.

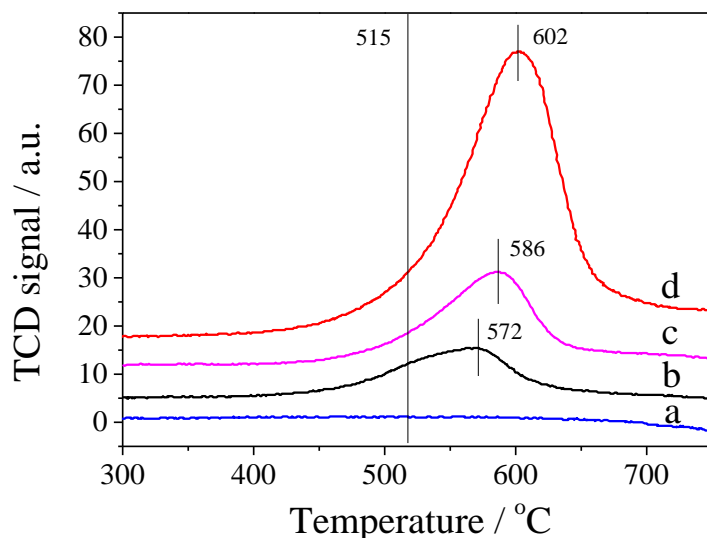


Figure 1. H<sub>2</sub>-TPR patterns of a. LUS, b. LUS-V(1.25)-I, c. LUS-V(2.5)-I, and d. LUS-V(5)-I.

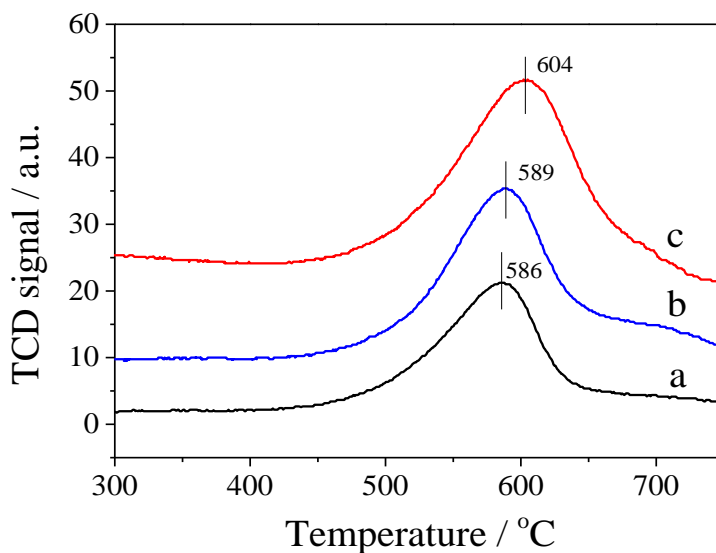


Figure 2. H<sub>2</sub>-TPR patterns of a. LUS-V(2.5)-I, b. Al(5)-LUS-V(2.5)-I, and c. Ti(7)-LUS-V(2.5)-I.

For a given loading the reduction temperature increased from pure siliceous LUS support to Al-LUS and Ti-LUS see reduction of LUS-V(2.5), Al(5)-LUS-V(2.5) and Ti(7)-LUS-V(2.5) (Figure 2). The high temperature shift of vanadium reduction on titanium-containing silicas was also observed by M. Setnicka *et al.* . The shift was

even more pronounced when increasing the titanium contents consistent with a stronger V-O-Ti bridge than a V-O-Si bridge. Conversely, the trend is inversed on pure TiO<sub>2</sub> support where V-O-V seems weaker than V-O-Ti.<sup>24</sup>

Along the same reasoning, when comparing LUS-V(2.5), LUS-Al(5)-V(2.5) and LUS-Ti(5)-V(2.5), it appeared that V-O-Ti bridges are stronger than V-O-Al and V-O-Si bridges.

### 6.3.2 Leaching test

It was interesting to correlate the reducibility of vanadium and the anchoring properties of Al and Ti with the leaching drawback of vanadium. The methanol was chosen as a solvent because of its stronger polarity than other current solvents and its relation with any product from alkane oxidation generating alcohol function in a primary step. The level of leaching in the LUS-V, Al(5)-LUS-V and Ti(7)-LUS-V series was reported in a bar diagram (Figure 3). The loss of vanadium species was calculated in percentage as the V mol% before leaching test minus the V mol% after

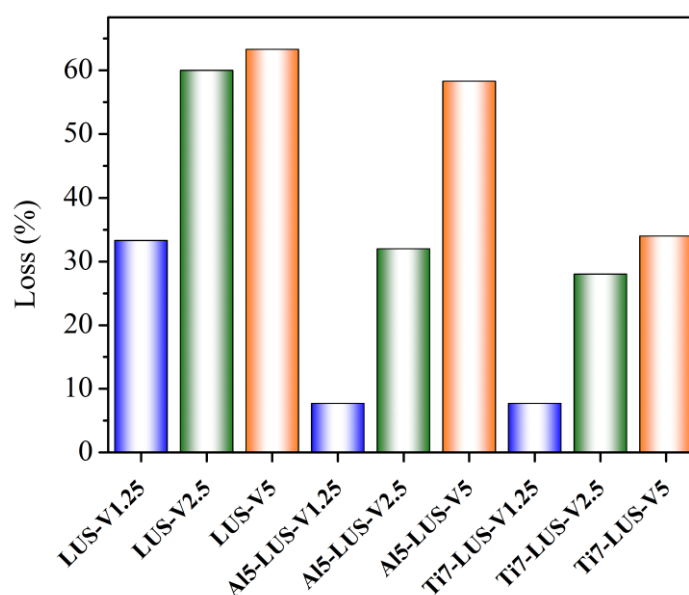


Figure 3. Loss of vanadium species of Si-LUS-V-I series, Al(5)-LUS-V-I series and Ti(7)-LUS-V-I series.

leaching test divided by V mol% before the leaching test.(Table 1 and Figure 3) The higher the vanadium loading, the higher the vanadium leaching whatever the series. This correlate is with a higher content of polymeric species. The vanadium loss is larger on pure silica than in the presence of Al or Ti anchors. Therefore the best retention is obtained for the lowest loading with al or Ti anchors though it remains about 8 % for both. Ti-LUS-V is obviously less than the LUS-V and Al-LUS-V. This may be rationalized using two different argumentations: 1) some of the titanium species are also leaching out from Ti-LUS (from 7.1 to 6.2 molTi%) (Table 1); 2) some vanadium species remain not linked to the anchor at low loadings. This is not elucidated yet.

Table 1. Elemental analysis of LUS-V, Al-LUS-V and Ti-LUS-V series before and after leaching test.

	Before leaching test		After leaching test		Loss
	X (mol %)	V (mol %)	X (mol %)	V (mol %)	V(%)
LUS-V(1.25)-I	-	1.2	-	0.8	33.3
LUS-V(2.5)-I	-	2.5	-	1.0	60.0
LUS-V(5)-I	-	4.9	-	1.8	63.3
Al(5)-LUS-V(1.25)-I	4.8	1.3	4.8	1.2	7.7
Al(5)-LUS-V(2.5)-I	4.8	2.5	4.8	1.7	32.0
Al(5)-LUS-V(5)-I	4.8	4.8	4.6	2.0	58.3
Ti(7)-LUS-V(1.25)-I	7.1	1.3	6.2	1.2	7.7
Ti(7)-LUS-V(2.5)-I	7.1	2.5	6.1	1.8	28.0
Ti(7)-LUS-V(5)-I	7.1	5.0	6.2	3.3	34.0

To further investigate the effect of washing using methanol, the states of vanadium species after washing was characterized by UV-visible spectroscopy, from which energy gaps were extracted using the Tauc's plot.(Figure 4) For the samples with larger vanadium particles i.e. LUS-V-I series, Al(5)-LUS-V(5) and Ti(7)-LUS-V(5), the energy gap (Table 1) shifted to higher value revealing that the largest aggregates (polymeric species) were preferentially leached out, leaving smaller aggregates linked to the support. This is particularly true for vanadium species on pure siliceous support. In the presence of Al, the effect is less pronounced and even inverted for the lowest V loading that presents the best dispersion before leaching tests. In the presence of the Ti anchor leading to better dispersion and the smallest oligomers, the inversion appears at the intermediate loading of 2.5 V mol%. This clearly indicated that methanol provide some mobility also for isolated and very small clusters (dimers) shifting the population towards intermediate oligomers (trimers, tetramers) whose

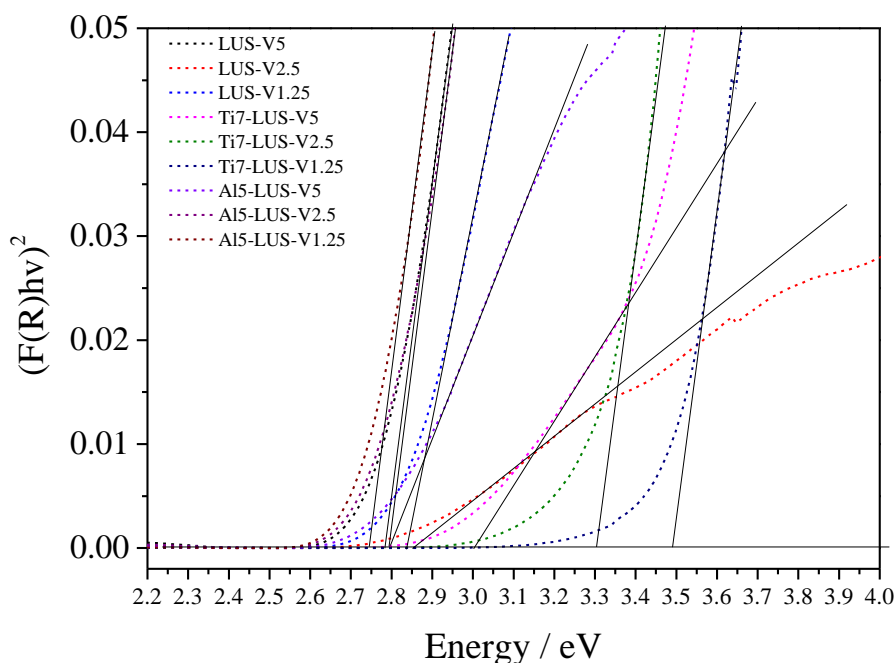


Figure 4. Tauc's plot based on UV-visible spectra of LUS-V(x)-I, Al(5)-LUS-V(x)-I and Ti(7)-LUS-V(x)-I after leaching test.

mobility remains small and resistance to leaching relatively high.

Table 2. Edge energies of obtained from Tauc's plot of LUS-V(x), Al(5)-LUS-V(x), and Ti(7)-LUS-V(x).

	Edge energy (eV)	
	Before leaching	After leaching
LUS-V(5)	2.61	2.79
LUS-V(2.5)	2.70	2.86
LUS-V(1.25)	2.70	2.84
Al(5)-LUS-V(5)	2.56	2.79
Al(5)-LUS-V(2.5)	2.79	2.79
Al(5)-LUS-V(1.25)	3.29	2.74
Ti(7)-LUS-V(5)	2.81	3.00
Ti(7)-LUS-V(2.5)	3.52	3.30
Ti(7)-LUS-V(1.25)	3.72	3.49

### 6.3.3 Catalytic performance of oxidation of cyclohexane

In order to study the catalytic behavior of vanadium-containing silica, oxidation of cyclohexane was decided as the probe liquid phase reaction because its potential in industrial application.

#### 6.3.3.1 Catalytic performance of vanadium-containing MCM-41 type silica prepared by impregnation

The catalytic performance of LUS-V series and Ti(7)-LUS-V series prepared in Chapter 4 was evaluated because these two series samples showed obvious difference of vanadium dispersion. The main products are cyclohexanol and cyclohexanone as

shown in GC. The main products were cyclohexanol and cyclohexanone as shown in GC. Note that the cyclohexane was also the solvent in the present protocol and its conversion remained low. As shown in Table 3, the cyclohexane conversion decreases with the decreasing of vanadium contents in the both series samples, but the turnover number (TON) increased inversely. Nonetheless, the turnover number (TON) increased and revealed that the proportion of active catalytic vanadium sites increased. Indeed, LUS-V(1.25)-I and Ti(7)-LUS-V(1.25)-I exhibited the better TON in each series. According to UV-visible characterization of Chapter 4, this observation is consistent with catalytic sites that match with the smallest clusters and even isolated vanadium sites. Furthermore, the TON of Ti(7)-LUS-V series is lower than the one of LUS-V series because titanium is less active than vanadium and it is the average  $TON_{V+Ti}$  that is taken into account for comparison. Indeed, grafted titanium in Ti(7)-LUS exhibited a clear catalytic activity. The TBHP efficiency is low in all samples, indicating that direct decomposition of hydro peroxide take places on surface silanol groups. The ratio of cyclohexanone over cyclohexanol is all around 0.5, indicating less cyclohexanone produced by deeper oxidation.

Table 3. Catalytic performance of LUS-V-I series and Ti(7)-LUS-V-I series.

	Cyclohexane Conversion (%)	TBHP Conversion (%)	TBHP Efficient (%)	K/A	TON
LUS-V(5)-I	0.87	74.7	14.2	0.54	6.4
LUS-V(2.5)-I	0.66	63.1	14.2	0.41	9.7
LUS-V(1.25)-I	0.58	46.4	16.5	0.51	14.6
Ti(7)-LUS-V(5)-I	1.20	77.3	18.9	0.79	3.0
Ti(7)-LUS-V(2.5)-I	0.77	72.1	14.5	0.41	3.2

Ti(7)-LUS-V(1.25)-I	0.71	49.5	19.3	0.48	3.6
Ti(7)-LUS	0.66	54.3	14.6	0.66	2.8

Reaction condition: 0.1 g catalyst, 4 g 7.5 wt% TBHP in cyclohexane, reaction time: 1 h, reaction temperature: 80 °C.

### 6.3.3.2 Recycling and reusing of vanadium-containing MCM-41 type silica prepared by impregnation

The recyclability of samples LUS-V(5)-I, Ti(7)-LUS-V(5)-I, LUS-V(1.25)-I and Ti(7)-LUS-V(1.25)-I were investigated comparing the conversion of cyclohexane and TBHP as well as the K/A ratios after reuse for several times as in Table 4, Figure 5 and Figure 6. The cyclohexane conversions of LUS-V series decrease at each new recycling run, showing a poor retention of vanadium on pure silica. It is interesting to note that the Ti(7)-LUS-V(5)-I exhibited a significant loss of at the first recycling run and then kept a relatively constant conversion in the following recycling runs. This clearly shows that the first run removes the weakly linked species that obviously correspond to the polymeric species with the most red shifted Charge transfer band on the UV-visible spectra. Conversely, the small clusters or oligomers are those better retained on the support in the reaction conditions. Indeed, at lower V loadings that generated better vanadium dispersion, the conversion loss was less pronounced as shown on pure silica with LUS-V(1.25)-I. Still at low loading, the anchoring effect of Ti is shown by a higher activity and a better retention (60 % instead of 40% without Ti). The TBHP conversion that is in excess follows basically the trend of the cyclohexane conversion does not bring much more information. In contrast, the K/A ratios follow a trend that depends on the presence of Ti and the vanadium loss. On titanium free catalysts this ratio ranged between 0.3-0.7 without any clear trend for high V loading while it increased from 0.5 to about 1.1 at low loading after the

successive recycling runs. When Ti is present this ratio remains low as far as the polymeric species were removed (2nd run and the following ones) at high V loading or when the Ti loading was low (all the recycling runs). This can be understood assuming that the polymeric or the largest clusters are producing less cyclohexanone than cyclohexanol. This shows that there is certainly different active species and the one with the lowest V nuclearity lead more readily to a deeper oxidation than those with a larger number of vanadium ions.

Table 4. Catalytic performance of LUS-V(5), Ti(7)-LUS-V(5), LUS-V(1.25) and Ti(7)-LUS-V(1.25) in reusing process.

	Reusing time	Cyclohexane	TBHP	K/A
		Conversion (%)	Conversion (%)	
LUS-V(5)-I	1 <sup>st</sup> run	0.87	74.7	0.54
	2 <sup>nd</sup> run	0.56	38.2	0.63
	3 <sup>rd</sup> run	0.44	24.0	0.73
	4 <sup>th</sup> run	0.12	17.6	0.32
Ti(7)-LUS-V(5)-I	1 <sup>st</sup> run	1.20	77.3	0.79
	2 <sup>nd</sup> run	0.75	53.7	0.55
	3 <sup>rd</sup> run	0.69	41.6	0.47
	4 <sup>th</sup> run	0.71	39.0	0.44
LUS-V(1.25)-I	1 <sup>st</sup> run	0.58	46.4	0.51
	2 <sup>nd</sup> run	0.43	27.4	0.73
	3 <sup>rd</sup> run	0.35	18.2	0.90
	4 <sup>th</sup> run	0.28	14.6	0.96
	5 <sup>th</sup> run	0.24	12.2	1.06
Ti(7) -LUS-V(1.25)-I	1 <sup>st</sup> run	0.71	49.5	0.48

---

2 <sup>nd</sup> run	0.64	40.7	0.51
3 <sup>rd</sup> run	0.55	21.1	0.41
4 <sup>th</sup> run	0.47	24.8	0.61
5 <sup>th</sup> run	0.39	15.6	0.67

---

Reaction condition: 0.1 g catalyst, 4 g 7.5 wt% TBHP in cyclohexane, reaction time: 1 h, reaction temperature: 80 °C.

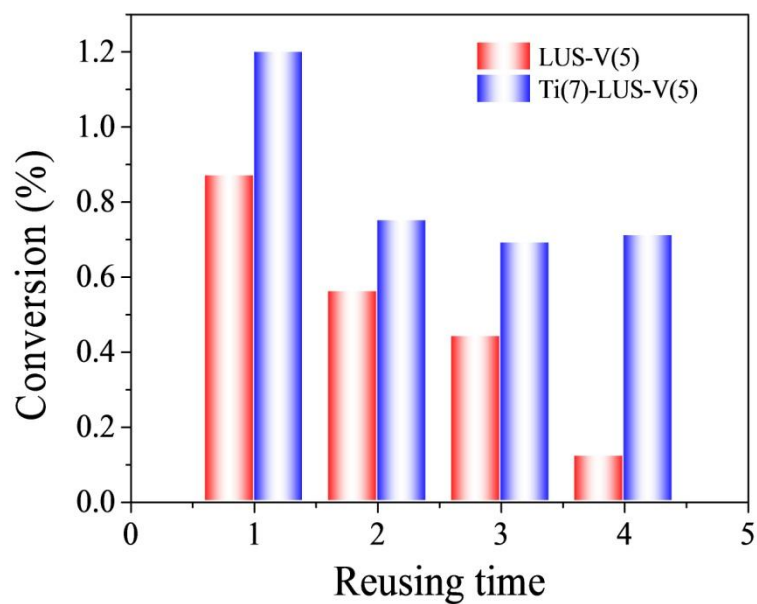


Figure 5. Cyclohexane conversion of LUS-V(5)-I and Ti(7)-LUS-V(5)-I during four times reusing.

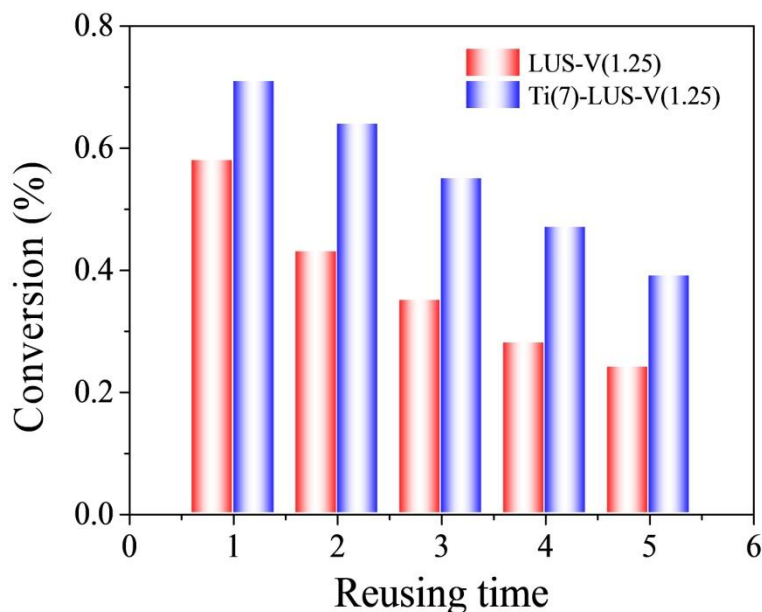


Figure 6. Cyclohexane conversion of LUS-V(1.25)-I and Ti(7)-LUS-V(1.25)-I during five times reusing.

### 6.3.3.3 Catalytic performance of vanadium-containing MCM-41 type silica prepared by grafting with or without molecular patterning stencil technique

The grafting method and molecular patterning stencil technique that produced worse dispersion or better dispersion of vanadium depending on the V loading (Chapter 5) led to catalysts that were tested in similar conditions than those prepared by impregnation (Chapter 4). The catalytic performance in oxidation of cyclohexane of this series of samples is shown in Table 5.

Basically, the samples based on the grafting method showed a similar trend than those obtained by impregnation, i. e., lower V contents samples led to lower conversions but higher TONs. For instance, compare the TON of 15.2 for LUS-V(1.25)-G to 7.5 of LUS-V(5)-G or 22.9 for LUS-E-V(1.25)-G to 8.0 of LUS-E-V(5)-G. Comparing now the former pair of materials to the latter pair of materials, one observes that only at

low vanadium loading, the TON is improved in the presence of the organic pattern of EBDMS. This is in adequacy with the nano-beaker effect that improves V dispersion at low loading. Note that these remarks are valid even in the presence of Ti acting as an anchor. In fact, the presence of titanium leads to better conversion increases but the TONs decrease since it refers to V and Ti center present in the samples. In this series, the titanium ions are grafted on the surface and accessible, in principle. The reason for low TONs is the poor activity of titanium species (last entry of Table 5, LUS-E-Ti(5)-G) that may be further decreased in the presence of grafted vanadium ions, below which they are likely buried. Indeed, if titanium atom were not counted among the potential active site, the TON reported on vanadium only would have been higher in the presence of Ti in all the cases, also in adequacy with a better dispersion.

Furthermore, a systematic increase of turnover is observed in the grafted series in comparison to the impregnated series, which exhibited a worse dispersion. This is obvious by comparing TONS of the grafted series LUS-V(5)-G, LUS-V(1.25)-G, LUS-Ti(5)-V(5)-G and LUS-Ti(5)-V(1.25)-G (7.5, 16.8, 4.5, 3.8, respectively) to the corresponding impregnated series LUS-V(5)-I, LUS-V(1.25)-I, Ti(7)-LUS-V(5)-I and Ti(7)-LUS-V(1.25)-I (6.4, 14.6, 3.0 and 3.6, respectively). Another proof is that dispersion directly impact the conversion is the effect of calcination that systematically produces a slight loss of activity (lower TON).

Apart from improving dispersion and catalytic reactivity, the organic patterning decreases the surface polarity of the silica support. As the consequence, less TBHP decomposition takes place improving the TBHP efficiency (compare LUS-E-Ti(5)-V(5)-G, LUS-E-V(5)-G, LUS-E-Ti(5)-V(1.25)-G and LUS-E-V(5)-G). Calcination that eliminated the capping trimethylsilyl groups suppress this advantage .

The selectivity in ketone and alcohol is the last parameter that remains to comment. As a general trend, the K/A ratio is smaller for impregnated materials than the grafted one. However, the low V loaded pure silica systems exhibited a high selectivity in ketone in the absence of Ti. Noticeably, the presence of titanium tends to increase this ratio, which may indicate that the oxidation is deeper than for vanadium alone. Note that in the impregnated catalysts the Ti is incorporated in the silica wall and as little or even no effect on the selectivity. Conversely, higher K/A are observed for grafted materials where all Ti are sitting on the surface. Note that titanium in absence of vanadium lead to high K/A. However, the Ti centers are much less active than V centers are not expected to impact the selectivity so significantly in the presence of the latter. Again, as a general trend high K/A appear to correlate with high dispersion of vanadium.

Apart from dispersion, another criteria seems to impact the K/A, this is the capping of the surface silanol by the organic masking treatment (Table 5). This effect is maximum even for high vanadium loaded support where dispersion is not optimum. Consistently, the selectivity in ketone is completely reversed after calcination and removal of the organic silanol capping. So that the most productive catalysts is the LUS-E-Ti(5)-V(5)-G that has the best compromise between dispersion and number of sites while the most efficient one is the LUS-E-Ti(5)-V(1.25)-G or LUS-E-V(1.25)-G that gathered the best qualitative criteria.

Since the grafting technique lead to a much better dispersion of vanadium, the effect of Ti anchoring is not as spectacular as that in the impregnated ones. It remains to be seen whether or not titanium improves the retention of vanadium under reaction condition like in impregnated samples.

Table 5. Catalytic performance of vanadium-containing MCM-41 type silica prepared by MSP technique.

	Cyclohexane	TBHP	TBHP		
	Conversion	Conversion	Efficiency	K/A	TON
	(%)	(%)	(%)		
LUS-E-Ti(5)-V(5)-G	1.48	65.7	27.9	1.32	4.7
LUS-E-V(5)-G	1.24	59.3	26.8	1.25	8.0
LUS-Ti(5)-V(5)-G	1.30	83.4	13.8	0.75	4.5
LUS-V(5)-G	1.14	86.1	18.0	1.11	7.5
LUS-E-Ti(5)-V(1.25)-G	0.93	35.6	34.4	1.09	5.9
LUS-E-V(1.25)-G	1.03	47.4	29.4	0.80	22.9
LUS-Ti(5)-V(1.25)-G	0.78	49.1	21.3	0.78	3.8
LUS-V(1.25)-G	0.76	47.9	21.4	0.67	15.2
LUS-E-Ti(5)-V(1.25)-G-cal	0.73	55.3	17.8	0.44	4.7
LUS-E-V(1.25)-G-cal	0.76	58.9	17.2	0.54	16.8
LUS-Ti(5)-V(1.25)-G-cal	0.66	54.3	17.0	0.44	3.2
LUS-V(1.25)-G-cal	0.57	42.7	17.6	0.57	11.8
LUS-E-Ti(5)-G	0.48	11.4	56.7	1.11	3.4

Reaction condition: 0.1 g catalyst, 4 g 7.5 wt% TBHP in cyclohexane, reaction time: 1h, reaction temperature: 80 °C.

### 6.3.3.4 Recycling and reusing of vanadium-containing MCM-41 type silica prepared by grafting with or without molecular patterning stencil technique

Considering the problem of the catalysts recycling, the most interesting case was that of the well dispersed V phase shown to be the most useful in the catalytic oxidation of cyclohexane. Then, the investigation was focused on the low loaded samples (1.25 Vmol%). In addition, it was interesting to see how calcination would affect the catalyst robustness. The catalytic performance of LUS-Ti(5)-V(1.25)-G and LUS-Ti(5)-V(1.25)-G-cal can be compared in and Table 6 as well as there equivalent with the organic EBDMS patterning, LUS-E-Ti(5)-V(1.25)-G-cal and LUS-E-V(1.25)-G-cal.

The bar diagram of Figure 7 give a more synthetic view of the catalytic performance than Table 6 and shows that calcination leads to a slight decrease of activity but ensures better stability. By contrast, the organic patterning does not bring any advantages when stability is at stake and the interest of titanium seems not to operate on stability as well. More should be done to understand these points.

Table 6. Catalytic performance of LUS-Ti(5)-V(1.25)-G, LUS-Ti(5)-V(1.25)-G-cal, LUS-E-Ti(5)-V(1.25)-G-cal and LUS-E-V(1.25)-G-cal in reusing process.

	Reusing time	Cyclohexane	TBHP	K/A
		Conversion (%)	Conversion (%)	
LUS-Ti(5)-V(1.25)-G	1 <sup>st</sup> run	0.78	49.1	0.78
	2 <sup>nd</sup> run	0.67	38.7	0.62
	3 <sup>rd</sup> run	0.57	26.8	0.57
	4 <sup>th</sup> run	0.52	25.3	0.52

---

LUS-Ti(5)-V(1.25)-G-cal	1 <sup>st</sup> run	0.66	54.3	0.44
	2 <sup>nd</sup> run	0.68	51.4	0.39
	3 <sup>rd</sup> run	0.59	32.4	0.59
	4 <sup>th</sup> run	0.63	38.4	0.47
LUS-E-Ti(5)-V(1.25)-G-cal	1 <sup>st</sup> run	0.73	55.3	0.44
	2 <sup>nd</sup> run	0.67	44.2	0.42
	3 <sup>rd</sup> run	0.56	21.5	0.65
	4 <sup>th</sup> run	0.45	11.2	0.96
LUS-E-V(1.25)-G-cal	1 <sup>st</sup> run	0.76	58.9	0.54
	2 <sup>nd</sup> run	0.55	28.8	0.69
	3 <sup>rd</sup> run	0.43	17.1	0.87
	4 <sup>th</sup> run	0.47	18.2	0.75

---

Reaction condition: 0.1 g catalyst, 4 g 7.5 wt% TBHP in cyclohexane, reaction time: 1 h, reaction temperature: 80 °C.

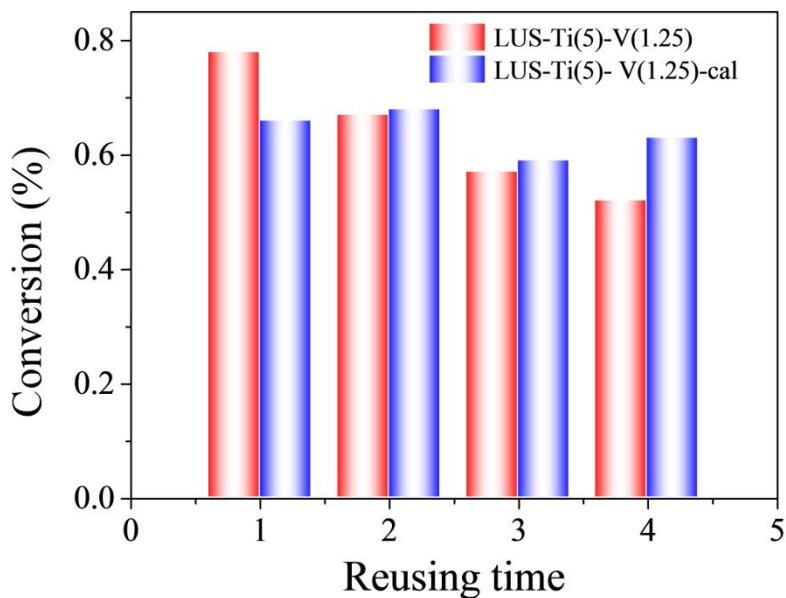


Figure 7. Cyclohexane conversion of LUS-Ti(5)-V(1.25)-G and LUS-Ti(5)-V(1.25)-G-cal during four times reusing.

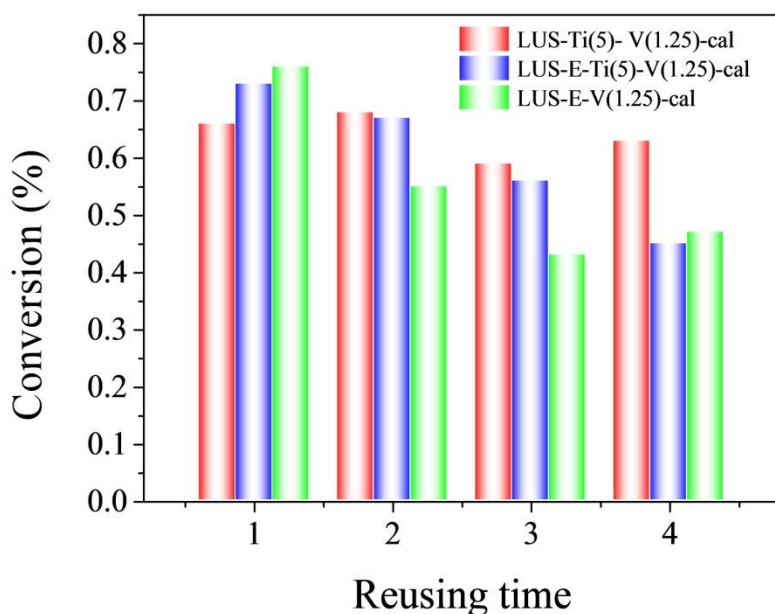


Figure 8. Cyclohexane conversion of LUS-Ti(5)-V(1.25)-G-cal, LUS-E-Ti(5)-V(1.25)-G-cal and LUS-E-V(1.25)-G-cal during four times reusing.

## 6.4 Conclusion

The catalytic properties of vanadium-containing mesoporous silicas prepared by two different methods in the last two chapters were evaluated in this work. The temperature programmed reduction technique was utilized to reveal the redox behavior of LUS-V, Al-LUS-V and Ti-LUS-V. The maximal reduction temperature shifted to higher temperatures when the vanadium content was increased and also the presence of titanium species acting as an anchor for vanadium species. The metal leaching known to be the weakness of vanadium was tested using methanol as extracting solvent. The polymeric species were shown the easiest to leach out while the small clusters and the monomeric species exhibited the best retention properties. The leaching test proved that the Ti-O-V bonds are stronger than Al-O-V bonds and Si-O-V bonds. The introduction of titanium species could reduce the leaching phenomenon.

Then, oxidation of cyclohexane was applied as a probe reaction to evaluate the reactivity of synthesized samples. As a consequence, the samples prepared by grafting method with molecular stencil patterning technique are more reactive than the samples prepared by impregnation. The introduction of organic patterning groups EBDMS improved the reactivity of vanadium sites in relation with a better dispersion of vanadium active sites. In addition, the organic groups on the surface increased the hydrophobicity, decreasing the inefficient decomposition of hydro peroxide. In the recycling and reusing tests, the reactivity and selectivity was maintained in some samples prepared by both impregnation and grafting method with incorporation of titanium species, proving the immobilization of vanadium species by titanium species.

Consequently, although the introduction of titanium species increase the temperature of reduction of active sites, it also reduce the leaching of vanadium species in the

liquid media of the oxidation reaction, which provides some potential in future industrial application. Besides, the MSP technique improved the reactivity of active sites of heterogeneous catalysts, though some improvement remained to be made on the robustness of this type of sophisticated hybrid catalysts.

## 6.5 Reference

- (1) Choudary, B. M.; Reddy, P. N. *Journal of Molecular Catalysis A: Chemical* **1995**, *103*, L1.
- (2) Neumann, R.; Levin-Elad, M. *Applied Catalysis A: General* **1995**, *122*, 85.
- (3) Chen, Y.-W.; Lu, Y.-H. *Industrial & Engineering Chemistry Research* **1999**, *38*, 1893.
- (4) Pe ña, M. L.; Dejoz, A.; Forn és, V.; Rey, F.; V ázquez, M. I.; López Nieto, J. M. *Applied Catalysis A: General* **2001**, *209*, 155.
- (5) Launay, H.; Loridant, S.; Nguyen, D.; Volodin, A.; Dubois, J.; Millet, J. *Catalysis Today* **2007**, *128*, 176.
- (6) Mori, K.; Miyamoto, A.; Murakami, Y. *The Journal of Physical Chemistry* **1985**, *89*, 4265.
- (7) Solsona, B.; Blasco, T.; López Nieto, J. M.; Pe ña, M. L.; Rey, F.; Vidal-Moya, A. *Journal of Catalysis* **2001**, *203*, 443.
- (8) Zhang, Q.; Wang, Y.; Ohishi, Y.; Shishido, T.; Takehira, K. *Journal of Catalysis* **2001**, *202*, 308.
- (9) Zhou, R.; Cao, Y.; Yan, S.; Deng, J.; Liao, Y.; Hong, B. *Catalysis Letters* **2001**, *75*, 107.
- (10) Liu, Y.-M.; Cao, Y.; Yi, N.; Feng, W.-L.; Dai, W.-L.; Yan, S.-R.; He, H.-Y.; Fan, K.-N. *Journal of Catalysis* **2004**, *224*, 417.
- (11) Kondratenko, E. V.; Cherian, M.; Baerns, M.; Su, D.; Schl ögl, R.; Wang, X.; Wachs, I. E. *Journal of Catalysis* **2005**, *234*, 131.
- (12) Liu, Y.-M.; Feng, W.-L.; Li, T.-C.; He, H.-Y.; Dai, W.-L.; Huang, W.; Cao, Y.; Fan, K.-N. *Journal of Catalysis* **2006**, *239*, 125.
- (13) Liu, W.; Lai, S.; Dai, H.; Wang, S.; Sun, H.; Au, C. *Catalysis Letters* **2007**, *113*, 147.
- (14) Rozanska, X.; Fortrie, R.; Sauer, J. *The Journal of Physical Chemistry C*

**2007**, *111*, 6041.

(15) Čapek, L.; Adam, J.; Grygar, T.; Bulánek, R.; Vradman, L.; Košová-Kučerová, G.; Čičmanec, P.; Knotek, P. *Applied Catalysis A: General* **2008**, *342*, 99.

(16) Ramaswamy, A. V.; Sivasanker, S. *Catalysis Letters* **1993**, *22*, 239.

(17) Walker, J. V.; Morey, M.; Carlsson, H.; Davidson, A.; Stucky, G. D.; Butler, A. *Journal of the American Chemical Society* **1997**, *119*, 6921.

(18) Bhunia, S.; Saha, D.; Koner, S. *Langmuir* **2011**, *27*, 15322.

(19) Zhang, Q.; Gong, S.; Liu, L.; Yin, H. *Process Safety and Environmental Protection* **2013**, *91*, 86.

(20) Sudhakar Reddy, J.; Liu, P.; Sayari, A. *Applied Catalysis A: General* **1996**, *148*, 7.

(21) Luna, F. J.; Ukawa, S. E.; Wallau, M.; Schuchardt, U. *Journal of Molecular Catalysis A: Chemical* **1997**, *117*, 405.

(22) Zhou, W.-J.; Wischert, R.; Xue, K.; Zheng, Y.-T.; Albela, B.; Bonneviot, L.; Clacens, J.-M.; De Campo, F.; Pera-Titus, M.; Wu, P. *ACS Catalysis* **2013**, *4*, 53.

(23) Selvam, P.; Dapurkar, S. *Journal of Catalysis* **2005**, *229*, 64.

(24) Setnička, M.; Čičmanec, P.; Bulánek, R.; Zúkal, A.; Pastva, J. *Catalysis Today* **2013**, *204*, 132.

## **Chapter 7. Conclusions and perspectives**

### **7.1 General conclusions**

The present dissertation concerned researches on the improvement of vanadium-containing heterogeneous catalysts for oxidation reaction. The solid supports chosen for vanadium were high surface area mesoporous silica materials according to its high potential on the basis of a literature survey on vanadium-based materials and their catalytic application reported in Chapter 2. Vanadium-containing MCM-41 silica modified by addition of Al or Ti heteroatoms were designed and developed because of its potential in catalytic industrial application. A panel of physical techniques and in particular pseudo-quantitative UV visible spectroscopy were applied to characterize the dispersion of Vanadium (IV) or (V) on the different materials and according to different preparation methods. In addition, their catalytic properties was tested by on the selective oxidation of cyclohexane as a probe liquid phase reaction as well as the resistance of vanadium to leaching and the capacity for catalysts recycling. A general conclusion is provided after the partial conclusion of each experimental results of chapter 4, 5 and 6.

### **Chapter 4. Effect of Al(III) and Ti(IV) additives on vanadium dispersion in MCM-41 type of silicas**

In this chapter, the chemical anchoring effect of Al(III) or Ti(IV) heteroatoms on the dispersion of vanadium (V) in MCM-41 type silica was investigated using a pseudo-quantitative analysis of diffuse reflectance UV-visible spectra. Vanadium species was incorporated using incipient wetness impregnation of an aqueous vanadyl sulfate salt and vanadium (IV) species was transformed to vanadium (V) via calcination in the air flow. The textual properties of supports and

vanadium-containing silica were determined by X-ray diffraction and N<sub>2</sub> sorption measurement. Electron paramagnetic resonance (EPR) spectra showed the change of vanadium oxidation state during the preparation and revealed that the average distance between isolated V(IV) species was larger in the Ti and Al-modified silica matrices. Then, Tauc's plot transformation and Gaussian fits of the composite charge transfer bands in UV-visible spectra of hydrated and dehydrated samples evidenced the coexistence of several V(V) species of different oligomerization and hydration levels. The introduction of Al(III) or Ti(IV) in the composition of the silica wall via direct synthesis produced a blue shift of the charge transfer bands assigned to a higher proportion of small clusters and isolated V(V) species. The stronger beneficial effect of Ti on the vanadium dispersion is consistent with a higher stability of the X-O-V bridges moving from X = Si to X = Al and Ti. The formation of Ti-O-V bond was evidenced using Raman spectra.

### **Chapter 5. Improvement of vanadium dispersion using molecular surface engineering**

In Chapter 5, a new method to disperse vanadium was applied for the first time where a surface pretreatment based on partial organic surface masking was at stake using a molecular stencil patterning technique (MSP). The goal consisted to restrict the growth of vanadium species in vanadium-containing MCM-41 silicas in order to obtain the better dispersion of vanadium species. The titanium species was chosen on the basis of the work reported in Chapter 4 to anchor vanadium species and improve further the dispersion of vanadium. The XRD, N<sub>2</sub> sorption techniques were used to characterize the textural properties. TGA, NMR and IR techniques were applied to confirm the states of organic group introduced via MSP technique. The UV-visible spectra were deconvoluted and analyzed thoroughly as in Chapter 4 to describe as much as possible the states of vanadium species depending on the different

environments (with or without organic surface patterning or Ti, and for different vanadium loadings). It was found that the introduction of EBDMS organic groups by MSP technique led to a decrease of vanadium aggregation particularly at low loading while at high loading the empty space left by the masking organic cover was saturated favoring medium size cluster formation. Grafting titanium on the surface with or without organic masking pattern yielded also anchoring for vanadium ions particularly for V/Ti mole ratio smaller or equal to 2. Increasing this ratio, was highly detrimental to the dispersion as polymeric vanadium oxides species were formed. Furthermore, combining the introduction of both organic functional groups and titanium species improved further the dispersion of vanadium and avoided the partial reduction of the vanadium (V) alkoxide precursor during grafting.

#### **Chapter 6. Investigation of catalytic application of vanadium containing mesoporous silica**

Lastly, the catalytic performance of the vanadium catalytic materials were tested in selective oxidation of cyclohexane. The reduction temperature correlated with the redox properties of the supported vanadium species were obtained using the temperature programmed reduction technique and correlated with the vanadium dispersion state. The metal leaching that is the weakness of vanadium was probed using methanol considered as a sever solvent since it is more polar than the reaction products. The results proved that a better retention is obtained with Ti-O-V covalent bridges than Al-O-V or Si-O-V bridges. The catalytic selective oxidation of cyclohexane of the materials produced in Chapter 4 and 5 were compared in terms of reactant conversion and turn over frequency, peroxide efficiency and cyclohexanone to cyclohexanol ratio noted as K/A. It appears that all the synthetic parameters that improved the vanadium dispersion improve the catalytic properties, the catalysts robustness upon recycling, minimizing the vanadium leaching as well in perfect

equation with the physical characterizations of chapter 4 and 5. In addition, it was found that the presence of the organic masking pattern first planned to improve the dispersion improves also the efficiency of the peroxide to produce the targeted ketone and alcohol.

In brief, the efforts put into the synthesis of the catalysts produced a significant improvement of the oxidation process of cyclohexane based not only on the improvement of the vanadium dispersion but also showing the importance of capping the surface silanol groups. The new catalysts was proved to possess the potential in the future catalytic application.

## **7.2 Future perspectives**

Although the vanadium-containing silica designed here showed lots of improvement to those one without modification, the materials are still far from perfect to satisfy the necessary of industrial application. More efforts should be dedicated to develop the vanadium-containing heterogeneous catalysts for real industrial application based on the understanding obtained in this dissertation. Several points for future perspectives were described in what follows.

- ♦ Since the mesoporous silica has few application in industry until now because of its hydrothermal stability, the support should be considered as an important element to improve the entirety of the catalysts. However, even though the zeolites are widely applied in industrial process for many years, the vanadium species in the vanadium-containing silicate is not stable enough to resist the catalytic properties in the liquid phase reaction due to the weak Si-O-V bonds. On the other hands, the pore sizes of microporous materials restrict its application of bulky substrate reaction. Therefore, the choice of better supports for vanadium species and the way to

introduce vanadium atoms into the supports should be thought over carefully in the future development.

♦ Although some catalytic properties of vanadium-containing materials were investigated in this dissertation, the details of the catalytic process or mechanisms should be understood so as to improve both the materials and the applications. Besides, more other reactions should be investigated such as the bromination process in green way to enlarge the application.

Despite of some inherent drawbacks using vanadium-based catalyst, there should still be enough potential for it to motivate new discoveries and developments.

## Acknowledgements

落其实者思其树，饮其流者怀其源。

——北周·庾信

As a Chinese idiom, never forget where the water comes from when you drink it. This dissertation would not be accomplished without the encouragement and assistance of others.

Firstly, I would like to thank both of my supervisors, Prof. He Mingyuan, the academician of Chinese Academy of Sciences, in East China Normal University and Prof. Laurent Bonneviot in École Normale Supérieure de Lyon. It was my great honor to be a graduated student of Professor He Mingyuan six years ago. I am always inspired by his idea of catalysis in green chemistry during my research. I am very grateful to him and Prof. Laurent Bonneviot for the opportunity to be a collaboration student between ECNU and ENS-Lyon to continue my research in Lyon. In the period of study and work in Lyon, Prof. Laurent Bonneviot offered me lots of suggestion and help. It was lucky and happy to work with him and his group. Furthermore, his talent of innovation and abundant knowledge of inorganic and material chemistry always provided deep and profound view of my results, which I appreciated a lot.

I am also thankful to my two advisors, Prof. Wu Peng and Prof. Belén Albela. Prof. Wu Peng provided me a basic idea of porous silica materials and oxidation catalysis during my Master study period. And also, he contributed a lot of suggestion and advice in the part of catalysis in this dissertation. On the other hand, I am so grateful for the help from Prof. Belén Albela, particularly in the experiments and details of my work. Belén never hesitated to help me with all her enthusiasm whenever and

whatever I asked for. It was my fortune to have her guidance during my stay in Lyon.

I owe a particular debt of gratitude to Ms. Qian Yunhua, who is responsible for the collaboration program between ECNU and Group de l'ENS. She contributed great efforts to offer us the opportunities to study in École Normale Supérieure in France, to negotiate for us to have a steady life abroad.

The accomplishment of this dissertation also owed to the assistance of my colleagues at both sides of ENS-Lyon and ECNU. The daily routine in the lab relied on the Dr. Nathalie Calin. The Electron Paramagnetic Resonance was finished with the help of Lhoussain Khrouz. Sandrine Denis-quanquin finished all the solid-NMR in this dissertation. Those students before me, Dr. Zhang Kun, Dr. Zhou Wenjuan, Dr. Fang Lin, Dr. Jérémy Chaignon and Dr. Wang Zhendong, gave me plenty of their experience and suggestion in all the aspects. I am thankful to those other students, professors and administrators in ECNU and ENS-Lyon, who helped me to finish the administrative affairs every year.

Last but not the least, my family is all my support to achieve the degree and this dissertation. As the unique child in the family, my parents always worried about me when I was in France. Even so, they still encouraged and supported me to pursue my dream and the life I wanted. I am so proud of them and they are the most precious treasure in my life.